ABSTRACT

MARGOLSKEE, ALISON J. A Whole Life Model of the Human Menstrual Cycle. (Under the direction of James F. Selgrade.)

Systems of ordinary and delay differential equations are presented to model hormonal control of the female reproductive cycle. We begin by presenting the hormonal feedback mechanisms governing the female reproductive cycle. We discuss related work, describing previous mathematical models of this phenomenon and providing motivation for the present work.

We improve the fit of an existing model to data by incorporating a time delay for the effect of inhibin on the synthesis of follicle stimulating hormone (FSH). Bifurcation analysis is carried out on this model to study the existence and stability of equilibria and periodic solutions while varying three important parameters. One parameter represents the level of estradiol adequate for significant synthesis of luteinizing hormone (LH). Bifurcation diagrams with respect to this parameter reveal an interval of parameter values for which a unique stable periodic solution exists and this solution represents a menstrual cycle during which ovulation occurs. The second parameter measures mass transfer between the first two stages of ovarian development and is indicative of healthy follicular growth. The third parameter is the time delay. Changes in the second parameter and the time delay affect the size of the uniqueness interval defined with respect to the first parameter. Saddle-node, transcritical and degenerate Hopf bifurcations are studied.

Next we explore a change in parameters that creates solution profiles exhibiting multiple waves of follicle growth throughout the cycle. The key parameter change that accomplishes this is a decrease in the exponent on LH in the transfer from recruited to growing follicle. We discuss refinements to the model such as incorporating the experimentally observed FSH threshold required for the initiation of follicle growth, and a term describing the necessary atresia of the nonovulatory second wave of follicles in the absence of an LH surge.

We then develop a variation on previous models with the goal of simulating the hormonal regulation of the menstrual cycle of a woman from age 20 to age 51. This mechanistic model predicts changes in follicle numbers and reproductive hormones that naturally occur over that time span. In particular, the model illustrates the decline in the pool of primordial follicles from age 20 to menopause as reported in the biological literature. Also, model simulations exhibit a decrease in antimüllerian hormone (AMH) and inhibin B and an increase in FSH with age corresponding to experimental data. Model simulations using the administration of exogenous AMH show that the transfer of non-growing primordial follicles to the active state can be slowed enough to provide more follicles for development later in life and to cause a delay in the onset of menopause as measured by the number of primordial follicles remaining in the ovaries. Other

effects of AMH agonists and antagonists are investigated in the setting of this model.

Finally we discuss possibilities for future research, touching on potential improvements to the present work, and other directions suggested by the present work.

A Whole Life Model of the Human Menstrual Cycle

by
Alison J. Margolskee

A dissertation submitted to the Graduate Faculty of
North Carolina State University
in partial fulfillment of the
requirements for the Degree of
Doctor of Philosophy

Applied Mathematics

Raleigh, North Carolina

2013

APPROVED BY:

Mette Olufsen	Hien Tran
Charles Smith	James F. Selgrade Chair of Advisory Committee

BIOGRAPHY

Alison was born in San Francisco, California, to Dorothy and Robert Margolskee. After one year, she, her parents and older brother Daniel moved to Montclair, New Jersey, where her younger brother Andrew was born two years later.

As a child Alison was stubborn, introverted, and a bit of a perfectionist. She had trouble understanding why she had to do things she did not want to do. This tended to get her into trouble in her early years at school. Alison's introverted nature allowed her to entertain herself with almost anything. Punishments such as sitting in the corner, or going to her room, were highly ineffective. At one point in Kindergarten, a simple punishment for getting distracted turned into a whole week sitting alone at a desk in the hallway, since Alison never asked to come back inside.

Alison's affinity for mathematical thinking was apparent from an early age. Around seven years old, Alison became involved in the Math-A-Thon fund-raiser for St. Jude's children's hospital, and was excited to work on the problems in the Math-A-Thon Funbook. Alison's family friends who sponsored her for every correct answer did not realize what they had gotten themselves into. Alison's enthusiasm for math was rediscovered and cemented in the 4th grade when her math and science teacher went above and beyond, introducing her to more advanced and challenging mathematics in after school programs. In the 5th grade, Alison became the Conrail-24 champion of her elementary school. Conrail-24 is a game involving cards upon which four numbers are printed. Players compete to determine a combination of addition, subtraction, multiplication, and division of the four numbers to result in the number 24. In middle school and high school, Alison was able to skip ahead in the mathematics curriculum, learning algebra in 7th grade, and geometry in 8th grade. By the end of high school, Alison had completed two years of calculus, passing her AP tests with flying colors.

From a very young age Alison also showed an interest in art. When asked if she wanted to become an artist when she was older, the 4-year old Alison would respond "I AM an artist." Alison always admired her grandmother's paintings which covered the walls in her grandparents' house in Massachusetts. Alison spent her high school and undergraduate years pursuing her loves of math and art. In high school, Alison learned mathematics during the day, and took drawing and painting classes at the local art museum in the evenings and on weekends. When she applied to undergraduate programs, the Bachelor's of Science and Arts program at Carnegie Mellon jumped out as the perfect fit.

As a junior at Carnegie Mellon, the results of a career interests test made Alison realize her strong interest in biology. Though it should have come as no surprise, since Alison grew up in a household where biology, physiology and medicine were frequent topics of discussion at the

dinner table (Alison's mother is an MD and a licensed physician working in the pharmaceutical industry, and her father is an MD/PhD doing research in genetic engineering). Once Alison's strong interest in physiology came to light, she began to search for biological applications of mathematics.

Alison's first experience in mathematical biology came in the summer after her Junior year of college. She was involved in a Research Experience for Undergraduates (REU) at North Carolina State University, where she worked on the problem of physiologically based pharmacokinetic modeling carbon tetrachloride exposure in rats. After that summer, Alison was sure that she wanted to continue in the field of the mathematical biology. Her search for graduate programs in biomathematics and applied mathematics with biological focus brought her back to NCSU. Alison spent the next five years in Raleigh, furthering her training through courses in applied mathematics and biology, and performing research on the hormonal control of the female reproductive cycle under the advisement of James Selgrade. A summer internship in 2012 at a small pharmaceutical company in Durham gave Alison a foot in the door in the field of pharmacokinetics and pharmacodynamics, and may be in large part responsible for her receiving an offer in the School of Pharmacy at the University of Manchester.

For the next two years, Alison plans to be living and working as a Research Associate at the University of Manchester in Manchester, England. She is both excited and anxious about living in a foreign country, even if she does speak the language. Alison will be moving to Manchester shortly after the defense of her thesis with her three cats Lucifer, Ginger, and Fisher, though it may be quite an ordeal to get them there. After her stay in Manchester, Alison hopes to find a modeling and simulation position at a pharmaceutical company back in the US.

ACKNOWLEDGEMENTS

I would like to thank my advisor James Segrade. I could not have done this without his support, and constant encouragement. I want to thank my parents for always pushing me and believing in me, and for their emotional and financial support. I would also like to thank my good friend Jerry McMahan for standing by me throughout my years at NCSU, and for being a walking talking encyclopedia of mathematics.

TABLE OF CONTENTS

LIST OF TABLES

LIST OF FIGURES

Chapter 1

Introduction

The female reproductive cycle is regulated by hormones secreted by the hypothalamic-pituitary-ovarian axis. Follicle stimulating hormone (FSH) and luteinizing hormone (LH) are produced by the pituitary which is prompted by signals from the hypothalamus. FSH and LH affect the growth and development of follicles in the ovaries. The ovarian hormones, primarily estradiol (E2), progesterone (P4) and the inhibins, are produced by follicles of various stages of development and in turn affect the production and release of FSH and LH. Chapter 2 describes in more detail the biological background of this hormonal feedback mechanism.

Differential equations have been used to model different aspects of hormonal control of the menstrual cycle, e.g., see Bogumil *et al.*, 1972a, 1972b [6, 7], Plouffe and Luxenberg, 1992 [34], Selgrade and Schlosser, 1999 [70], Schlosser and Selgrade, 2000 [66], Harris-Clark *et al.*, 2003 [30], Reinecke and Deuflhard, 2007 [32], Pasteur, 2008 [57], and Selgrade, 2010 [68]. Chapter 3 discusses these related works in more detail, and provides context and motivation for the work presented in subsequent chapters.

Chapter 4 presents the numerical and computational methods utilized in Chapters 5, 6 and 7. We discuss the numerical software package used to perform the bifurcation analysis in Chapter 5, the numerical optimization schemes utilized in Chapter 7, and sensitivity and correlation of parameters used during parameter identification in Chapter 7.

Chapter 5 presents bifurcation analysis on the model from Selgrade, 2010 [68]. This model is a system of 13 ordinary differential equations with 42 parameters. The model's fit to data is improved by including a time delay for the effect of inhibin A on the synthesis of FSH. Biological reasons for this improvement are discussed. Bifurcations with respect to changes in three important parameters are examined. One parameter represents the level of E2 adequate for significant synthesis of LH. Bifurcation diagrams with respect to this parameter reveal an interval of parameter values for which a unique stable periodic solution exists and this solution represents a menstrual cycle during which ovulation occurs. The second parameter measures

mass transfer between the first two stages of ovarian development and is indicative of healthy follicular growth. The third parameter is the time delay. Changes in the second parameter and the time delay affect the size of the uniqueness interval defined with respect to the first parameter. Saddle-node, transcritical and degenerate Hopf bifurcations are studied.

The solution profiles corresponding to follicular stages of previous models, and those presented in Chapter 5, depicted a single wave of follicular development, beginning in the follicular phase and ending with ovulation. However, experimental evidence suggests that many women experience waves of follicles maturing to pre-ovulatory size throughout the monthly cycle, e.g. Baerwald 2003 [3]. In Chapter 6 we present a parameter set for the model of Selgrade, 2010 [68], that simulates a wave of two follicles in one monthly cycle. We also present a variation on this model to include atresia of the second wave.

In Chapter 7 we develop a variation on the models discussed in Chapters 3 through 6 with the goal of simulating key hormonal changes with advancing age. We use a single parameter set to represent women of different ages. Previous studies modeled the phenomenon on the time scale of days and months, and could model women of various ages only by using different parameter sets. The model presented in Chapter 7 is a system of 16 nonlinear, delay differential equations with 66 parameters, and models the hormonal regulation of the menstrual cycle of a woman from age 20 to age 51. This mechanistic model predicts changes in follicle numbers and reproductive hormones that naturally occur over that time span. In particular, the model illustrates the decline in the pool of primordial follicles from age 20 to menopause as reported in the biological literature. Also, model simulations exhibit a decrease in antimüllerian hormone (AMH) and inhibin B and an increase in FSH with age corresponding to experimental data. Model simulations using the administration of exogenous AMH show that the transfer of non-growing primordial follicles to the active state can be slowed enough to provide more follicles for development later in life and to cause a delay in the onset of menopause as measured by the number of primordial follicles remaining in the ovaries. Other effects of AMH agonists and antagonists are investigated in the setting of this model.

Chapter 2

Biological Background

Regulation of the reproductive cycle in adult women involves hormones produced by the hypothalamic-pituitary-ovarian axis (see Figure 2.1). The pituitary, prompted by signals from the hypothalamus, secretes follicle stimulating hormone (FSH) and luteinizing hormone (LH) which control ovarian follicle development and ovulation (Yen [86]). The ovaries produce estradiol (E2), progesterone (P4), inhibin A (InhA) and inhibin B (InhB) which affect the synthesis and release of FSH and LH (Karsch *et al.* [35]). The ovaries also produce antimüllerian hormone (AMH) which affects early follicular development (Skinner [72], Durlinger *et al.* [16]).

The menstrual cycle of a normally cycling adult female ranges from 25 to 35 days in duration (Ojeda [54]) and consists of the follicular phase, ovulation and then the luteal phase. The menstrual cycle begins with the follicular phase (days 1 to 13 of the average 28-day cycle) when a number of follicles are chosen to grow in response to elevated levels of FSH released from the pituitary. These growing follicles produce InhB and E2 in increasing amounts. By the middle of the follicular phase, a single follicle has been selected to mature to dominance. Increasing levels of E2 produced by the dominant follicle stimulate the release of an LH surge from the pituitary at mid-cycle. The LH surge is responsible for ovulation, causing the dominant follicle to rupture and release its ovum. After ovulation, the empty follicle becomes the corpus luteum. The second half of the cycle (days 15 to 28 of the average 28-day cycle) is referred to as the luteal phase. During the luteal phase, the corpus luteum produces P4 which primes the uterus for implantation and suppresses LH synthesis. The corpus luteum also produces InhA which suppresses FSH production, and E2 suppressing FSH and LH release. If at the end of the luteal phase fertilization has not occurred then the corpus luteum regresses, P4, InhA, and E2 decline, FSH rises and the cycle begins again.

Figure 2.2 plots the pituitary and ovarian hormone concentrations of the average young woman throughout her 28-day cycle, scaling each hormone to show their relative changes in magnitude across the cycle. These hormone profiles are taken from Welt *et al.*, 1999 [83] which

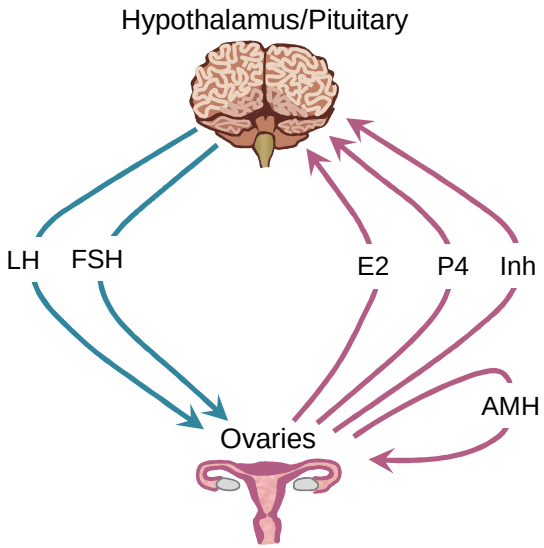

Figure 2.1: Hormonal control of the menstrual cycle via the hypothalamic-pituitary-ovarian axis. Luteinizing hormone (LH) and follicle stimulating hormone (FSH) are produced by the pituitary. Estradiol (E2), progesterone (P4), the inhibins and antimüllerian hormone (AMH) are produced by the ovaries.

collected daily plasma concentration levels of FSH, LH, E2, P4, InhA, and InhB from women of two age groups, 20-34 year (Table 2.1) and 35-46 year (Table 2.2). This data set is one of the first that sampled all six hormones. Most notably, it contains daily concentration data for both inhibins A and B, as it was collected after a biochemical assay for distinguishing between the inhibins was developed in the mid 1990's (see Groome *et al.* 1996 [23]). The hormone data from Welt *et al.* [83] is used in subsequent chapters for parameter identification and model validation. The model analyzed in Chapter 5 simulates the hormone concentration data for the younger women from Welt *et al.*. In Chapter 7, a model is developed that can simulate key hormonal changes with advancing age, including the decline in follicular phase InhB and rise in follicular phase FSH that are observed between the two age groups of the Welt data.

Figure 2.3 depicts the stages of development of follicles inside the ovaries. The primordial pool is the pool of follicles that a woman is born with. A primordial follicle consists of an oocyte surrounded by a layer of squamous (flat) granulosa cells. Primordial follicles pass to the primary stage of development where the granulosa cells become cuboidal and theca cells are recruited. This transition is stimulated and inhibited by a variety of ovarian factors (Skinner [72] and Reddy *et al.* [60]). One important hormone that inhibits the primordial to primary transition is antimüllerian hormone (AMH). AMH is produced by primary, preantral, and small antral

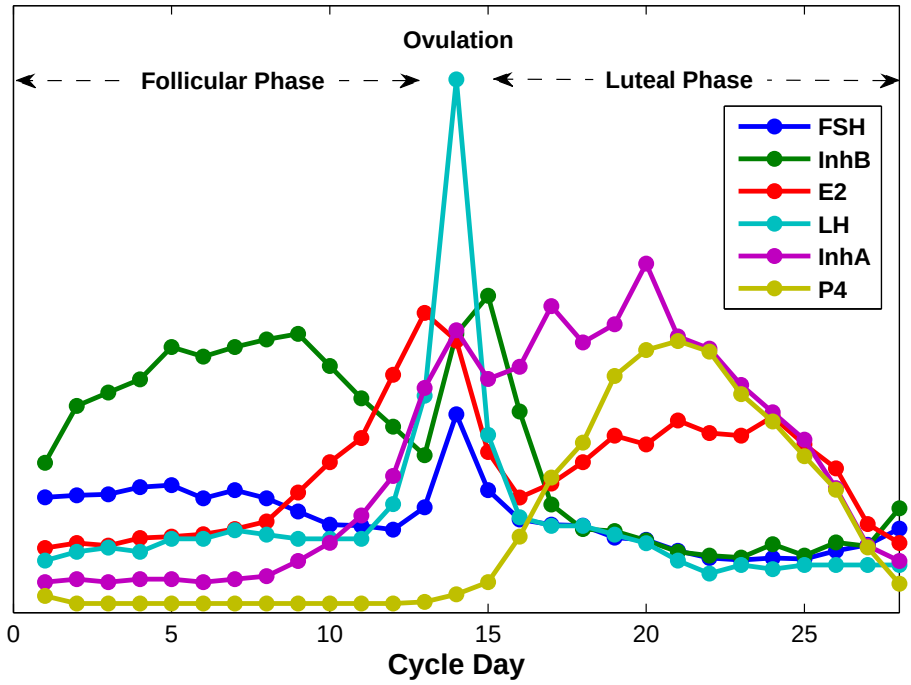

Figure 2.2: Hormone concentrations throughout the typical 28-day cycle of the average woman, taken from Welt *et al.* 1999 [83] who sampled 23 women between the ages of 20 and 34 years. The hormone levels have been scaled to show their relative changes in magnitude across the cycle. Elevated FSH stimulates follicle growth in the first half of the cycle. Growing follicles produce InhB and E2. Increased levels of E2 produced by the dominant follicle at mid-cycle causes the LH surge, which is responsible for ovulation. The second half of the cycle marks the luteal phase where the corpus luteum is producing P4, priming the uterus for implantation, and InhA and E2, suppressing the production and release of FSH and LH.

Table 2.1: Plasma concentrations for younger women from Welt *et al.* 1999 [83], extracted by and reported in Pasteur, 2008 [57].

Day	LH (IU/L)	FSH (IU/L)	E2 (pg/mL)	P4 (ng/mL)	InhA (IU/mL)	InhB (pg/mL)
1	12	11.4	51	1.1	1	79
2	14	11.6	55	0.6	1.1	109
3	15	11.7	53	0.6	1	116
4	14	12.4	59	0.6	1.1	123
5	17	12.6	60	0.6	1.1	140
6	17	11.3	62	0.6	1	135
7	19	12.1	66	0.6	1.1	140
8	18	11.3	72	0.6	1.2	144
9	17	10	95	0.6	1.7	147
10	17	8.7	119	0.6	2.3	130
11	17	8.6	138	0.6	3.2	113
12	25	8.2	188	0.6	4.5	98
13	50	10.4	237	0.7	7.4	83
14	123	19.6	215	1.2	9.3	147
15	41	12.1	127	2	7.7	167
16	22	9.2	91	5	8.1	106
17	20	8.7	102	8.9	10.1	57
18	20	8.6	119	11.2	8.9	44
19	18	7.4	140	15.6	9.5	43
20	16	7.2	133	17.3	11.5	38
21	12	6.1	152	17.9	9.1	32
22	9	5.4	142	17.2	8.7	30
23	11	5.2	140	14.4	7.5	29
24	10	5.4	155	12.6	6.6	36
25	11	5.3	133	10.3	5.7	30
26	11	6.1	114	8.1	4.1	37
27	11	6.7	70	4.3	2.2	35
28	11	8.3	55	1.9	1.7	55

Table 2.2: Plasma concentrations for older women from Welt *et al.* 1999 [83].

Day	LH (IU/L)	FSH (IU/L)	E2 (pg/mL)	P4 (ng/mL)	InhA (IU/mL)	InhB (pg/mL)
1	17	12.2	58	0.8	0.9	76
2	15	11.9	57	0.8	1.1	86
3	16	13	53	0.7	1.2	94
4	14	13.4	65	0.7	1.1	113
5	16	13.5	68	0.6	1.1	111
6	16	13.6	88	0.6	1.3	111
7	16	12.6	94	0.6	1.1	122
8	14	11.3	104	0.6	1.3	118
9	16	9.9	124	0.6	1.7	118
10	15	8.6	153	0.6	2.4	106
11	15	8.2	196	0.7	2.9	93
12	20	8.2	256	0.6	4.7	84
13	39	10	341	0.7	6.7	72
14	155	24.2	267	1.4	8.2	86
15	48	15.7	132	2.1	4.4	114
16	22	12.5	114	5.3	7.1	66
17	24	11.3	152	9	8.2	43
18	18	9.7	169	12.9	8.1	36
19	18	8.3	168	14.8	8	34
20	12	7.2	172	17.3	7.6	23
21	11	6.2	155	16.6	7.2	19
22	12	6.1	154	15.8	5	19
23	13	6	165	14.3	6	18
24	14	6.1	148	13.9	4.8	19
25	8	5.7	128	10.2	3.2	18
26	10	6.8	111	8.8	2.2	19
27	11	7.8	86	5.8	1.4	26
28	11	10.1	64	2.7	0.9	40

follicles and has emerged as an important indicator of follicle reserve [75, 82]. Primordial and primary follicles are gonadotropin-independent. The next stage of development is the pre-antral follicle. These follicles develop FSH-receptors, growing in response to FSH, and maturing to the small antral stage.

This point in the maturation process is where the monthly cycle begins. Small antral follicles, growing under the influence of FSH, begin producing InhB in large amounts. Six to ten follicles are selected to grow beyond the small antral stage. These follicles continue to grow in response to FSH, and some may develop LH receptors, grow in response to LH, and begin to produce E2. By mid-cycle, a dominant follicle has emerged. The dominant follicle produces E2 in large amounts and this increase in E2 causes a surge in LH which is responsible for ovulation. The dominant follicle becomes the ovulatory follicle, rupturing in response to the LH surge and releasing its ovum. The empty follicle becomes the corpus luteum and produces P4, InhA, and E2 preparing the uterus for fertilization. The stages represented in Figure 2.3 correspond to the follicular equations modeled in Chapter 7. The follicular stages starting from recruited through the corpus luteum correspond to those modeled in Chapters 5 and 6.

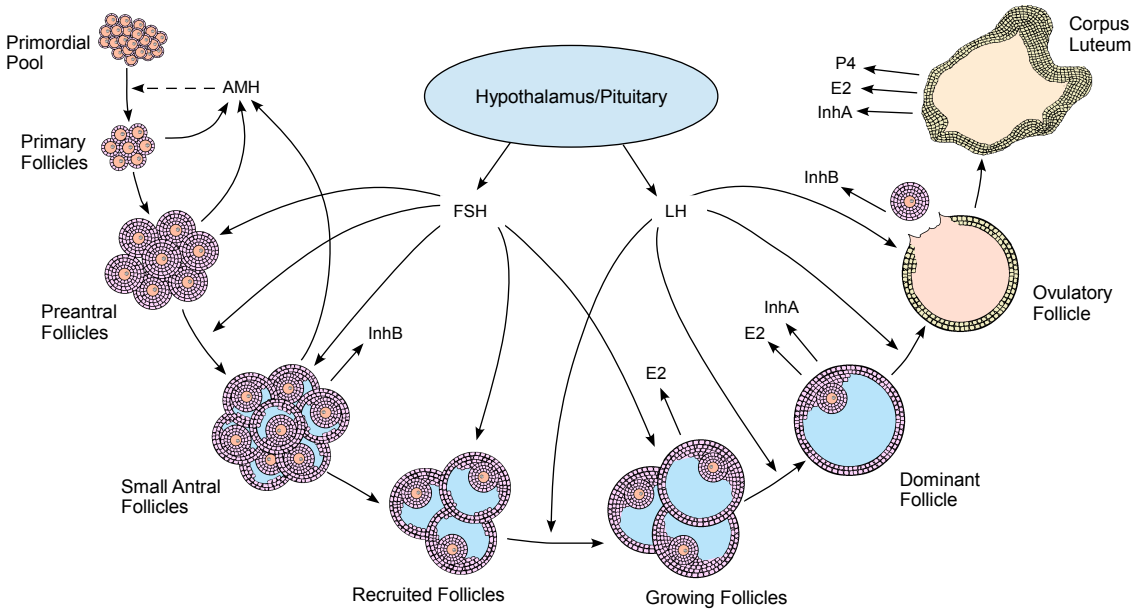

Figure 2.3: Depicted are the stages of follicular development, starting with the primordial follicles, primary follicles and continuing through to the ovulatory follicle and corpus luteum. Arrows between each stage represent a transition from one follicle type to the next. Arrows pointing away from follicles represent hormones secreted by these follicles. FSH and LH are produced and released by the Hypothalamus/Pituitary. Arrows pointing from FSH and LH represent the effects of these hormones on follicle growth and transition. The dashed arrow pointing from AMH indicates the inhibitory role that AMH plays on the primordial to primary transition.

Chapter 3

Previous Work and Model Development

Systems of ordinary and delayed differential equations have been used to model different aspects of hormonal control of the menstrual cycle, e.g., see Bogumil *et al.*, 1972a, 1972b [6, 7], McIntosh and McIntosh, 1980 [48], Plouffe and Luxenberg, 1992 [34], Selgrade and Schlosser, 1999 [70], Schlosser and Selgrade, 2000 [66], Harris-Clark *et al.*, 2003 [30], Reinecke and Deuflhard, 2007 [32], Pasteur, 2008 [57], and Selgrade, 2010 [68].

Harris, Pasteur, Schlosser and Selgrade [29, 30, 57, 66, 70] developed a model for this endocrine control system based on 13 ordinary differential equations (S) with three auxiliary equations (A) and with discrete time delays. Four of these differential equations (S1-S4) describe the synthesis, release and clearance of LH and FSH. Pulses of FSH and LH are secreted by the pituitary in response to pulses of gonadotropin-releasing hormone (GnRH) produced by the hypothalamus on a time scale of minutes. Because the ovaries respond to average daily blood levels (Odell [53]), the model tracks average daily concentrations of FSH and LH, lumping the effects of the hypothalamus and the pituitary together and just considering the synthesis and release of FSH and LH on the time scale of days. The state variables RP_{LH} and RP_{FSH} represent the amounts of these hormones stored in a releasable pool in the pituitary and LH and FSH represent the plasma concentrations of these hormones.

For each pituitary hormone there are two equations, one representing the amount of the hormone in a releasable pool in the pituitary, and a second representing the blood concentration. If we let H be a placeholder for LH or FSH, then the pituitary equations have the general

form of

$$\frac{d}{dt}RP_H = synthesis - release$$
$$\frac{d}{dt}H = \frac{1}{v}release - clearance$$

where RP_H stands for the amount of the hormone in the "releasable pool" and H stands for the plasma concentration of the hormone. In the second equation, the release term is divided by plasma volume, v, to convert hormone amounts to hormone concentrations. This model structure allows for differential responses in synthesis and release to ovarian factors (such as the biphasic response of LH to E2 indicated in the literature [35, 42, 86]). Figure 3.1 provides a schematic diagram for the effects of E2, P4 and Inh on the synthesis and release of the pituitary hormones, LH and FSH. E2 has a stimulatory role and P4 an inhibitory role on the synthesis of LH. Inh inhibits FSH synthesis. E2 inhibits and P4 stimulates the release of both LH and FSH. Clearance rates of LH and FSH are assumed constant.

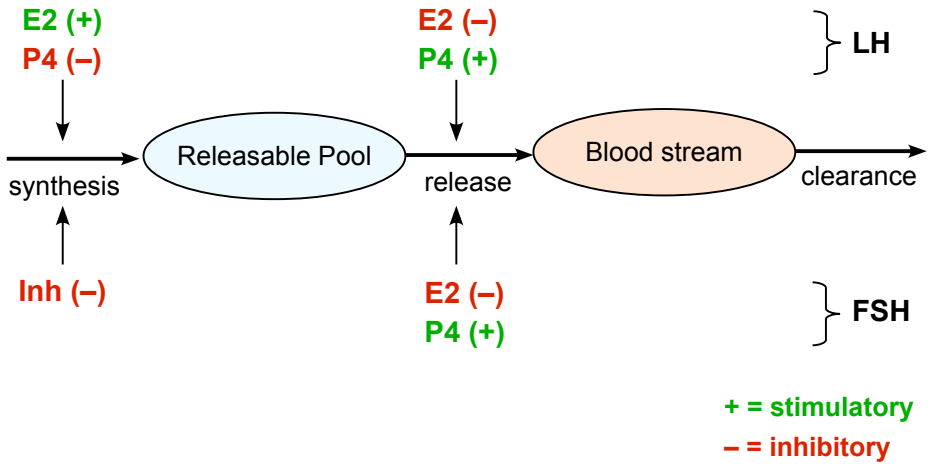

Figure 3.1: Schematic for the effects of E2, P4, and Inh on the synthesis and release of LH and FSH.

The biological literature (e.g., [35, 42, 86]) indicates that LH exhibits a biphasic response to E2, where low levels of E2 inhibit plasma LH concentrations while high levels of E2 stimulate LH. To capture this the model assumes that the effect of E_2 on LH synthesis is different than the effect on LH release, i.e., E_2 inhibits release (see the denominator of the second term in (S1)) but at high levels E_2 promotes synthesis. The stimulatory effect of E_2 on LH

synthesis is modeled as a Hill function in the numerator of the first term of (S1). Hill functions are frequently used to model the effect of substrate concentrations on the rate of an enzyme catalyzed reaction. They have the general form $\frac{Vmax \cdot S^a}{Km^a + S^a}$. The constant $Vmax$ represents the maximum rate for the reaction. Km is referred to as the half-saturation constant and is the concentration of substrate at which the reaction is running at half $Vmax$. The exponent a is referred to as the Hill coefficient. When a is greater than 1, higher concentrations of substrate accelerate the rate of reaction, representing cooperativity between substrates [36]. Figure 5.4 plots Hill functions for various values of the Hill coefficient, a, keeping $Vmax$ and Km fixed.

In contrast to the effects of E2, P4 inhibits LH synthesis and promotes release. These effects are included in the model as the denominator of the first term in (S1), and the numerator of the second term in (S1). The release term appears in (S1) as a decay term and in (S2) as a growth term, where it is divided by blood volume v. The equations (S3-S4) for FSH are similar except the synthesis term has Inh inhibition. The parameters in (S1-S4) are named according to the traditional usage for chemical reactions, e.g., $V_{1,LH}$ denotes the velocity of the reaction (see Keener and Sneyd, 2009, [36]).

Since synthesis is a complex process, it is assumed that the effect of the ovarian hormones are not immediately observed as changes in LH and FSH reserve in the releasable pool. Thus, time delays (d_E, d_P, d_{Inh}) are included in the synthesis terms for LH and FSH and represent a lag in the effect of serum concentrations of the ovarian hormones on the production of the pituitary hormones.

System (S1)-(S4)

$$\frac{d}{dt} RP_{LH} = \frac{V_{0,LH} + \dfrac{V_{1,LH}\, E_2(t-d_E)^8}{Km_{LH}^8 + E_2(t-d_E)^8}}{1 + P_4(t-d_P)/Ki_{LH,P}} - \frac{k_{LH}\ [1 + c_{LH,P}\, P_4]\ RP_{LH}}{1 + c_{LH,E}\, E_2} \tag{S1}$$

$$\frac{d}{dt} LH = \frac{1}{v} \frac{k_{LH}\ [1 + c_{LH,P}\, P_4]\ RP_{LH}}{1 + c_{LH,E}\, E_2} - a_{LH}\, LH \tag{S2}$$

$$\frac{d}{dt} RP_{FSH} = \frac{V_{FSH}}{1 + Inh(t-d_{Inh})/Ki_{FSH,Inh}} - \frac{k_{FSH}\ [1 + c_{FSH,P}\, P_4]\ RP_{FSH}}{1 + c_{FSH,E}\, E_2^2} \tag{S3}$$

$$\frac{d}{dt} FSH = \frac{1}{v} \frac{k_{FSH}\ [1 + c_{FSH,P}\, P_4]\ RP_{FSH}}{1 + c_{FSH,E}\, E_2^2} - a_{FSH}\, FSH \tag{S4}$$

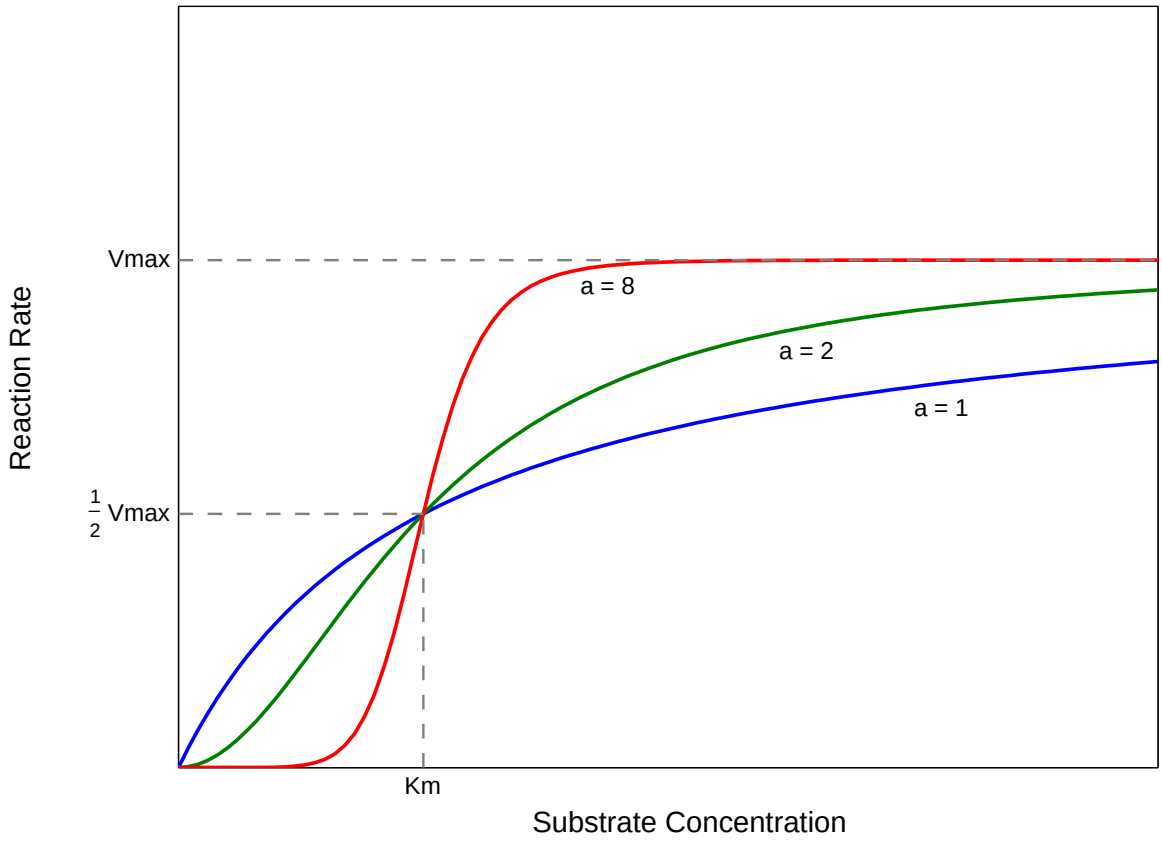

Figure 3.2: Graphs of Hill functions, $Vmax \cdot S^a/(Km^a + S^a)$, for three values of the Hill coefficient a, with Km and $Vmax$ fixed. A value of a greater than 1 represents positive cooperativity among substrates. The dashed lines indicate $Vmax$, $\frac{1}{2}Vmax$, and Km. Note that when the substrate concentration is equal to Km, the reaction is running at half $Vmax$.

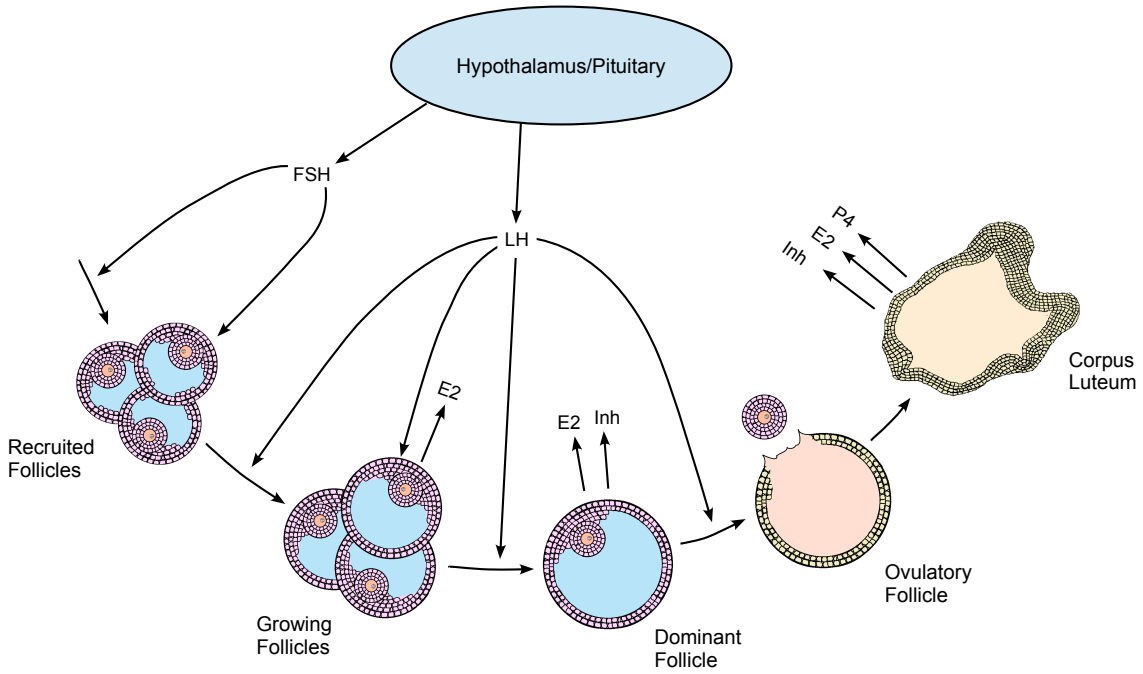

Figure 3.3: Depicted are the stages of follicle development as modeled by equations (S5-S13). The first three follicle stages in this diagram (recruited, growing, and dominant follicle) correspond to the state variables ReF, GrF, and $DomF$ in equations (S5-S7), the ovulatory follicle is modeled by Ov_1 and Ov_2 in equations (S8) and (S9), and the corpus luteum is represented by the four luteal phases Lut_1 through Lut_4 in equations (S10 - S13). Arrows between follicle stages represent transitions from one stage to the next. Arrows pointing to follicle stages represent growth in response to LH or FSH, and arrows pointing away from follicles represent the ovarian hormones produced by those stages of development.

Because of the quasi-steady state assumption mentioned below, the ovarian hormones are modeled as linear combinations of the different follicle stages that produce them. Equations (S5-S13) model the dynamics of 9 distinct stages of ovarian follicle development during the follicular and luteal phases of the cycle. Figure 3.3 illustrates the follicle stages as modeled by this system. ReF, GrF and $DomF$ denote the recruited follicles, the growing follicles and the preovulatory or dominant follicle, respectively. Note that we have changed the notation of previous models ([30], [57], [68]), replacing the old notation of PrF with the new notation $DomF$. The reason for this change is that the reference to the dominant follicle as primary is not in agreement with biological references, e.g., Skinner [72] and Hansen *et al.* [28]. These references use "primary follicle" to refer to the very early stage of follicle growth in which granulosa cells have become cuboidal and theca cells are being recruited. Ov_1 and Ov_2 represent periovulatory stages and Lut_i, $i = 1, ..., 4$, denote four luteal stages. LH and FSH promote tissue growth within a stage and the transformation of tissue from one stage to the next. Since clearance from the blood of the ovarian hormones is on a fast time scale, we assume that blood levels of E_2, P_4, and Inh are at quasi-steady state [36] as did Bogumil *et al.* [6]. Hence, these concentrations are taken to be proportional to the follicle stages during the appropriate phases of the cycle giving the three auxiliary equations (A1-A3) for the ovarian hormones. The forty-two parameters listed in Table 3.1 correspond to those which Selgrade [68] used to analyze bifurcation diagrams. The parameters represent a set for which the model output is a close fit to the Welt data for women age 20-34, with time delays set to zero.

System (S5)-(S13)

$$\frac{d}{dt}\,ReF = b\,FSH + \left[c_1\,FSH - c_2\,LH^{\alpha}\right]\,ReF \tag{S5}$$

$$\frac{d}{dt}\,GrF = c_2\,LH^{\alpha}\,ReF + \left[c_3\,LH^{\beta} - c_4\,LH\right]\,GrF \tag{S6}$$

$$\frac{d}{dt}\,DomF = c_4\,LH\,GrF - c_5\,LH^{\gamma}\,DomF \tag{S7}$$

$$\frac{d}{dt}\,Ov_1 = c_5\,LH^{\gamma}\,DomF - d_1\,Ov_1 \tag{S8}$$

$$\frac{d}{dt}\,Ov_2 = d_1\,Ov_1 - d_2\,Ov_2 \tag{S9}$$

$$\frac{d}{dt}\,Lut_1 = d_2\,Ov_2 - k_1\,Lut_1 \tag{S10}$$

$$\frac{d}{dt}\,Lut_2 = k_1\,Lut_1 - k_2\,Lut_2 \tag{S11}$$

$$\frac{d}{dt}\,Lut_3 = k_2\,Lut_2 - k_3\,Lut_3 \tag{S12}$$

$$\frac{d}{dt}\,Lut_4 = k_3\,Lut_3 - k_4\,Lut_4\ . \tag{S13}$$

Auxiliary Equations (A)

$$E_2 = e_0 + e_1\,GrF + e_2\,DomF + e_3\,Lut_4 \tag{A1}$$

$$P_4 = p_0 + p_1\,Lut_3 + p_2\,Lut_4 \tag{A2}$$

$$Inh = h_0 + h_1\,DomF + h_2\,Lut_2 + h_3\,Lut_3\ . \tag{A3}$$

Harris, Pasteur, Schlosser and Selgrade [30, 57, 66, 70] identified model parameters using two different clinical data sets for normally cycling women (McLachlan *et al.*, 1990 [50], and Welt *et al.*, 1999 [83]). The McLachlan data was the only available data when their modeling started and it was obtained before inhibin A and inhibin B were separately identifiable (see Groome *et al.* 1996 [23]). The Welt data includes data for both inhibins, and for two different age groups of women, unlike the McLachlan data. Comparison of the inhibin profiles in Welt with the single inhibin profile in McLachlan suggests that it is likely that inhibin A is the reported hormone in McLachlan *et al.* 1990.

Model simulations with parameters from the McLachlan data [50] revealed two stable periodic solutions [30] — one fitting the McLachlan data for normally cycling women and the other being non-ovulatory because of no LH surge. The non-ovulatory cycle has similarities to an

Table 3.1: Parameters and values for system (S) and auxiliary equations (A).

Eqs. (S1-S4)	
k_{LH}	2.42 day^{-1}
a_{LH}	14.0 day^{-1}
$V_{0,LH}$	500 IU/day
$V_{1,LH}$	4500 IU/day
Km_{LH}	200 pg/mL
$Ki_{LH,P}$	12.2 ng/mL
$c_{LH,E}$	0.004 mL/pg
$c_{LH,P}$	0.26 mL/ng
V_{FSH}	375 IU/day
a_{FSH}	8.21 day^{-1}
k_{FSH}	1.90 day^{-1}
$c_{FSH,E}$	0.0018 mL^2/pg^2
$Ki_{FSH,Inh}$	3.5 IU/mL
$c_{FSH,P}$	12.0 mL/ng
v	2.50 L

Eqs. (S5-S13)	
b	0.05 L μg/(IU day)
c_1	0.08 L/(IU day)
c_2	0.07 $(\text{L/IU})^{\alpha}$/day
c_3	0.13 $(\text{L/IU})^{\beta}$/day
c_4	0.027 L/(IU day)
c_5	0.51 $(\text{L/IU})^{\gamma}$/day
d_1	0.50 day^{-1}
d_2	0.56 day^{-1}
k_1	0.55 day^{-1}
k_2	0.69 day^{-1}
k_3	0.85 day^{-1}
k_4	0.85 day^{-1}
α	0.79
β	0.16
γ	0.02

Eq. (A)			
e_0	30 pg/mL	p_2	0.048 kL^{-1}
e_1	0.11 L^{-1}	h_0	0.4 IU/mL
e_2	0.21 L^{-1}	h_1	0.009 IU/(μg mL)
e_3	0.45 L^{-1}	h_2	0.029 IU/(μg mL)
p_0	0 ng/mL	h_3	0.018 IU/(μg mL)
p_1	0.048 kL^{-1}		

abnormal cycle of a woman with polycystic ovarian syndrome (PCOS) [87], the leading cause of female infertility. However, model simulations corresponding to the Welt parameters produced only one stable periodic solution and it fits the Welt data for normally cycling women. Selgrade *et al.*, 2009 [69], explained this apparent inconsistency by showing that a change in only one sensitive parameter of the Welt system would result in the Welt model exhibiting bistability like the McLachlan model.

In an effort to understand what parameter ranges result in normal and abnormal cycling, Selgrade [68] set the time-delays to zero in the Welt model and used the software XPPAUT [19] to study bifurcation diagrams with respect to two of the most sensitive parameters. Bifurcation diagrams for the resulting autonomous system could be drawn with the features of AUTO [15] in XPPAUT. In Chapter 5 we re-introduce the time-delays to provide a superior fit to the Welt data. We carry out bifurcation analysis for the system of delayed differential equations using the Matlab package DDE-BIFTOOL [18], which is designed to handle the delay.

Each of the models mentioned in this section simulate the daily hormone levels of a woman of a certain age. Solutions to these systems are purely periodic, and lack the long-term trends associated with ovarian aging. These models can and have been used to simulate hormone levels in women of different ages by providing separate parameters sets for women of different ages (e.g. see Pasteur 2008 [57]). It has been suggested (e.g. see Broekmans *et al.* [9]) that the changes in reproductive hormones during the menopausal transition can be directly attributed to a decrease in the number available follicles to grow to maturity. The goal of Chapter 7 is to incorporate the constantly declining primordial pool of follicles that a woman is born with, and use this as the driving force behind the key hormone changes with advancing age.

Chapter 4

Methods

4.1 Computational methods

Numerical computations are performed using Matlab version 7.12 on a quad-core PC equipped with a 7th generation Intel chip and 8.00 GB installed RAM. Delay differential equations are solved using Matlab's built-in delay differential equations solver dde23, which numerically integrates delay differential equations with constant delays. It employs the Runge Kutta (2,3) pair to perform a variable step integration, and uses a Hermite cubic interpolant to determine lagged values from stored history [71]. When equations are decoupled, and the result produces a smaller system of equations with no delays, this system is integrated using Matlab's ode23.

Numerical drift can result when the local truncation errors of a numerical approximation are compounded with each iteration, causing the numerical approximation to drift away from the true solution [58]. Numerical drift resulting during numerical integration will accumulate over longer periods of integration. The extent of numerical drift is dependent upon the step size used during integration, with smaller step sizes resulting in less numerical drift. Thus, the extent of numerical drift can be analyzed with a grid-refinement study. For periodic solutions of differential equations, numerical drift can present itself as a phase shift in the time direction. Since solutions of our system that are of interest are exponentially attracting, we expect to see numerical drift primarily in the time direction.

To determine the extent of numerical drift of Runge Kutta methods on our model, we performed a grid-refinement study using a fixed step 4th order Runge Kutta method for delay differential equations which we coded and implemented in Matlab. We refer to this integrator as ddeRK4 [45]. The solutions obtained by using different time steps in the integrator ddeRK4 were compared to determine the extent of numerical drift. We found that a step size of 0.1 days limits the numerical drift in the time direction to less than 0.25 days when the model is integrated over a period of 30 years, from age 20 to age 50 (see Figure 4.1). When the phase

Step size (Days)	Phase Shift (Days)
0.1	0
0.05	0.2161
0.025	0.2415
0.0125	0.2436

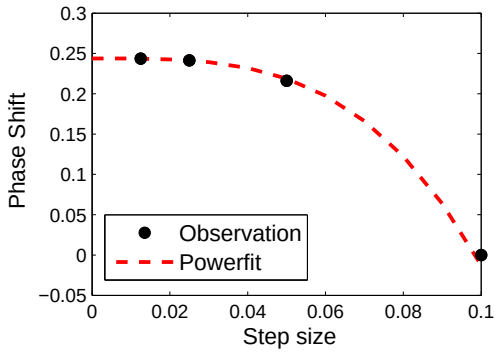

Figure 4.1: Summary of grid-refinement study of phase shift in time direction of numerical simulation after integrating from age 20 to age 50 using ddeRK4. Column 1 is the step size used in integration, Column 2 is the difference in day of LH peak (phase shift) at the end of 30 years when compared to the solution obtained using the step size of 0.1 days. Fitting a simple power function $(a + bx^c)$ to these data gives an intercept of $a = 0.2438$ days, which implies a phase shift for the simulation with step size 0.1 approaches 0.2438 days with successively smaller step sizes. (The other two parameters of the powerfit are $b = -578.6814$ and $c = 3.3533$.)

shift in the time direction is accounted for, i.e. the solution profiles are centered at the LH peak, then a time step of 0.1 days limits the deviation in the solution profiles to less than 0.5% for integration spans of more than 30 years. In an analogous grid refinement study, the numerical drift in the noncycling stages, $Primor$ and $Primar$ of Chapter 7, was observed. These stages are affected by numerical drift to a lesser extent than the monthly cycling stages. The numerical drift in the solution profiles for $Primor$ and $Primar$ can be limited to less than 0.1% across the 30 year span by using a step size of 80 days during integration.

The longest time span of integration reported here is from age 20 to age 51, but only the noncycling equations ($Primor$ and $Primar$, see equations (SS1) and (SS2) in Chapter 7) are integrated for this time span (see Section 7.3.4). These equations also contain no delay, so they are simulated using Matlab's ode integrator ode23. The numerical drift in the magnitudes of these noncycling equations can be limited to less than 0.1% when a step size of 80 days is used. So we integrate this small system using ode23 with the option MaxStep set to 80.

The monthly cycling differential equations (Equations (SS3) through (SS16)) are simulated for two-month time spans (see Section 7.3.4). The numerical drift in the time direction over this short time span is negligible. The numerical drift in the magnitude of the solution profiles can be limited to less than 0.5% by using a time step of 0.1 days. So we integrate these equations using dde23 with the option MaxStep set to 0.1.

4.2 Bifurcation analysis

Meiss 2007 [51] described a bifurcation as a "qualitative change in dynamics occurring upon a small change in a parameter." Bifurcations can occur when equilibria are created or destroyed or when a change in the stability of an equilibrium is observed in response to a change in parameter value. For some examples of basic bifurcations such as saddle-node, pitchfork, transcritical, and hopf bifurcations, see Appendix B.

Bifurcation diagrams for systems of delay differential equations are computed using the numerical bifurcation toolbox DDE-BIFTOOL [18]. This package uses continuation to compute branches of steady state and periodic solutions. Branches of periodic solutions can be started from a Hopf point or from a previously supplied periodic solution.

Unlike ordinary differential equations, the linearized equations (variational equations) corresponding to a system of delay differential equations (see Hale, 1977 [26]) produces a system with an infinite number of characteristic roots which determine stability. However, there are only a finite number of characteristic roots in the right half of the complex plane, and the existence of at least one eigenvalue with positive real part signifies an unstable equilibrium. DDE-BIFTOOL uses these facts to determine the stability of a steady state solution by computing the rightmost roots to the characteristic equation [18]. The stability of a periodic solution is determined by the Floquet multipliers. The Floquet multipliers are the eigenvalues of a time integration operator that integrates the linearization of the delay differential equation from time 0 to T, where T is the period of the periodic orbit. If all Floquet multipliers (except the trivial multiplier of 1 corresponding to the vector tangent to the periodic solution) are within the unit circle, then a periodic solution is stable.

The algebraic systems which determine steady state solutions, periodic solutions, and various bifurcations are approximated by Newton iteration methods (Engelborghs *et al.* [18]). Continuation of a branch of solutions is performed by a combination of prediction and correction. Previously computed points are used to predict the next point via a secant prediction method, and the prediction is then corrected by solving the appropriate determining system.

4.3 Least squares data fitting

In least squares data fitting, the objective function to be optimized has the form [37]:

$$f(\vec{q}) = \sum_{j=1}^{M} |d^j - y(t_j; \vec{q})|^2 = R(\vec{q})^T R(\vec{q})$$

where $\vec{q}$ is the parameter vector, y is a single model output and d is the data sampled at M time points. R is a column vector of length M with components $(d^j - y(t_j; \vec{q}))$ and is referred to

as the residual between the data and the model output. If the output is a vector of observations $\vec{y}$ of length N with components y_i then we have

$$f(\vec{q}) = \sum_{j=1}^{M} \|\vec{d^j} - \vec{y}(t_j; \vec{q})\|_2^2 = \sum_{j=1}^{M} \sum_{i=1}^{N} |d_i^j - y_i(t_j; \vec{q})|^2 = R(\vec{q})^T R(\vec{q})$$

where R is of length MN with components $(d_i^j - y_i(t_j; \vec{q}))$.

Fitting the model output to data involves finding a $\vec{q}$ that minimizes the function $f(\vec{q})$. There are many optimization algorithms that can be implemented to find a minimum to a least squares objective function. Public domain codes for many of these optimization algorithms can be found online in the Numerical Analysis and Modelling software repository at Zuse Institut Berlin (ZIB) [89]. These codes are based on the algorithms presented in a book by P. Deuflhard [14]. Of these codes we explored the use of NLSQ_ERR, which is an implementation of unconstrained Gauss-Newton with an error oriented convergence criterion. In order to insure that the parameters of our system are positive, we optimize the natural log of the parameter values and then exponentiate after optimization.

4.4 Sensitivity, correlation, and uncertainty quantification

The models presented here have a large number of parameters, and a number of state variables for which there are no direct experimental data. Attempting to identify all of the parameters at once leads to poor convergence of the numerical optimization schemes, and limited parameter identifiability [33]. In the presence of poor convergence, it may be helpful to examine the sensitivity of the model to the parameters and correlations among the parameters. Insensitivity of a model to a parameter means that large changes in the parameter have little effect on the model output. This leads to greater uncertainty of the optimal parameter value and can prevent an optimization algorithm from converging. If a pair of parameters is correlated then changing one parameter is related to changing the other parameter, which may limit parameter identifiability.

The sensitivity of a model output y with respect to a parameter set $\vec{q}$ is determined by the matrix $\frac{\partial y}{\partial \vec{q}}$ (also called the Jacobian of y) evaluated at the time points $t_1, t_2, \ldots t_M$ associated

with the data [4],

$$S(\vec{q}) = \frac{\partial y}{\partial \vec{q}} = \begin{bmatrix} \frac{\partial y(t_1;\vec{q})}{\partial q_1} & \frac{\partial y(t_1;\vec{q})}{\partial q_2} & \cdots & \frac{\partial y(t_1;\vec{q})}{\partial q_p} \\ \frac{\partial y(t_2;\vec{q})}{\partial q_1} & \frac{\partial y(t_2;\vec{q})}{\partial q_2} & & \\ \vdots & & \ddots & \\ \frac{\partial y(t_M;\vec{q})}{\partial q_1} & & & \frac{\partial y(t_M;\vec{q})}{\partial q_p} \end{bmatrix}.$$

It describes the sensitivity of the model to the parameters at the chosen time points. Here p is the number of parameters in $\vec{q}$ and M is the number of data points, which makes S a matrix of size $M \times p$. If the model output is a vector $\vec{y}$ of length N then the sensitivity matrix will be a matrix of size $MN \times p$. Note that sensitivities will vary depending on the parameter values, $\vec{q}$, and the times, $t_1, \ldots, t_M$, at which they are evaluated. For comparison across parameters and outputs of differing magnitudes, it is often helpful to consider the *relative* sensitivities which are obtained by multiplying each element $\partial y(t_i;\vec{q})/\partial q_j$ by $q_j/y(t_i;\vec{q})$, for $y \neq 0$ [55].

The covariance of parameters can be used to determine correlations among parameters and to quantify the uncertainty in a parameter set. Normally covariance of a set of random variables would be estimated from a sample distribution of the variables, but here we do not have any information about how $\vec{q}$ varies with the model output. We do however have information about how the model output varies with changes in $\vec{q}$, namely we know the sensitivity matrix $S(\vec{q}) = \frac{\partial y}{\partial \vec{q}}$.

Given knowledge of the sensitivity matrix, $S(\vec{q})$, the covariance matrix, cov, of the parameters $\vec{q}_j$ can be estimated via the unbiased estimator, $\widehat{\mathrm{cov}}(\vec{q})$, given by [55, 11]

$$\widehat{\mathrm{cov}} = \sigma^2 (S^T S)^{-1}.$$

Here the variance, σ^2, is assumed constant and can be estimated as

$$\widehat{\sigma}^2 = R^T(\vec{q}) R(\vec{q}) / (n - p),$$

where R is the residual between the model and data (see Section 4.3), n is the number of data points (length of R), and p is the number of parameters (length of $\vec{q}$). The square root of the diagonal entries of the covariance matrix are the standard errors associated with the parameters, thus the covariance matrix can be used to estimate the uncertainty in the choice of parameters. The covariance matrix can also be used to determine correlations among the

parameters. Correlation of parameters can be given by [55, 11]

$$C_{ij} = \frac{\mathrm{cov}_{ij}}{\sqrt{\mathrm{cov}_{ii}\mathrm{cov}_{jj}}}$$

where cov is the covariance matrix, and can be estimated using $\widehat{\mathrm{cov}}$ in place of cov.

The correlation matrix C is symmetric with 1's on the diagonal, and values between -1 and 1 elsewhere. The closer the C_{ij} entry is to ± 1, the more correlated are the parameters q_i and q_j. A reasonable rule proposed in Olufsen and Ottesen [55] is to consider all entries greater than 0.9 in magnitude to imply correlation. Note that $S^T S$ must have full rank in order to be inverted, and since $rank((S^T S)_{p\times p}) = rank(S_{n\times p}) \leq min(n, p)$, it is necessary that p be less than n. There need to be at least as many data points as there are parameters. If there are too many parameters compared to data, then there will necessarily be correlations among the parameters. If a pair of parameters is determined to be correlated, it may be possible to decouple the parameters or reduce the parameter set through nondimensionalization [73].

Chapter 5

Dynamics and Bifurcation of a Menstrual Cycle Model with Inhibin Delay

5.1 Introduction

Abnormal cycling and non-ovulatory cycling have serious health and reproductive consequences. In fact, between 6% and 9% of adult women exhibit some symptoms of polycystic ovary syndrome (PCOS), see Azziz *et al.*, 2004 [2], and Alvarez-Blasco *et al.*, 2006 [1]. Since cycle irregularities are usually associated with abnormal hormone levels, mathematical models of hormonal regulation may provide information about parameter variations which result in abnormal cycling and may provide insights about possible hormonal therapies.

In an effort to understand what parameter ranges result in normal and abnormal cycling, Selgrade [68] set the time-delays to zero in the Welt model and used the software XPPAUT [19] to study bifurcation diagrams with respect to two of the most sensitive parameters (Km_{LH} and c_2). Bifurcation diagrams for the resulting autonomous system could be drawn with the features of AUTO [15] in XPPAUT. This autonomous model gives an acceptable fit to the 28 day Welt data set [83] except some hormone peaks are lower than the data and the period for the normal cycle is only about 26 days, see Figure 5.1.

Based on model sensitivity analysis [57, 69], the two key parameters for study in [68] were Km_{LH} and c_2. Km_{LH} is the half-saturation constant which represents the level of E2 sufficient for significant LH synthesis and the LH surge. c_2 indicates the ovarian mass transfer rate between the first two stages of ovarian development. The bifurcation diagram with respect to Km_{LH} reveals an interval of Km_{LH} parameter values for which a unique stable periodic

solution exists and this solution represents a menstrual cycle with an LH surge adequate for ovulation. If Km_{LH} lies outside this cycle uniqueness interval then either no LH surge occurs or there are two stable cycles — one is ovulatory and the other may be non-ovulatory because of an insufficient LH surge. Changes in c_2 affect the size of this interval because of the positions of Hopf, saddle-node and transcritical bifurcations as discussed in [68].

In this study, we carry out a bifurcation analysis for the system of delayed differential equations using the Matlab package DDE-BIFTOOL [18], which is designed to handle the delay. The original model in Harris et al. 2003 [30] had three discrete time-delays (one corresponding to each ovarian hormone) which represented the time interval between changes in ovarian hormone concentrations and subsequent changes they cause in synthesis rates of the pituitary hormones. Selgrade 2010 [68] set the delays to zero in order to use XPPAUT to perform bifurcation analysis on the system. Here we show that including only a delay of $\tau = 1.5$ days for the effect of the peptide inhibin on the pituitary's secretion of FSH improves the fit to the Welt data (see Figure 5.1) and this time lag in the effect of inhibin is consistent with observations from experiments with rhesus monkeys (Ramaswamy *et al.* [59]). The other two delays, which pertain to the steroids E2 and P4, were less than a day and did not contribute significant additional improvement. So they are set to zero for this study. The system with the inhibin delay has larger uniqueness intervals than the model with no delay (see Table 5.1). Hence, an inhibin delay may enhance the possibility of ovulation. In Section 5.2 we speculate about the biological reasons for this improvement in model behavior due to inhibin delay. We examine bifurcation diagrams with respect to Km_{LH} for the delayed system and show that the cycle uniqueness interval is usually determined by two saddle-node bifurcations. For the delay τ fixed at 1.5 days, we illustrate how this interval may be enlarged by varying c_2 due to the occurrence of two degenerate Hopf bifurcations. Then for fixed c_2, we increase the delay parameter τ from 0 to 1.5 to unfold transcritical bifurcations and produce large cycle uniqueness intervals. Finally, we illustrate how loops in the Km_{LH} bifurcation diagrams may appear and disappear by varying the parameters τ and c_2.

5.2 Effect of inhibin delay on model fit to data

Inhibin is a glycoprotein secreted by the ovaries and has a more complicated molecular structure than the steroids E2 and P4. It is well-known, e.g., see [20, 67, 86], that inhibin inhibits FSH synthesis. However, its mode of action has not been determined definitively but may involve competition with activin (which stimulates FSH) for the activin receptor or may bind with its own receptor (Robertson *et al.* [64]). Biological evidence indicates that this process of FSH suppression requires a significant time lag which is species-specific. For instance, it has been

observed that, *in vitro*, inhibin suppresses FSH synthesis in bovine (Franchimont *et al.* [20]) and ovine (Scott and Burger [67]) pituitary cells with a time lag of up to 72 hours. *In vivo* experiments with rhesus monkeys by Ramaswamy *et al.* [59] reported FSH suppression with a time delay of about 48 hours but, in rats, Robertson *et al.* [63] observed only a 4-8 hour delay. In menstrual cycle "time-lagged analyses," Robertson *et al.* [62] computed a negative correlation between inhibin and FSH follicular phase data 72 hours later. Our mathematical model requires an inhibin time delay of 36 hours to obtain a very good approximation to the clinical data of Welt *et al.* [83]. This delay is consistent with current biological evidence and may suggest hypotheses for future biological experimentation.

System (S) and (A) with the parameters in Table 3.1 and the inhibin delay has a stable periodic solution of period 28 days and this solution represents an ovulatory menstrual cycle. This periodic solution gives a very good approximation (see Figure 5.1) to the 28 day data set of Welt *et al.* [83] which contains daily average hormone values computed from blood samples of 23 normally cycling women ranging in age from 20 to 34 years. Because of various intrinsic and extrinsic factors, it is highly unlikely that the cycle length of an individual woman will be always 28 days or that her cycle will be exactly periodic even for a short span of time. The extensive study of Treloar *et al.* [78] indicated wide variation in inter-person and intra-person cycle length. In fact, a recent dynamical systems analysis (Derry and Derry [13]) of cycle length data over a 20 year span suggested that the menstrual cycle should be described by a chaotic dynamical system. Also, apparent quasi-periodic behavior [65] has been exhibited by a model for the bovine estrous cycle (Boer *et al.* [5]), which has some structural similarities to our system. In spite of this variability, Treloar *et al.* [78] concluded that the "menstrual interval for many persons and covering a wide span of chronologic age should, however, be expected to average within a few days of the oft-quoted 28."

System (S) and (A) with the parameters in Table 3.1 and the inhibin delay has an asymptotically stable cycle of period 28 days instead of 26 days for the no-delay model [68]. The LH data indicates a 14 day follicular phase and the position and height of the LH surge for the delay model is consistent with that (see Figure 5.1). Also, the delay E_2 follicular and luteal peaks are higher than E_2 for the no-delay model. To understand from a mathematical point of view why the inhibin delay is responsible for these differences we examine hormone profiles and ovarian stages for both models over three carefully chosen consecutive cycles. MATLAB simulations of both models were run with the following initial conditions (rounded to two decimal places) given in the order of the 13 state variables in (S), {29.65, 6.86, 8.47, 6.15, 3.83, 11.51, 5.48, 19.27, 45.64, 100.73, 125.95, 135.84, 168.71}. The simulations were aligned so that both delay and no-delay periodic orbits are as close to one another as possible at the beginning of their second cycle, indicated by the vertical line at day 29 in Figures 5.1, 5.2 and 5.3. This was done so that the point of our comparison would be the second cycle in these figures and the

preceding cycle would also be plotted because hormone profiles during the luteal phase of the preceding cycle influence behavior in our comparison cycle.

The key feature to observe in Figure 5.2 is that the no-delay FSH (red curve) is higher than the delay FSH from day 19 until day 34, which includes the first six days of the follicular phase of our comparison cycle. Since FSH stimulates follicular development, the no-delay ovarian stages of the second cycle increase sooner than the delay ovarian stages and the no-delay cycle is advanced ahead of the delay cycle (see Figure 5.3). No-delay FSH is higher because delay Inh has a greater inhibitory effect than no-delay Inh on FSH synthesis (see (S3)) during that period. Delay Inh (green curve) is greater than no-delay Inh from day 15 to day 22 where the curves cross and then both curves decrease in parallel until day 33.5. These Inh curves are so close to one another (see Figure 5.2) from day 22 to day 33.5 that the delay of 1.5 days results in delay $Inh(t-1.5)$ being greater than no-delay $Inh(t)$ for this time interval. In fact, model simulations indicate that delay $Inh(t-1.5)$ is greater than no-delay $Inh(t)$ for $14.5 \leq t \leq 33.5$. Effectively, for this interval of 19 days, the synthesis of delay FSH is suppressed more than the synthesis of no-delay FSH. This causes the no-delay follicles to develop sooner than the delay follicles with the consequence via (A1) that no-delay E_2 rises sooner (see Figure 5.1). Since E_2 inhibits FSH release (see (S3-S4)), this earlier rise in E_2 tends to decrease no-delay FSH sooner than delay FSH with the result that the no-delay follicular stages develop to a lesser extent than the delay stages (Figure 5.3). Also, because E_2 promotes LH synthesis, the LH surge is earlier and smaller for the no-delay model (Figure 5.1). The cumulative effect of these profile differences is a shortening of the no-delay cycle length by 2 days and a reduction in no-delay hormone peaks.

The differences between the no-delay system and the delay system hormone profiles is similar to the observed hormone changes that occur in older reproductive women, e.g., see Welt *et al.* [83], Klein *et al.* [38] and Hale *et al.* [25]. After age 35 a decrease in the number of follicles results in a decrease in inhibin and a consequential earlier follicular rise in FSH and E2 and reduced cycle length as compared to younger women. Hence, the timing and serum concentration of inhibin appear to have significant effects on ovarian development during the follicular phase of the cycle.

Inhibin, secreted by the ovaries, is responsible for inhibiting FSH synthesis in the pituitary. There is evidence that this process of FSH suppression requires significant time lag [20, 59, 67]. Including an inhibin delay in our model improves the model fit to the daily hormone data from Welt *et al.*. The effect of this delay on the model is an increased and delayed effect of inhibin on FSH production in the luteal and early follicular phases, which results in suppressed FSH synthesis and a longer and more fully developed follicular phase.

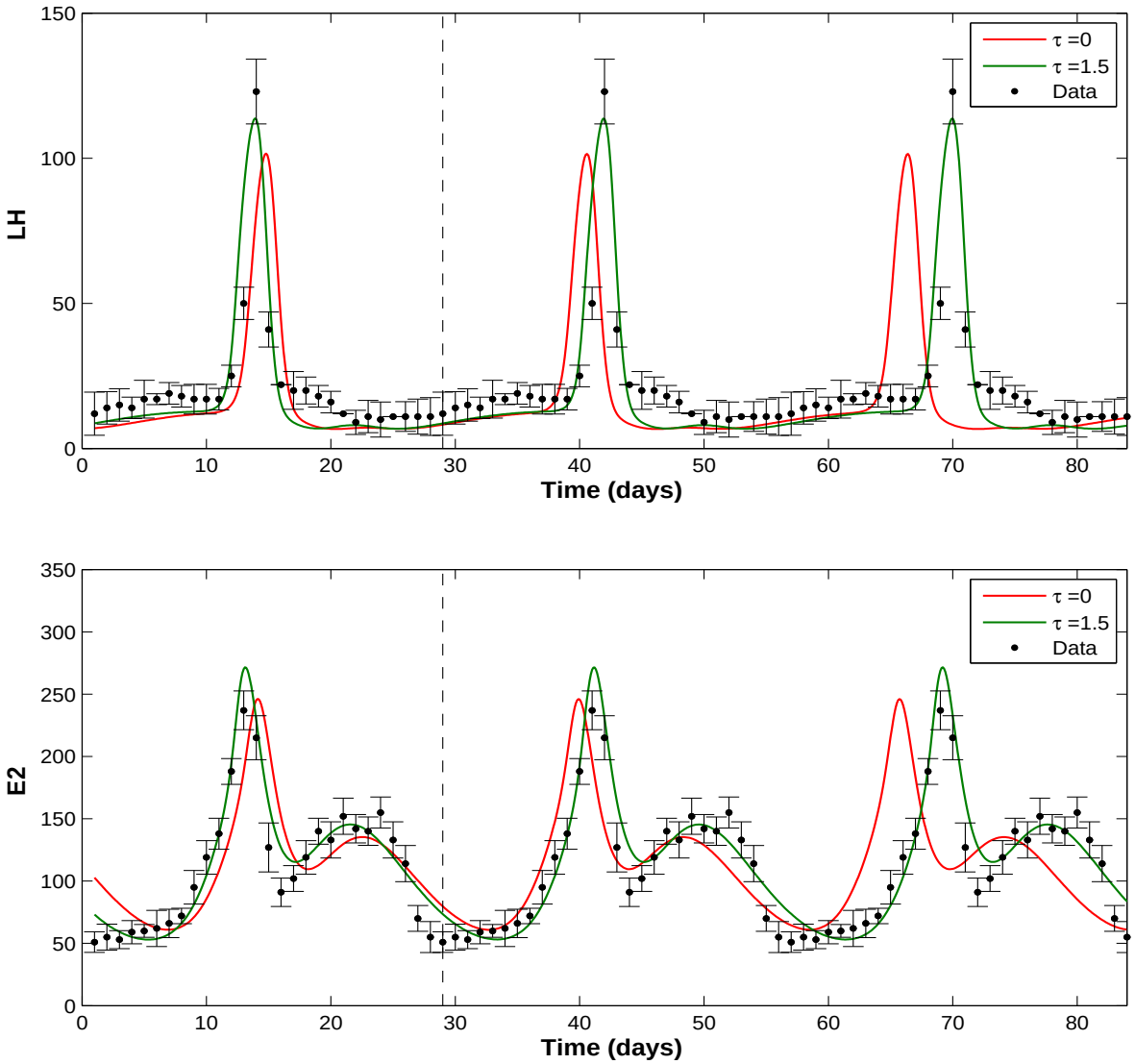

Figure 5.1: LH and E_2 simulations for 3 cycles of the Welt model with inhibin delay τ of 1.5 days (green curves) and no delay (red curves) with data points (84 black dots, mean $\pm$ SD) corresponding to the 28 day data from Welt et al. [83] plotted 3 times. The vertical dashed line indicates day 29, where the second cycle begins and where both solution orbits are very close to one another.

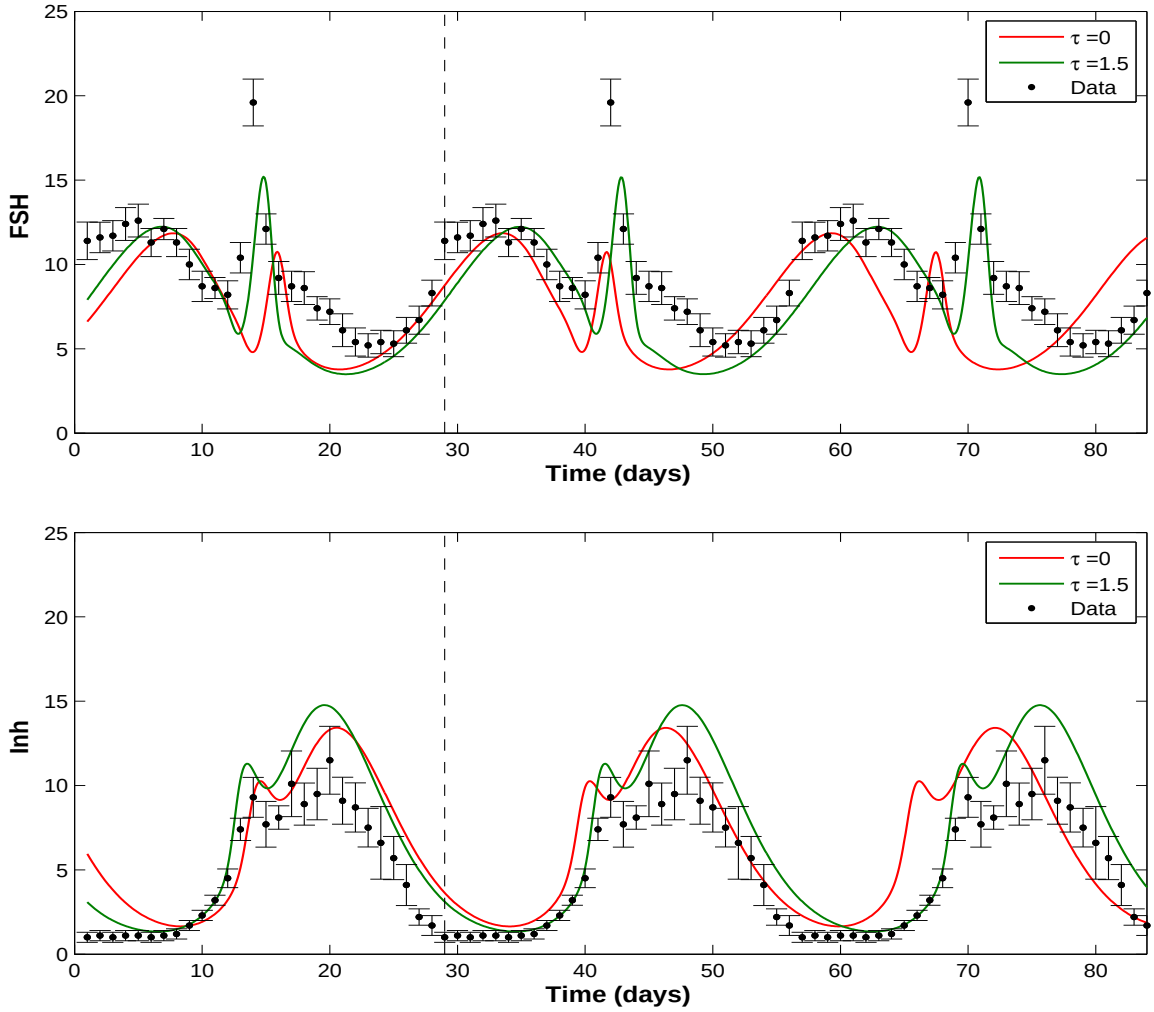

Figure 5.2: FSH and Inh simulations for 3 consecutive cycles of the delay model (green curves) and the no-delay model (red curves) with 84 data points (black dots, mean ± SD) from Welt et al. [83]. The vertical dashed line indicates day 29, the beginning of the second cycle. From day 14.5 to day 33.5 the synthesis of delay FSH is suppressed more than the synthesis of no-delay FSH because of inhibin differences.

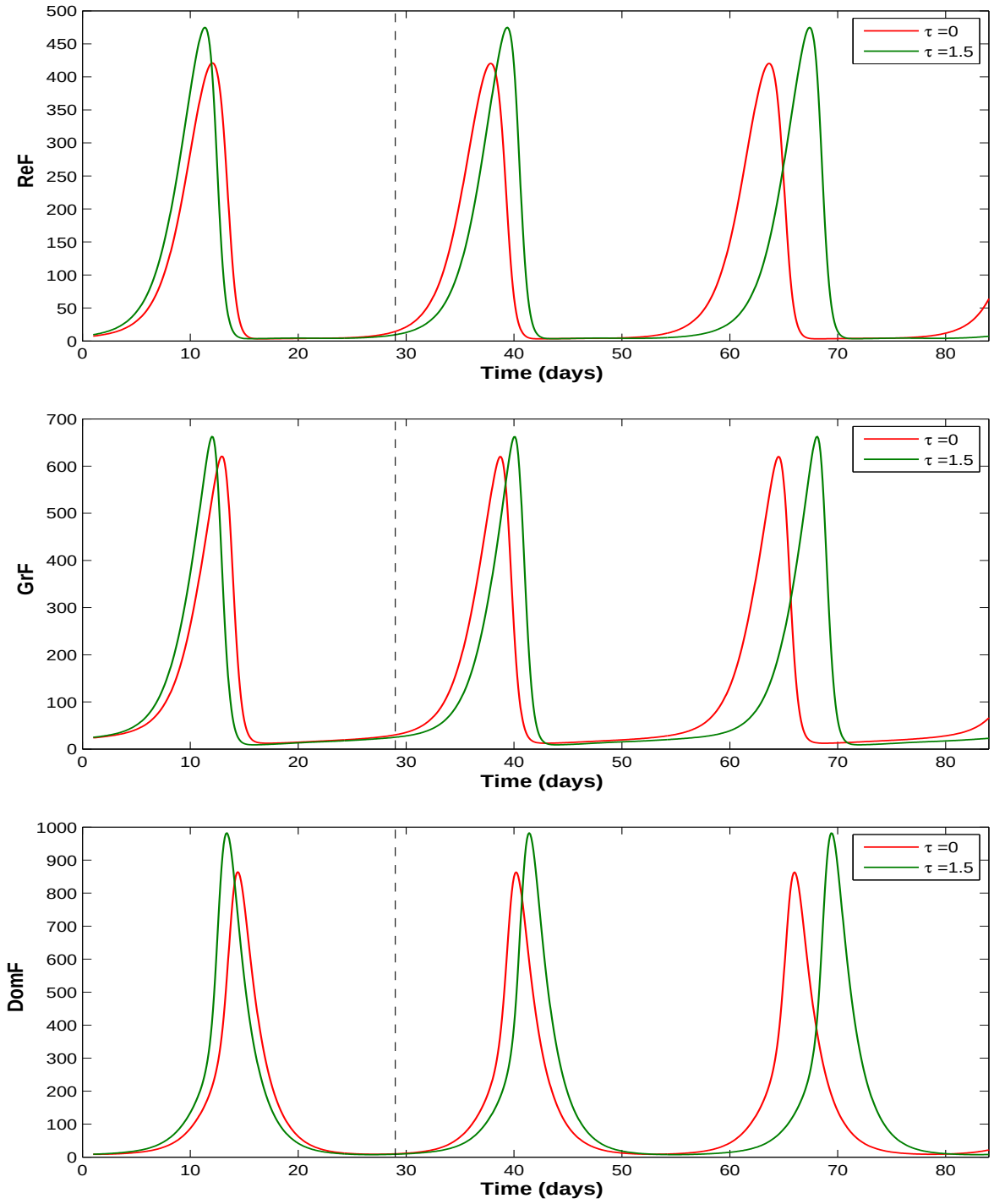

Figure 5.3: First 3 ovarian stages ReF, GrF and $DomF$ for 3 consecutive cycles of the delay model (green curves) and the no-delay model (red curves). Notice the no-delay stages of the 2nd cycle develop sooner and to a lesser extent than the delay stages because of an earlier rise and fall of FSH.

5.3 Cycle uniqueness interval

The parameters Km_{LH} and c_2 are two of the three most sensitive parameters when sensitivity is measured with respect to the E_2 follicular peak as system output [57, 69]. This E_2 peak is chosen as system output because a significant follicular E2 level is necessary for the LH surge to occur. The parameter Km_{LH} is the half-saturation constant in the Hill function in (S1), $\frac{V_{1,LH}\, E_2^8}{Km_{LH}^8 + E_2^8}$. This sigmoidal shaped function (see Figure 5.4) acts like a threshold for the synthesis of LH in response to E_2 blood levels. Once E_2 concentration reaches the value Km_{LH}, half way up the sigmoid as indicated by the dashed line in Figure 5.4, then the pituitary is synthesizing LH in large amounts, which is necessary for ovulation. For larger values of Km_{LH}, E_2 must reach a higher level to produce the same LH synthesis rate. Because higher follicular E2 levels may suggest a greater probability of abnormal cycling [68, 69], we construct bifurcation diagrams where LH is plotted against the parameter Km_{LH} to determine the number of stable cycles for a given Km_{LH} value and to determine LH surge height along each cycle. When similar bifurcation diagrams were drawn for the no-delay model [68], an interval of Km_{LH} values was observed for which a unique stable periodic solution existed and it represented an ovulatory cycle. The length of this cycle uniqueness interval varied as the parameter c_2 was changed [68]. The present study reveals that these uniqueness intervals are larger for the model with inhibin delay, (A) and (S), as indicated in Table 5.1.

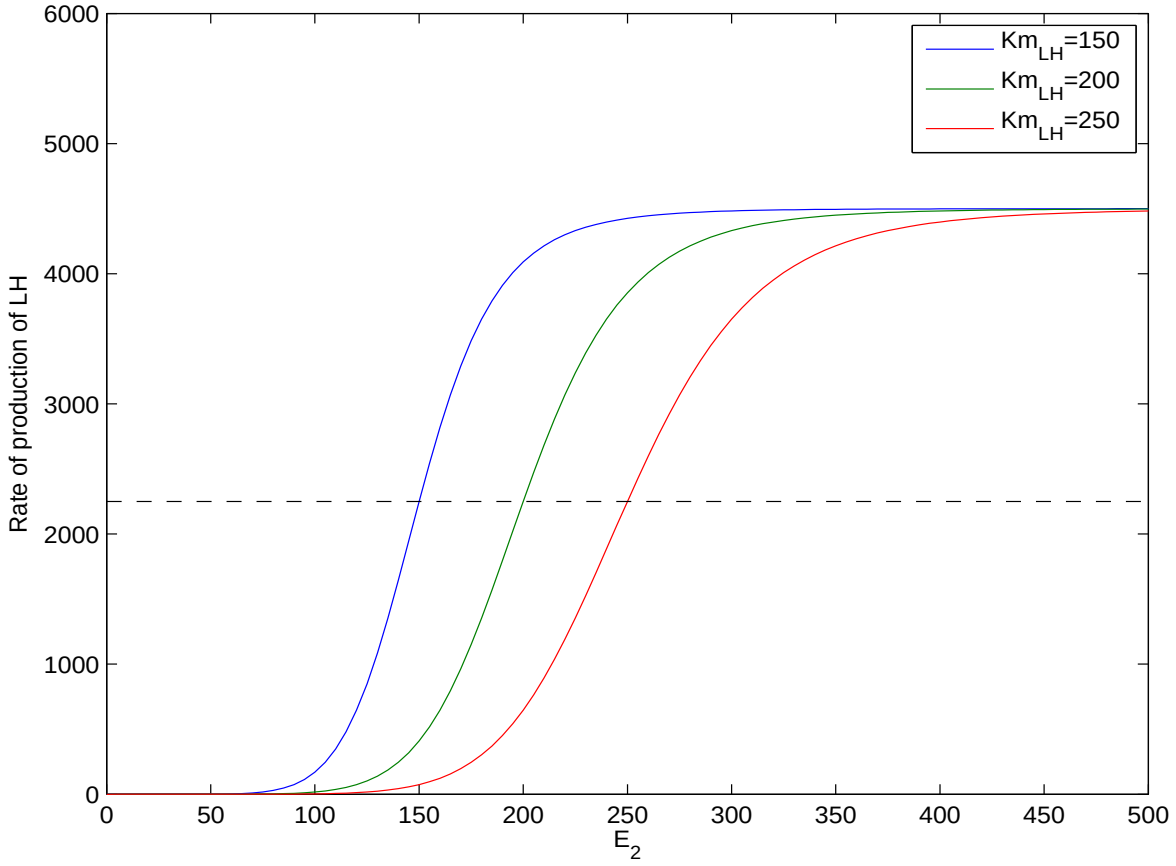

Figure 5.4: Graphs of Hill functions, $(V_{1,LH}\, E_2^8)/(Km_{LH}^8 + E_2^8)$, for three values of Km_{LH}. The dashed line indicates the synthesis rate when $E_2 = Km_{LH}$, half-saturation.

Here, the software DDEBIFTOOL [18] is used to construct bifurcation diagrams where the maximal LH value along a periodic solution or at a steady-state solution is plotted against the parameter Km_{LH}. Figure 5.5 displays the bifurcation diagram where the remaining parameters are those in Table 3.1. For the MATLAB code used to generate this bifurcation diagram, see Appendix C. Stable and unstable periodic orbits and equilibria are depicted. Saddle-node (SN) and Hopf (HB) bifurcations are labeled. For a review of these and other basic bifurcations, see Appendix B. The curve along the lower portion of Figure 5.5 tracks an equilibrium, which undergoes a supercritical Hopf bifurcation as Km_{LH} increases through 64 and another supercritical Hopf bifurcation at $Km_{LH} = 248$. A supercritical Hopf bifurcation is when a stable periodic solution comes out of the de-stabilization of an equilibrium, as opposed to a subcritical Hopf bifurcation in which an unstable periodic solution emerges from the stabilization of an equilibrium [51]. The bifurcation at $Km_{LH} = 64$ results in a small amplitude, stable, periodic orbit which persists until $Km_{LH} = 73$. Stable and unstable cycles appear together at $Km_{LH} = 68$ via a saddle-node bifurcation of periodic orbits. The unstable orbit coalesces with the small amplitude stable Hopf orbit at $Km_{LH} = 73$ and both disappear in another saddle-node. The stable cycle appearing at $Km_{LH} = 68$ grows in amplitude, continues across the top portion of the diagram and disappears in a saddle-node at $Km_{LH} = 282$. This branch of periodic solutions represents the ovulatory cycles of the model (S) with (A), where the $*$ indicates the cycle corresponding to the Km_{LH} value of Table 3.1, 200 pg/ml. Analogous behavior occurs at the right side of the bifurcation diagram where the hysteresis character of the curve of periodic orbits is evident. Clearly, for Km_{LH} from 227 to 282 there is a stable, large amplitude ovulatory cycle and a stable, small amplitude non-ovulatory cycle or stable equilibrium. Figure 5.6 plots LH and E_2 solution profiles for the stable ovulatory, unstable, and stable anovulatory cycles at $Km_{LH} = 240$. For Km_{LH} in the interval between the lower SN's in Figure 5.5 ($73 < Km_{LH} < 227$), there is only one stable cycle and it is ovulatory. Selgrade [68] referred to this Km_{LH} interval as the cycle uniqueness interval. In the context of this cycle regulation model, a woman's Km_{LH} parameter must fall within her cycle uniqueness interval for her to be assured of only a normal cycle. From Figure 5.5, we observe that decreasing Km_{LH} from 200 pg/mL keeps it within the interval and increases the height of the LH surge. However, increasing Km_{LH} to 227 moves Km_{LH} to a region of multiple stable cycles and possible non-ovulation. For $c_2 = 0.07$, the diameter of this cycle uniqueness interval is 154 for the delay model and only 114 for the no-delay model (see Table 5.1).

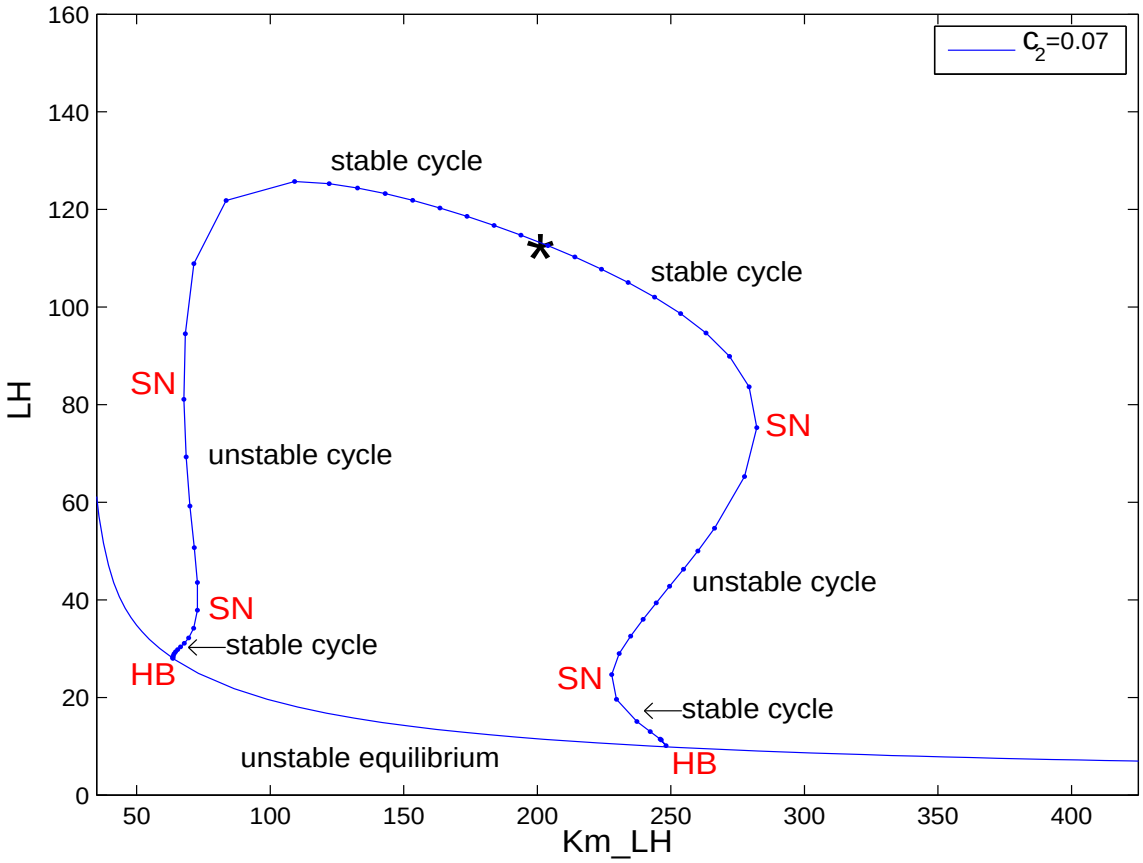

Figure 5.5: In this bifurcation diagram the maximal LH value along a periodic solution or at an equilibrium is plotted against Km_{LH} when $\tau = 1.5$ and $c_2 = 0.07$. HB and SN denote Hopf and saddle-node bifurcations. The $*$ indicates the position of the cycle for the parameters of Table 3.1 and this cycle is the only stable solution at $Km_{LH} = 200\,\mathrm{pg/mL}$. The cycle uniqueness interval is the interval between the lower saddle-nodes, i.e., $73 < Km_{LH} < 227$.

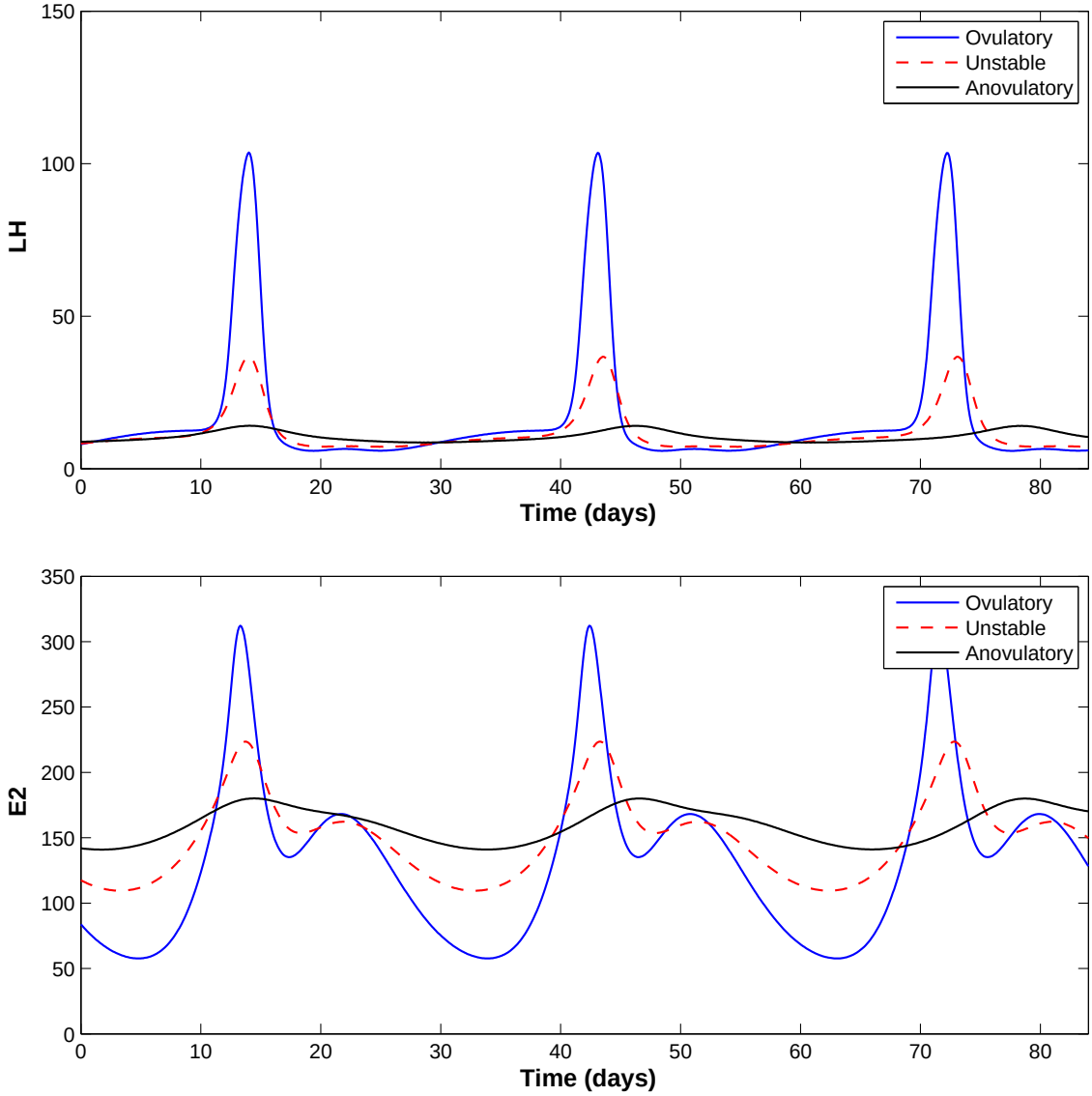

Figure 5.6: Stable ovulatory (blue), unstable (dashed red), and stable anovulatory cycles (black) simulations for LH (top) and E_2 (bottom) corresponding to $Km_{LH} = 240\,\text{pg/mL}$ are plotted against time for three cycles. The decreased mid-cycle E_2 in the anovulatory cycle signifies that a dominant follicle has not emerged. The absence of an LH surge in the anovulatory cycle corresponds to a lack of ovulation.

Table 5.1: Size of cycle uniqueness interval for inhibin delay $\tau = 0$ (column 2) and $\tau = 1.5$ days (column 4) for increasing values of c_2. $c_2 = 0.07$ and $Km_{LH} = 200$ pg/mL give the best fit to data.

c_2	size ($\tau = 0$)	Km_{LH} bounds ($\tau = 0$)	size ($\tau = 1.5$)	Km_{LH} bounds ($\tau = 1.5$)
0.03	126	$147 < Km_{LH} < 273$	271	$40 < Km_{LH} < 311$
0.04	50	$181 < Km_{LH} < 231$	226	$44 < Km_{LH} < 270$
0.05	81	$153 < Km_{LH} < 234$	173	$85 < Km_{LH} < 258$
0.06	118	$122 < Km_{LH} < 230$	167	$80 < Km_{LH} < 247$
0.07	114	$98 < Km_{LH} < 212$	154	$73 < Km_{LH} < 227$
0.08	102	$84 < Km_{LH} < 186$	141	$63 < Km_{LH} < 204$

For the no-delay model, Selgrade [68] investigated how variations in the ovarian transfer parameter c_2 changed the size of the cycle uniqueness interval. Increasing c_2 from $c_2 = 0.07$ causes an increased transfer of mass from the first follicular stage ReF to the second stage GrF which diminishes the development of not only ReF but of all subsequent ovarian stages. Effectively, ovarian hormone production is reduced and the cycle uniqueness interval is decreased for both delay and no-delay models. For a biological interpretation, we conjecture that too large a c_2 parameter stunts the growth of small recruited follicles and results in diminished ovarian mass during the follicular phase. However, ovulation may still occur. Table 5.1 lists the cycle uniqueness intervals for various values of c_2 which we compute for the delay model ($\tau = 1.5$) and which were reported in [68] for the no-delay model ($\tau = 0$). Decreasing c_2 from 0.07 in increments of 0.01 widens the cycle uniqueness interval for the delay model but shrinks it for the no-delay model until $c_2 = 0.03$. This is an important difference between the delay and the no-delay models and indicates a certain amount of biological inexplicability in the no-delay model. Mathematically, for the no-delay model as c_2 decreases, the cycle uniqueness interval shrinks because the hysteresis curves enlarge and the Hopf points move closer together resulting in a narrowing of the gap between the lower two saddle-nodes. Then, as described in [68], an unfolding of a transcritical bifurcation occurs as c_2 decreases through 0.0305 and this results in the disappearance of the left hysteresis curve and a rapid expansion of the cycle uniqueness interval (see Table 5.1 for $\tau = 0$, $c_2 = 0.04$ and $c_2 = 0.03$). In contrast, for the delay model, decreasing c_2 from 0.07 causes the hysteresis curves to enlarge only slightly (compare Figures 5.5 and 5.7) and the Hopf points to move apart. Instead of disappearing due to a transcritical bifurcation, the left hysteresis curve in the delay bifurcation diagram disappears due to two degenerate Hopf bifurcations described below. The uniqueness interval for $\tau = 1.5$

when $c_2 = 0.03$ (Figure 5.8) is over twice as large as that for the no-delay model. The inhibin delay ($\tau = 1.5$) and the additional growth of the first follicular stage (smaller c_2) result in a large interval of Km_{LH} values where there is a unique ovulatory menstrual cycle.

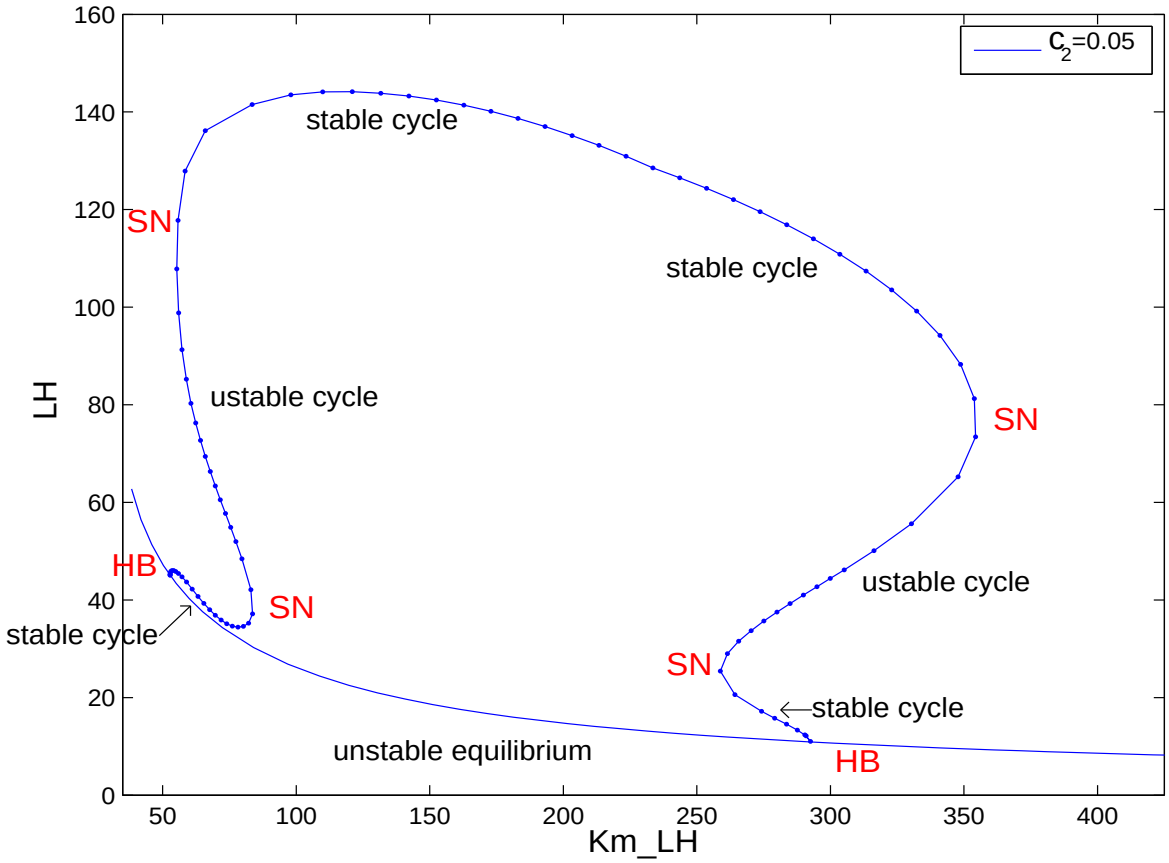

Figure 5.7: Bifurcation diagram with respect to Km_{LH} when $\tau = 1.5$ and $c_2 = 0.05$. HB and SN denote Hopf and saddle-node bifurcations. The length of the cycle uniqueness interval is 173, i.e., $85 < Km_{LH} < 258$.

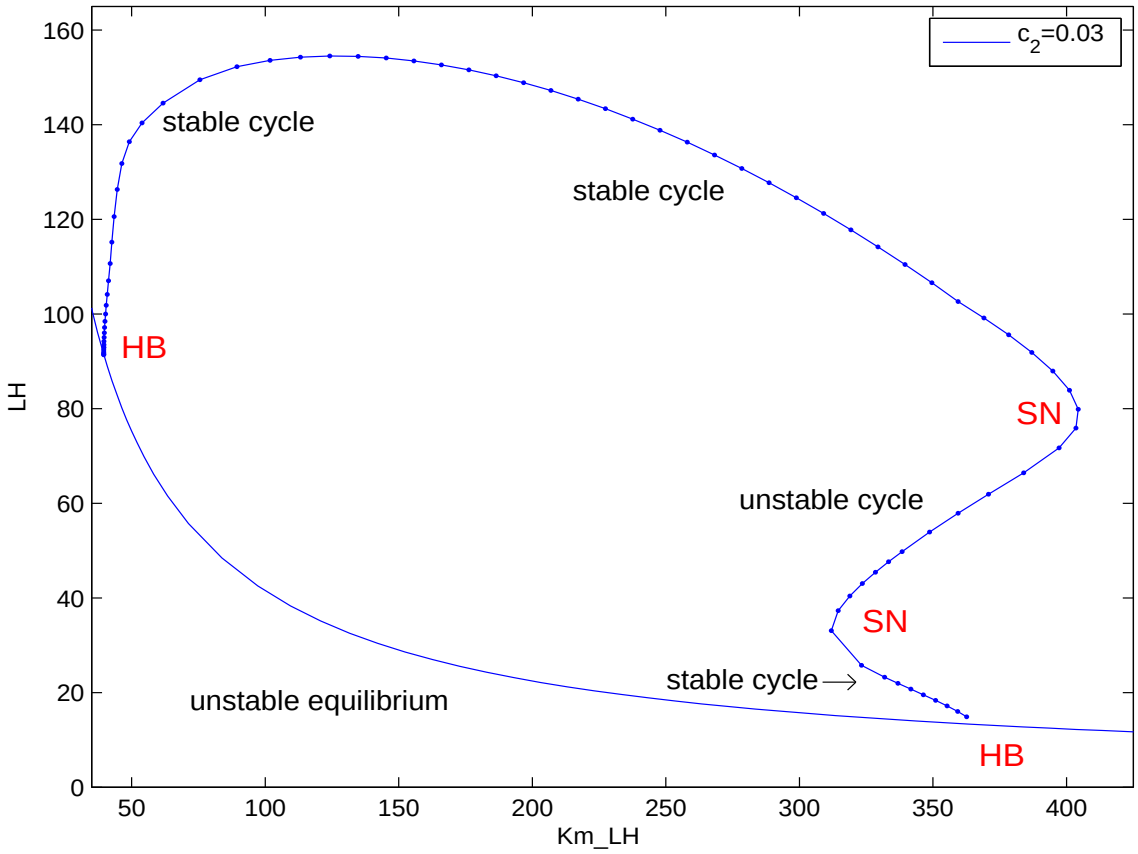

Figure 5.8: Bifurcation diagram with respect to Km_{LH} when $\tau = 1.5$ and $c_2 = 0.03$. HB and SN denote Hopf and saddle-node bifurcations. The left hysteresis curve has disappeared and the length of the cycle uniqueness interval is 271, i.e., $40 < Km_{LH} < 311$.

The broad expansion of the cycle uniqueness interval for c_2 less than 0.05 is due to two different unfoldings of degenerate Hopf bifurcations which occur for c_2 near 0.05. Each Hopf bifurcation is degenerate because the real part of the eigenvalue pair crossing the imaginary axis has a zero derivative with respect to the parameter at crossing. One of these degeneracy occurs when two Hopf points coalesce at $c_2 = 0.05147$ and $Km_{LH} = 69.8458$. At $c_2 = 0.05$, the left side of Figure 5.7 displays a branch of stable cycles lying just above a branch of unstable equilibria. Figure 5.9(a) blows these curves up at $c_2 = 0.051$. They touch when $c_2 = 0.05147$ producing a degenerate Hopf point. Then as c_2 increases, the degenerate Hopf point separates into two nondegenerate, supercritical Hopf points with stable equilibria in between them pictured at $c_2 = 0.0516$ in Figure 5.9(b). As discussed in Golubitsky and Schaeffer [22], p. 375, the unfolding of this bifurcation may be described roughly by the equation

$$-x^3 + (Km_{LH} - 69.8458)^2\, x + (0.05147 - c_2)\, x = 0 \qquad \text{(DegHB1)}$$

where x represents the state variable LH and the line $\{x = 0\}$ represents the curve of equilibria. As c_2 continues to increase above 0.052, the two Hopf points on the left in Figure 5.10(a) coalesce in a second degenerate Hopf point at $c_2 = 0.05209$ and $Km_{LH} = 61.0174$ and that Hopf point disappears for $c_2 > 0.05209$. The unfolding of this bifurcation may be represented by the equation (see [22])

$$x^3 + (Km_{LH} - 61.0174)^2\, x + (c_2 - 0.05209)\, x = 0\,. \qquad \text{(DegHB2)}$$

As c_2 increases above 0.05209, the saddle-nodes which determine the cycle uniqueness interval move closer together causing the interval to shrink and move to the left, see Table 5.1.

As c_2 increases from 0.04 to 0.045, the left hysteresis curve forms because of the appearance of a kink and two saddle-nodes along the left edge of the large loop of periodic solutions. Bifurcation diagrams for c_2 values of 0.04, 0.045, 0.05 and 0.055 are plotted in Figure 5.11. The kink occurs between $c_2 = 0.04$ and $c_2 = 0.045$ (top two frames) and the two degenerate Hopf unfoldings (DegHB1 and DegHB2) occur between $c_2 = 0.05$ and $c_2 = 0.055$ (bottom two frames).

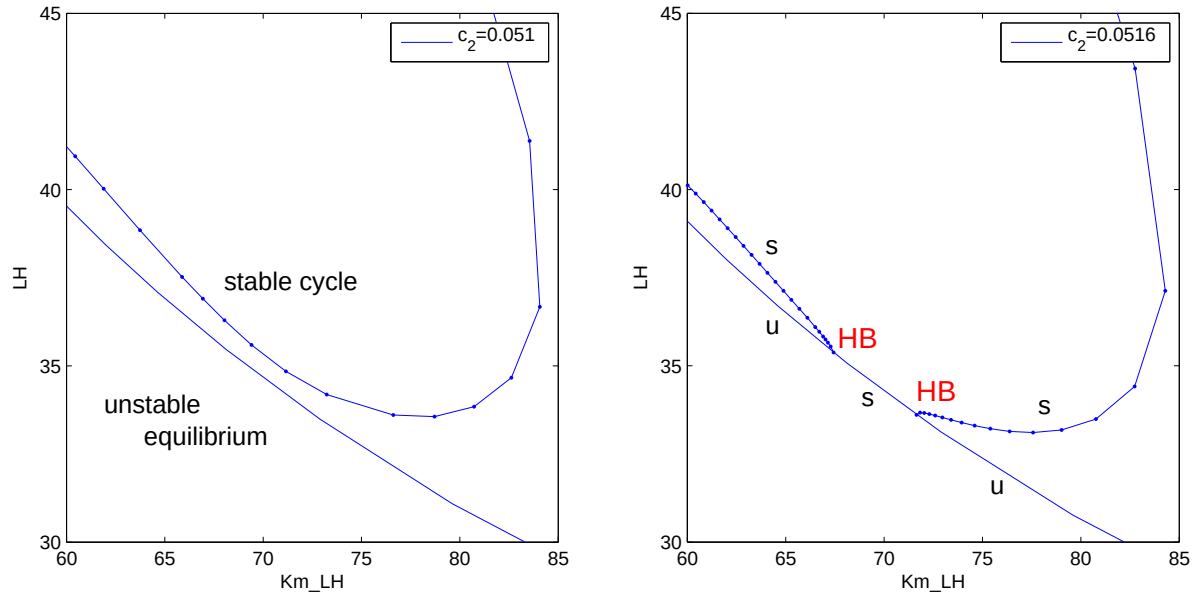

Figure 5.9: (a): Blow up for $c_2 = 0.051$ (b): Blow up for $c_2 = 0.0516$
s indicates a stable and u, an unstable cycle or equilibrium. HB denotes a Hopf point.

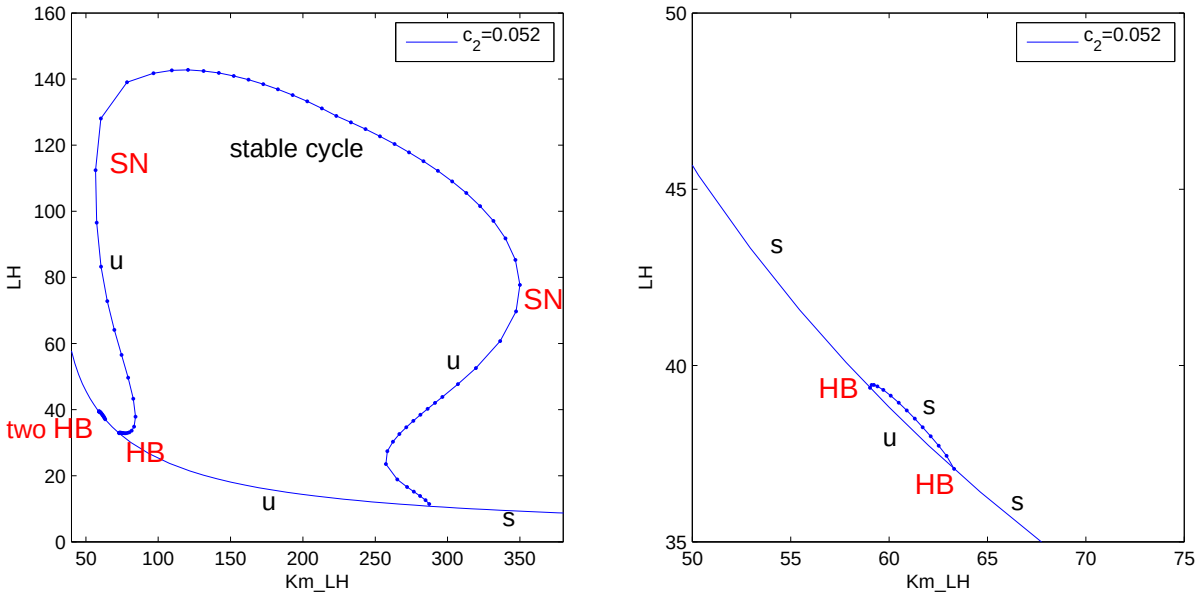

Figure 5.10: (a): $c_2 = 0.052$ (b): Blow up of "two HB" for $c_2 = 0.052$
s indicates stable and u indicates unstable. HB denotes a Hopf point.

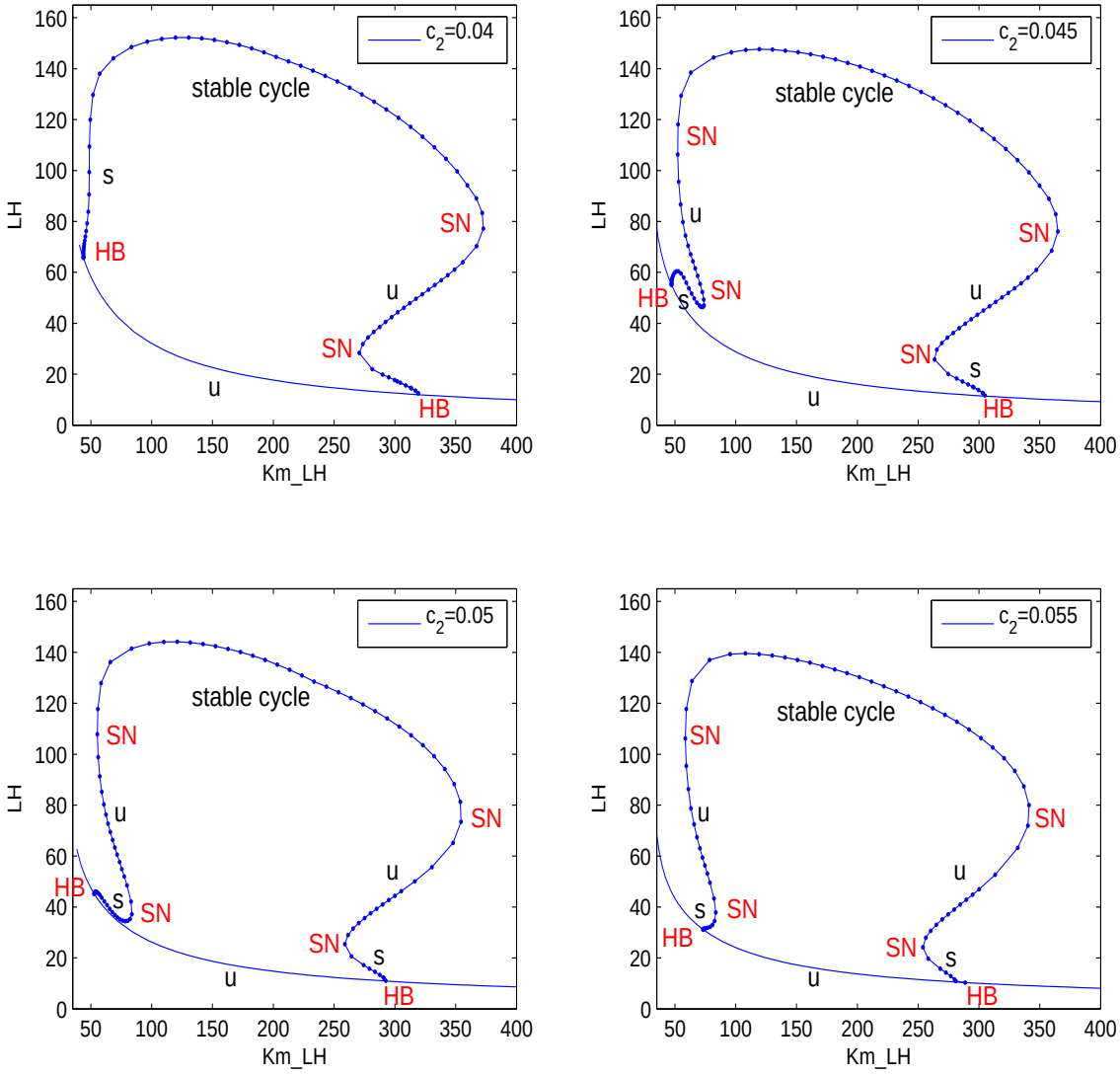

Figure 5.11: Bifurcation diagrams with respect to Km_{LH} for $\tau = 1.5$ as c_2 increases from 0.04 to 0.055 by increments of 0.005. A kink appears in the large loop at the left and bends to touch the curve of equilibria causing a degenerate Hopf bifurcation. s indicates stable and u indicates unstable.

5.4 Comparing bifurcation diagrams as delay τ varies

For all c_2 values in Table 5.1, the delay model has a larger cycle uniqueness interval than the no-delay model. As discussed previously, when $Km_{LH} = 200$ and $c_2 = 0.07$ the delay in the effect of inhibin on FSH results in more vigorous growth of ovarian stages, a longer cycle and higher hormone peaks. Numerical simulations indicate that this is also true after reasonable variations in both model parameters, Km_{LH} and c_2. It is conceivable that the more robust ovarian development of the delay model permits a broader range of half-saturation constants Km_{LH} for the successful surge response of LH to E_2 priming and, hence, a larger cycle uniqueness interval. Bifurcation diagrams for various values of τ support this suggestion.

First we fix $c_2 = 0.07$, which is the parameter value fitting the data best (see Table 3.1). We draw bifurcation diagrams with respect to Km_{LH} to study how the cycle uniqueness interval opens up as the delay τ increase from 0 to 1.5. Figure 5.12 illustrates these diagrams for τ values increasing from $\tau = 0$ to $\tau = 1.5$ by increments of 0.5. As τ increases the Hopf points (HB) along the curve of equilibria spread apart as do the saddle-nodes (SN), which determine the cycle uniqueness interval. The qualitative features of these diagrams are similar. In particular, there are hysteresis curves on both the left and right edges of a large loop of periodic solutions. The hysteresis curves give rise to two regions of periodic bistability.

For other values of c_2, these two hysteresis curves do not persist for all values of τ. For instance, if $c_2 = 0.04$ then the hysteresis curve on the left disappears as τ increases. The cycle uniqueness interval enlarges from 50 when $\tau = 0$ to 226 when $\tau = 1.5$. The primary reason for this drastic increase is a sequence of bifurcations that occur as τ increases from 0.7 to 1.2. A degenerate Hopf bifurcation similar to that described by (DegHB2) occurs at $\tau = 0.73$ resulting in a bump of stable cycles to the left of the large loop of periodic solutions as pictured in Figure 5.13. This Hopf bump of stable solutions is just below the branch of unstable cycles in the left hysteresis curve and, as τ increases, this bump grows and touches the curve of cycles above producing a transcritical bifurcation of periodic solutions in the parameter Km_{LH} when $\tau = 1.06$. The unfolding of this transcritical bifurcation is analogous to that discussed in [68] except here the second parameter is τ instead of c_2. For τ values just above 1.06 the bump of stable cycles appears on the other side of the large loop of cycles (see Figure 5.13) and disappears via the following sequence of bifurcations. At $\tau = 1.11$ a degenerate Hopf bifurcation like (DegHB1) causes the Hopf bump to separate from the curve of equilibria producing a small closed loop of periodic solutions (Figure 5.14). Then this loop shrinks and disappears because the two saddle-nodes at each end of the loop coalesce and annihilate one another at $\tau = 1.173$. The unfolding of these bifurcations as τ increases from 0.7 to 1.2 is depicted in Figure 5.13 .

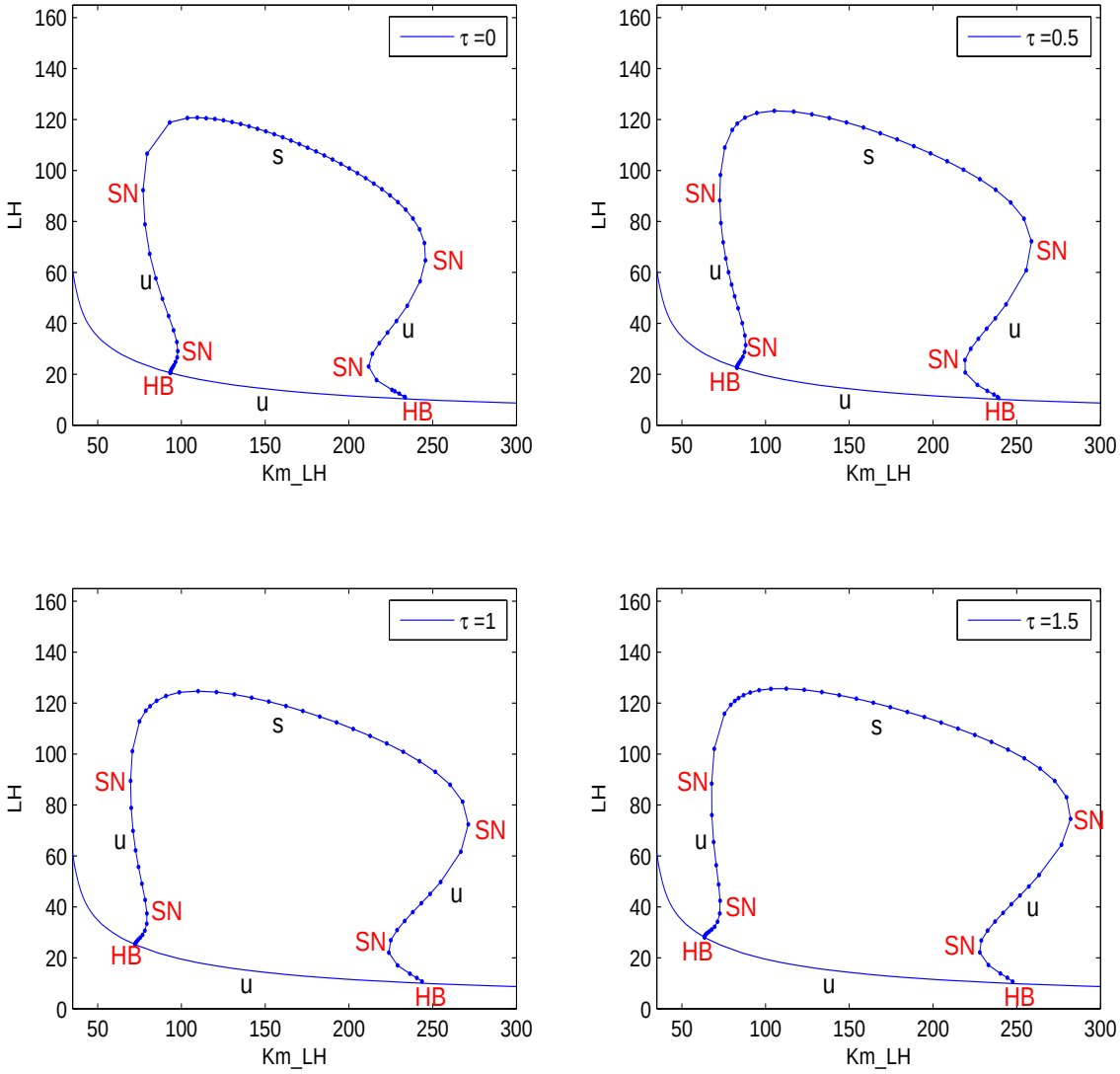

Figure 5.12: Bifurcation diagrams with respect to Km_{LH} for $c_2 = 0.07$ as τ increases from $\tau = 0$ to $\tau = 1.5$ by increments of 0.5. The cycle uniqueness interval enlarges from 114 to 154. HB and SN denote Hopf and saddle-node bifurcations. s indicates a stable and u, an unstable cycle or equilibrium.

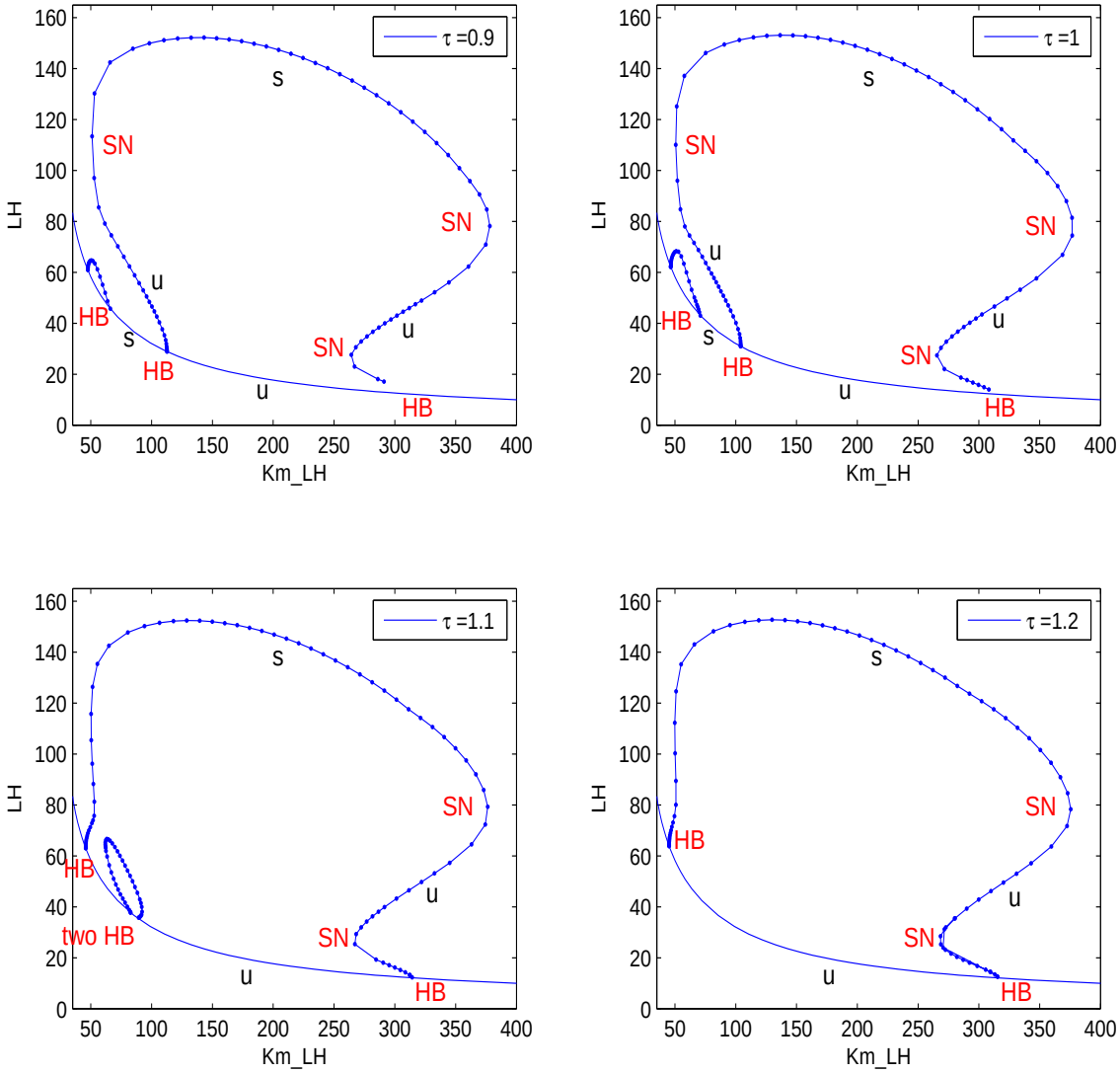

Figure 5.13: Bifurcation diagrams with respect to Km_{LH} for $c_2 = 0.04$ as τ increases from $\tau = 0.9$ to $\tau = 1.2$ by increments of 0.1. HB and SN denote Hopf and saddle-node bifurcations. s indicates a stable and u, an unstable cycle or equilibrium. Transcritical and degenerate Hopf bifurcations occur as τ increases from 0.7 to 1.2.

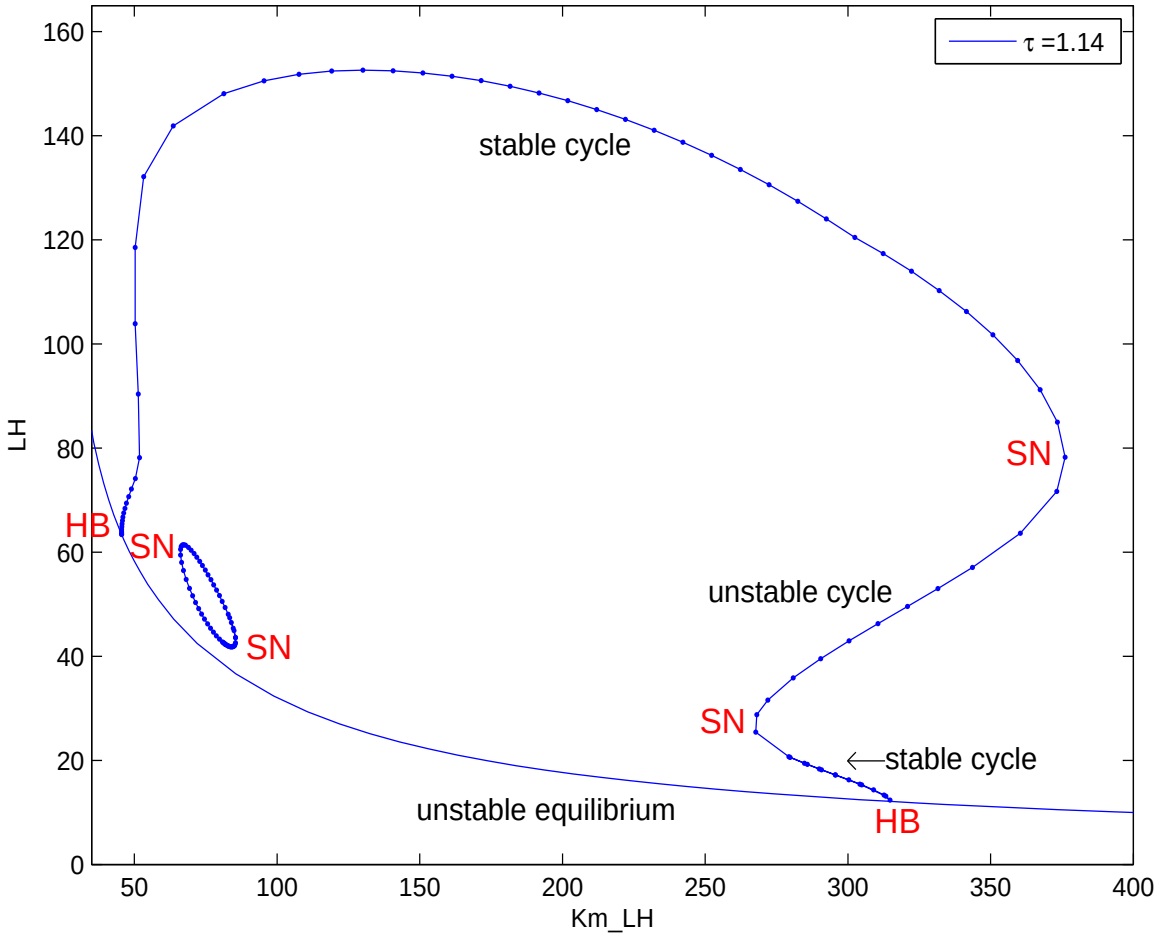

Figure 5.14: Bifurcation diagram with respect to Km_{LH} when $\tau = 1.14$ and $c_2 = 0.04$. HB and SN denote Hopf and saddle-node bifurcations. The small closed loop of cycles has saddle-nodes at each end.

The transcritical bifurcation is a prominent feature of the left side of the bifurcation diagrams for smaller values of τ. When this bifurcation is present in the diagram, the cycle uniqueness interval has reduced length, e.g., only 125 for the first frame of Figure 5.15. The transcritical bifurcation persists for the parameter pairings in Figure 5.15 until the transcritical bifurcation point coalesces with a saddle-node for $\tau \approx 1.45$. As τ increases, the cycle uniqueness interval grows although c_2 is also increasing. Hence, a larger delay in the effect of inhibin may compensate for an apparent reduction in growth of the first follicular stage of a cycle. In fact, an increase in FSH inhibition during the luteal phase of the previous cycle due to the delay in inhibin results in greater early follicular development during the next cycle (see the middle cycle in Figure 5.3).

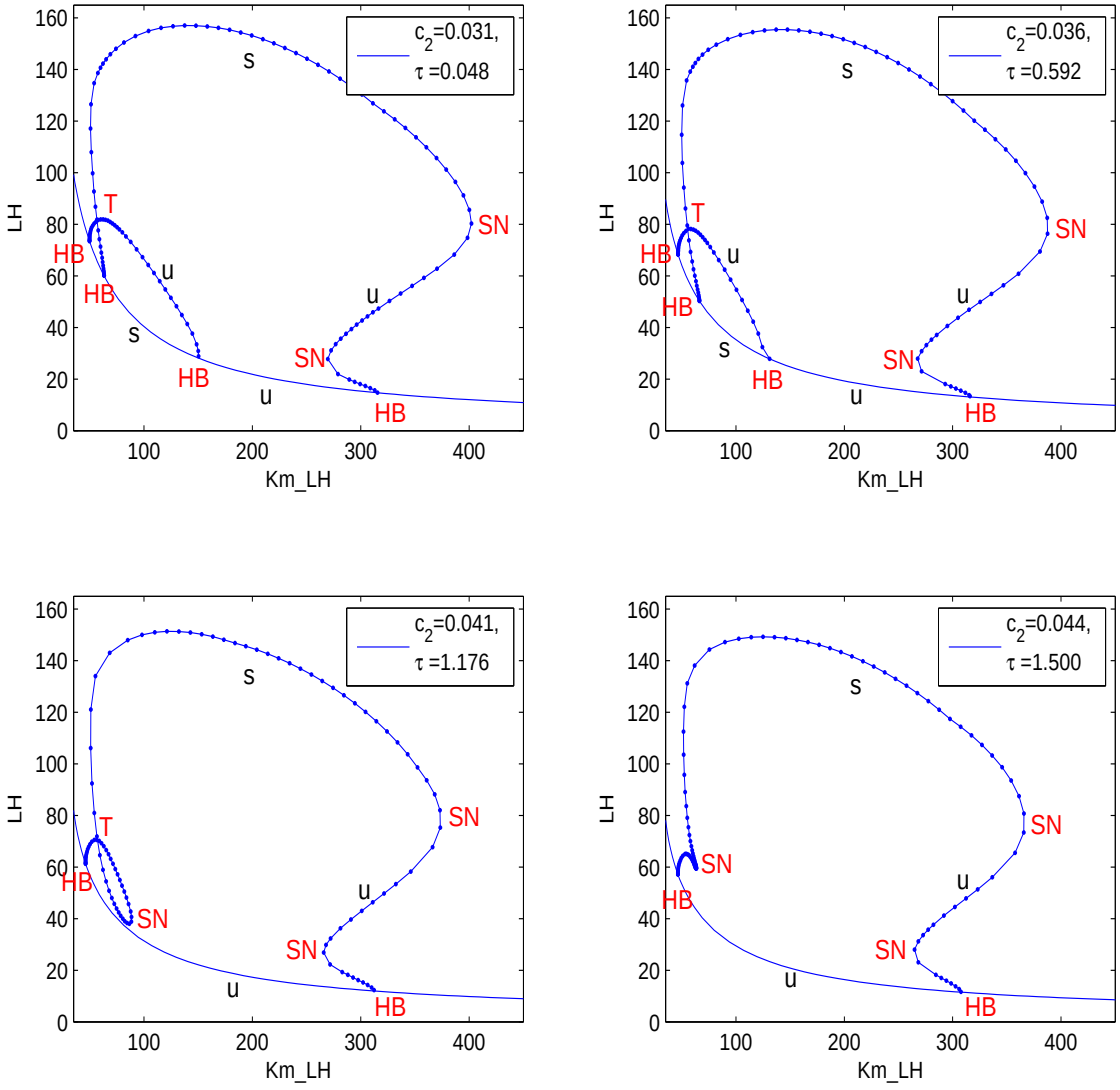

Figure 5.15: Bifurcation diagrams with respect to Km_{LH} as τ increases from 0.048 to 1.5 and c_2 increases from 0.031 to 0.044. HB, SN and T denote Hopf, saddle-node and transcritical bifurcations. s indicates a stable and u, an unstable cycle or equilibrium. As τ and c_2 increase, a loop is created in the bifurcation diagram and the cycle uniqueness interval broadens.

5.5 Summary and conclusion.

The half-saturation parameter Km_{LH} in the Hill function in (S1) indicates the level of E2 sufficient for significant LH synthesis. This chapter studies bifurcation diagrams where maximum LH along a periodic or equilibrium solution is graphed against Km_{LH}. We observe an interval of Km_{LH} values for which the model admits a unique stable periodic solution and this solution represents an ovulatory cycle. A large cycle uniqueness interval signifies a wide range of follicular E2 levels which promote a LH surge sufficient for ovulation. This cycle uniqueness interval is usually determined by two saddle-nodes bifurcations which lie on hysteresis curves at the left and right sides of the bifurcation diagram.

The parameter τ is the time delay for the inhibition of FSH synthesis caused by inhibin. In Section 5.2, we explain why a delay of 1.5 days (the value of τ fitting the data best) is consistent with biological evidence and permits increased ovarian development during the follicular phase of the cycle and a larger interval of Km_{LH} values which result in a unique cycle. The ovarian growth parameter c_2 promotes mass transfer between the first two stages of ovarian development and is indicative of healthy follicular growth. For various values of c_2, we illustrate how the cycle uniqueness interval grows as τ increases due to the occurrences of transcritical and degenerate Hopf bifurcations, e.g., see Figure 5.13. Also, for delay τ near 1.5 days, Section 5.3 asserts that the cycle uniqueness interval increases as c_2 decreases because of additional growth of the first follicular stage, which represents small antral follicles.

Model simulations and bifurcation diagrams studied here imply that parameter combinations which provide for the sustained growth of small antral follicles at the beginning of the cycle may result in a greater possibility of normal cycling.

The material in this chapter was previously published in the paper "Bifurcation analysis of a model for hormonal regulation of the menstrual cycle with inhibin delay" by Margolskee and Selgrade, 2011 [46]. We would like to thank Georgina E. Hale and Claude L. Hughes for helpful conversations and an anonymous reviewer for suggestions which improved the paper.

Chapter 6

Follicle Waves

The presence of follicle waves, or multiple maturing follicles staggered throughout the monthly cycle, has been long observed in other species. For example see Ginther *et al.* 1989 [21] on follicular waves during the bovine estrous cycle. Interestingly, recent experiments have also observed this phenomenon in women (i.e. see Baerwald *et al.* 2003 [3]). During these cycles, multiple follicles grow up out of the recruitable pool of follicles, becoming large antral follicles with the potential for ovulation. These follicles emerge in a staggered manner, maturing during different phases of the cycle. However, only the follicles that mature prior to an LH surge will experience ovulation. Follicles that mature in the absence of an LH surge, for example during a normal luteal phase when elevated P4 suppresses LH synthesis, fail to ovulate and subsequently undergo atresia.

Here we investigate follicle wave solutions to the equations of Selgrade (2010) [68], equations (S1)-(S13) (see Chapter 3). We focus on the ovarian equations (S5)-(S13), solved using time-dependent input functions for $FSH(x)$ and $LH(x)$, where $x = t \mod (28)$. These functions are approximations to data from Welt et al. (1999) [83] (see Figure 6.1).

$$\begin{aligned} FSH(x) =& 4 + 8.5\left(e^{-\frac{(x-4.5)^2}{47}} + e^{-\frac{(x-32.5)^2}{47}}\right) + 11.4e^{-\frac{(x-14)^2}{0.75}} + 4.5e^{-\frac{(x-17)^2}{20}} - 1.2e^{-\frac{(x-25.5)^2}{14}} \\ LH(x) =& 9.5 + 105.5e^{-\frac{(x-14)^2}{0.8}} + 8.5e^{-\frac{(x-7.5)^2}{35}} + 10e^{-\frac{(x-17)^2}{14}} \end{aligned}$$

6.1 Original System

Typical solutions to the system (S5)-(S7) using the time-dependent input functions for FSH and LH produce follicular profiles that each form one peak per cycle. For example see Figure 6.2, which is the solution to the system using the parameters in Table 3.1 and $c_1 = 0.0783$, and

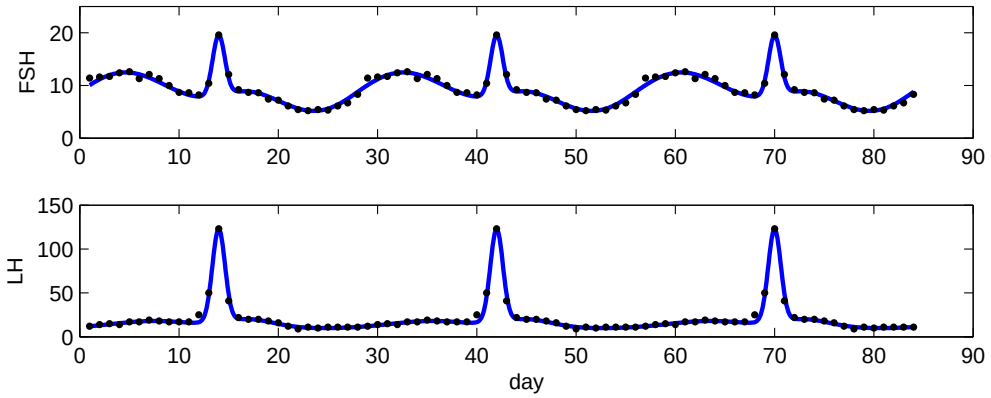

Figure 6.1: Time-dependent input functions for FSH and LH plotted against Welt data

initial conditions $ReF = 29.1731$, $GrF = 66.4904$, and $DomF = 33.9723$.

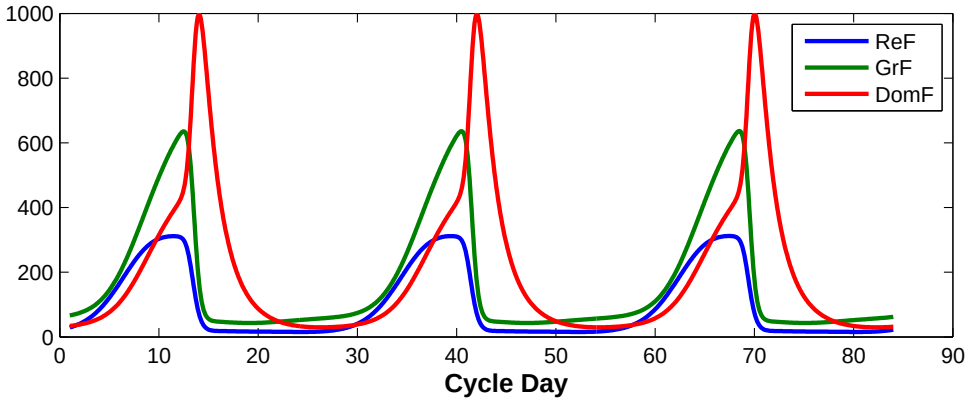

Figure 6.2: Solution to the system (S5)-(S7) with time-dependent input functions for FSH and LH, using the parameters in Table 3.1 and $c_1 = 0.0783$, and initial conditions $ReF = 29.1731$, $GrF = 66.4904$, and $DomF = 33.9723$. This solution exhibits the typical growth in the follicular phase of the cycle, with no large follicles after the LH surge (i.e. no follicle waves).

6.2 Systems with follicle waves

6.2.1 Decreasing α creates follicle waves

Follicle waves form when a recruited follicle matures to a pre-ovulatory stage during the luteal phase of the cycle. In the absence of an LH surge, this additional wave of follicles fails to ovulate. In order to capture this behavior, the transition from ReF to GrF should be less dependent upon an LH surge than the present model predicts. The decay term of ReF (and growth term of GrF) is the term $c_2\, LH^{\alpha}$. The parameters governing the transition from ReF to GrF are α, the exponent on LH in the decay term of ReF (and growth term of GrF), and c_2, the coefficient of LH^{α}. Decreasing α and increasing c_2 maintains the magnitude of the stage $DomF$, while decreasing the impact of the LH surge on recruitment from ReF to GrF. The result is a second wave of follicles in the ReF and GrF profiles following the LH surge (see Figure 6.3).

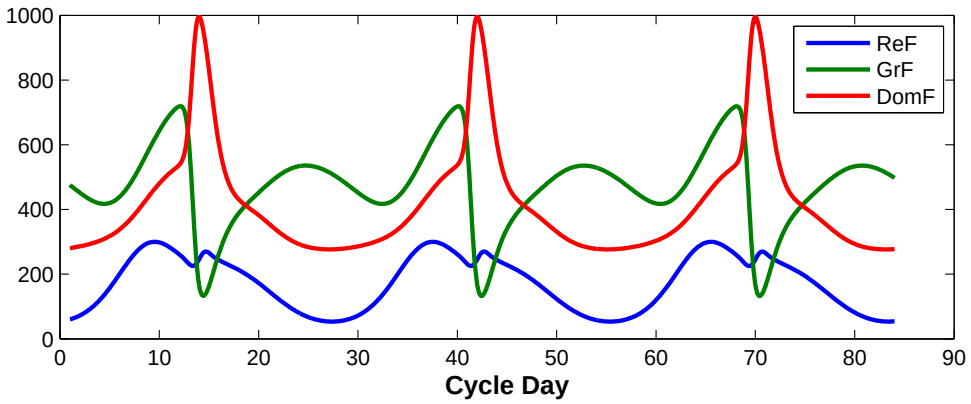

Figure 6.3: Decreasing α from 0.79 to 0.3 (and adjusting c_2 from 0.07 to 0.3084) produces a solution with follicle waves in ReF and GrF stages but not $DomF$. Plotted is the solution with initial conditions $ReF = 60.2279$, $GrF = 475.5458$, and $DomF = 280.7008$.

6.2.2 Smoother profiles with a Hill function

There is indication of an "FSH threshold," above which FSH levels must rise to initiate follicular development [88]. Following this suggestion, we replace the growth terms in equation (S5) with Hill functions in FSH (see equation (S5') below).

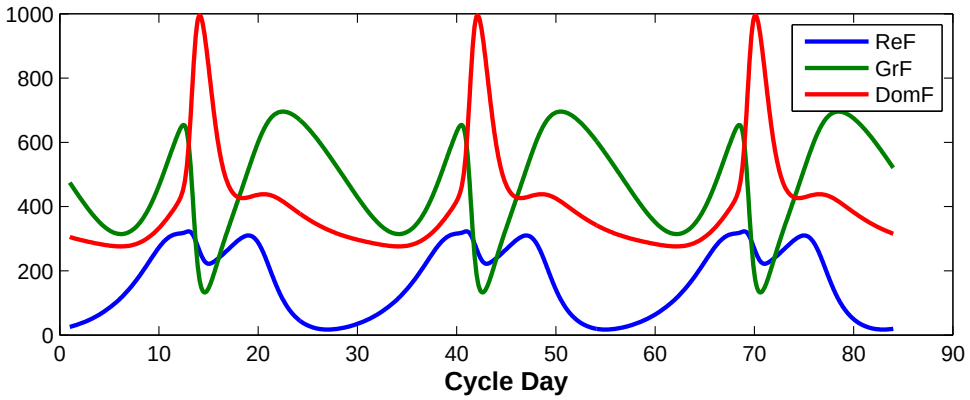

Figure 6.4: Replacing FSH stimulated growth of ReF with Hill functions in FSH smoothes the $DomF$ profile, and makes the follicle waves in ReF and GrF more pronounced. Plotted is the solution using the parameters in Table 6.1 and the initial conditions $ReF = 25.5517$, $GrF = 474.7875$, and $DomF = 305.2963$.

$$\frac{d}{dt}ReF = \frac{b \cdot FSH^{p_{F1}}}{Km_{F1}^{p_{F1}} + FSH^{p_{F1}}} + \left[\frac{c_1 \cdot FSH^{p_{F2}}}{Km_{F2}^{p_{F2}} + FSH^{p_{F2}}} - c_2 \cdot LH^{\alpha}\right] ReF \qquad \text{(S5')}$$

After selecting $Km_{F1} = Km_{F2} = 7$, and $p_{F1} = p_{F2} = 8$, and adjusting parameter b to 1.002, the system formed by equations (S5'), (S6) and (S7) produces a smoother profile for $DomF$, and more pronounced follicle waves in the profiles for ReF and GrF (see Figure 6.4).

These follicle wave solutions produce a small bump in the profile for $DomF$. It may seem insignificant, but if we look at the later stages of the system, this small bump is carried forward, contributing to trailing tails of the luteal stages. This is detrimental to the P4 profile which is determined by the luteal stages (see Figure 6.5).

Table 6.1: Parameters for the system with follicle waves, and a Hill function for growth of ReF. Changes are indicated in bold.

$b =$	**1.002**	$Km_F =$	**7**
$c_2 =$	0.3084	$p_F =$	**8**
$\alpha =$	0.3		

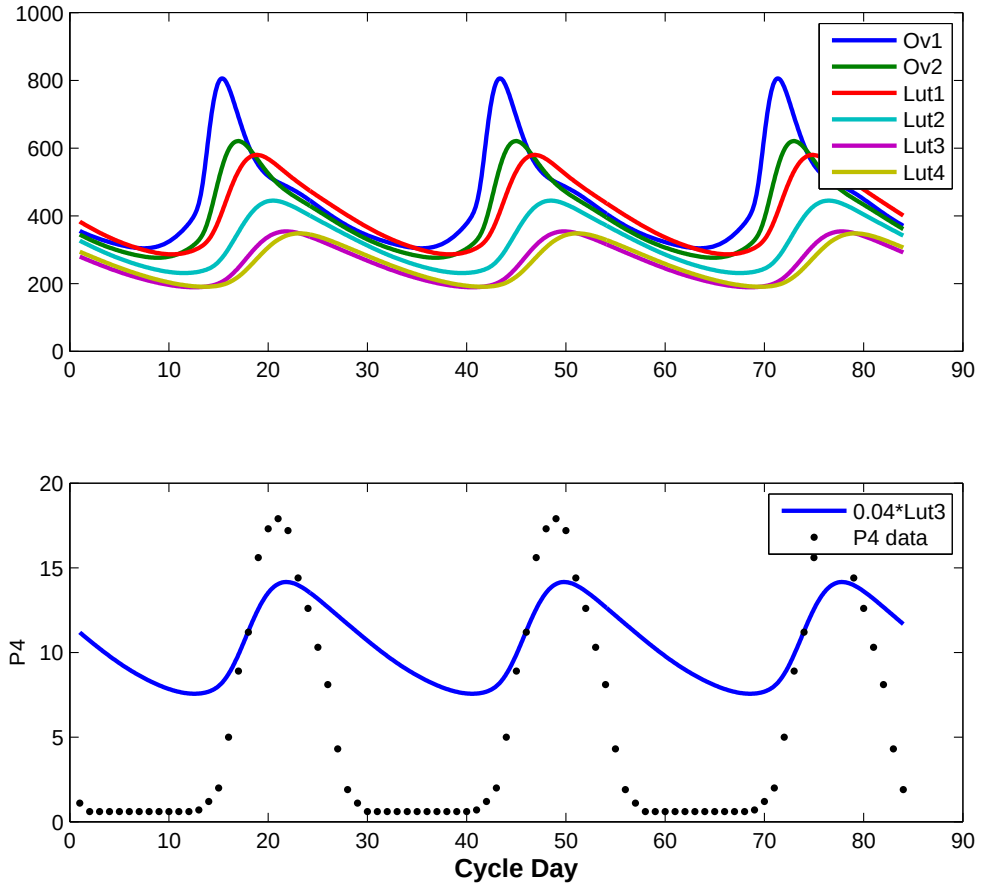

Figure 6.5: The second follicle wave persists in subsequent stages, which does not agree with the biology, and the effect on these stages is enough to change the shapes of the luteal stages so that they do not agree with the P4 profile. Plotted is the solution to the model with the initial conditions as in Figure 6.4, and $Ov_1 = 355.4037$, $Ov_2 = 344.8754$, $Lut_1 = 383.0573$, $Lut_2 = 326.6730$, $Lut_3 = 279.5955$, $Lut_4 = 294.0251$.

6.2.3 Including atresia of the second wave

To remain true to the biology, we should note that in the absence of an LH surge the growing follicle cannot reach ovulation, and instead undergoes atresia. However, in the present model, there is no atresia of the second wave of follicles. The influence of the second wave can be observed as an elevated post-ovulation $DomF$ mass (see Figure 6.4), and in the trailing luteal stages of Figure 6.5. Since progesterone is produced by the corpus luteum, we can compare the luteal stages of the current model with P4 data from Welt *et al.* 1999 [83]. It is apparent that the right tails of the luteal stages do not satisfactorily capture the biology of this phase of the menstrual cycle (see Figure 6.5).

To remedy this situation, we include a decay term representing atresia of the stage $DomF$ in equation (S7):

$$\frac{d}{dt}DomF = c_4 \cdot LH \cdot GrF + \left[-c_5 \cdot LH^{\gamma} - \frac{atr}{1 + \left(\frac{LH}{Ki_L}\right)^{p_{atr}}} \right] \cdot DomF \qquad (S7')$$

Using the same parameters as in Table 6.1, choosing $atr = 180$, $Ki_L = 10$, and $p_{atr} = 4$, the solution for $DomF$ no longer has the small bump after ovulation (see Figure 6.6). Also, the shapes of the luteal stage profiles are now in agreement with experimentally observed P4. Solutions to the model with the parameters from Table 6.2 are included in Figure 6.6.

Table 6.2: Parameters for the system with follicle waves, Hill functions for the growth of ReF, and atresia included in the decay of $DomF$. Changes are indicated in bold.

$b =$	1.002	$Km_F =$	7	$atr =$	**180**
$c_2 =$	0.3084	$p_F =$	8	$Ki_L =$	**10**
$\alpha =$	0.3			$p_{atr} =$	**4**

6.3 Summary and Conclusion

Decreasing the effect of LH on the transition from recruitable to growing follicles allows for the emergence of a second wave of follicles maturing during the luteal phase. The model does not track actual follicle numbers, but models the follicle wave phenomenon as multi-modal profiles in the development of the recruitable and growing follicles. Staying true to the biology, we incorporate a decay term in the equation for $DomF$ to ensure that a follicle reaching this stage in the absence of an LH surge will necessarily undergo atresia.

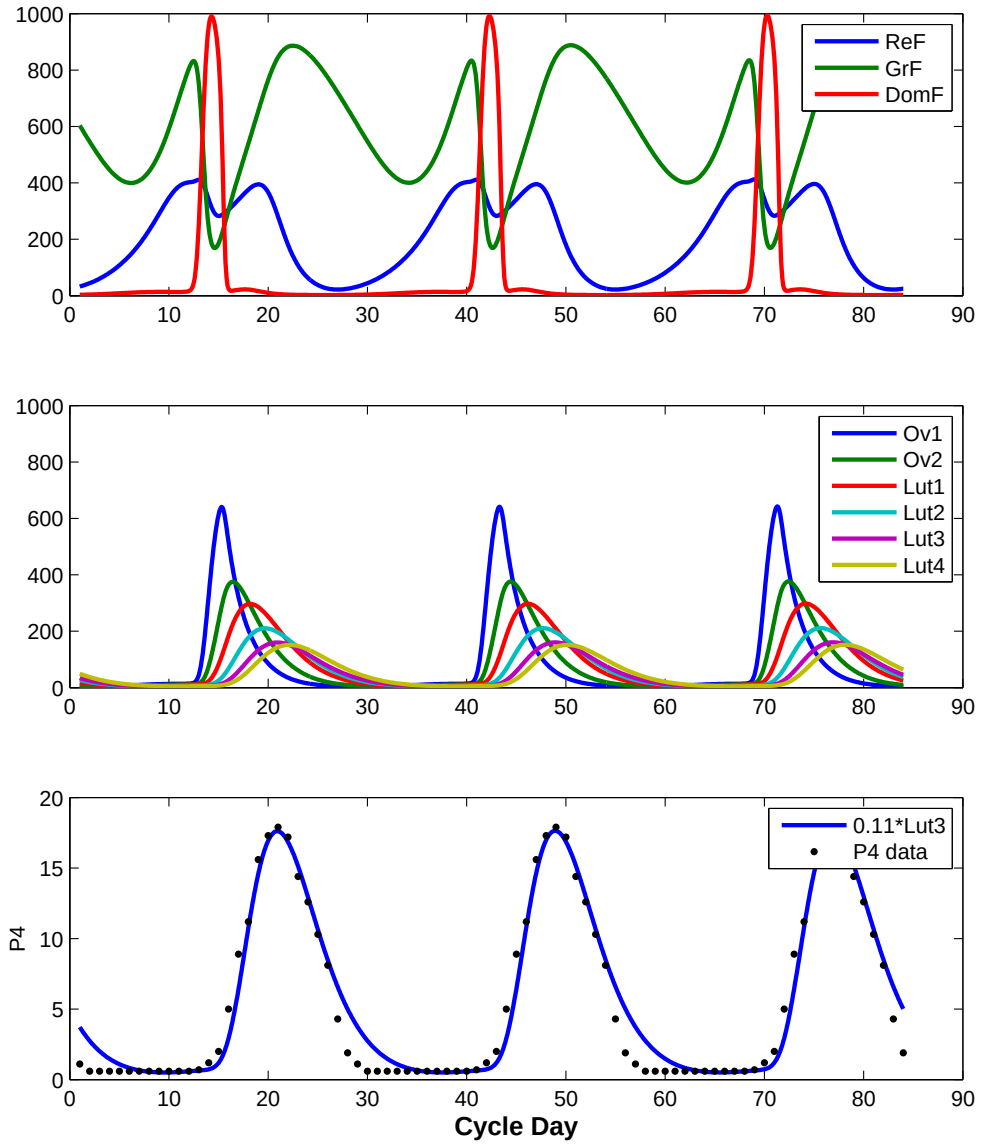

Figure 6.6: Including atresia in the equation for $DomF$ erases the second follicle wave from the profile for $DomF$, and improves the shapes of the luteal stages for their contribution to the $P4$ profile. Plotted is the solution to the system $(S5')$,(S6),$(S7')$,(S8)-(S13), using parameters from Table 6.2, and initial conditions: $ReF = 32.4748$, $GrF = 603.6958$, $DomF = 3.3381$, $Ov_1 = 3.9724$, $Ov_2 = 7.0361$, $Lut_1 = 18.1854$, $Lut_2 = 27.0960$, $Lut_3 = 33.8966$, $Lut_4 = 49.4114$

Chapter 7

A lifelong model for the female reproductive cycle with an AMH treatment to delay menopause

7.1 Introduction

As a woman ages, her ability to produce offspring decreases because of decreasing follicle numbers and changes in reproductive hormones (Broekmans *et al.* [9]). Peak fertility occurs between the ages of 20 and 30 (Soules *et al.* [74]). By the average age of 41, a woman is considered infertile because conception often takes longer than 12 months [9]. However, in North America and Europe more women are postponing childbearing until their 30's and must deal with the consequences of reduced natural fertility. A mathematical model for hormonal regulation of the menstrual cycle throughout a woman's reproductive life would be useful for studying age-related changes in menstrual cyclicity. Such models may help to identify parameter variations which are associated with subtle hormonal variations occurring in women in their 30's and model simulations may assist in the testing of hormonal therapies.

Previous studies using differential equations to describe different aspects of hormonal control of the menstrual cycle modeled the phenomenon on the time scale of days and months, and could model women of various ages by using different parameter sets. Here we develop a variation on these models with the goal to simulate key hormonal changes with advancing age, using a single parameter set to represent women of different ages.

We present a system of 16 delay differential equations with 66 parameters which models a woman's reproductive years between age 20 and 51 from the point of view of hormonal control. Our model simulations approximate data in the literature (Welt *et al.* [83]) for two age groups of women, 20-34 years old and 35-46 years old. Our model reflects changes in hormone levels and

follicle numbers that occur during that time span, e.g., the continual drop in AMH (see [41, 31]), the decrease in InhB between ages 35 and 45 (see [83]), and the subsequent rise in follicular phase FSH, while E2 and P4 levels remain unaffected [25]. The biological mechanism which initiates these changes is the gradual loss of primordial follicles (Skinner [72]). The "primordial pool" refers to the dormant follicles that a woman is born with and this pool continually decreases over time due to atresia or due to transfer to the active state. White *et al.* [84] recently reported the discovery of stem cells in a woman's ovaries which may produce oocytes after birth. However, we model primordial follicles formed only before birth, their transfer to growing follicles and then these follicles as they mature through primary, preantral, antral and dominant status followed by ovulation and luteinization. Our previous models (see Chapters 5 and 6) did not include state variables representing primordial, primary, preantral and small antral follicles nor did they include AMH and InhB. The decline of the primordial pool is eventually realized in a decreased number of preantral and small antral follicles, which directly translates to decreased levels of AMH and InhB (which are produced by these follicles), and the decreased InhB causes increased FSH production (since InhB inhibits FSH production). A goal of our modeling endeavor is to investigate possible hormonal treatments which may improve the fertility of women in their 30's and early 40's. To this end, we show that the administration of exogenous AMH mitigates the loss of primordial follicles and, hence, provides more and possibly healthier follicles for development later in life.

Section 7.2 develops the model under study and describes the model system of 16 differential equations (SS1)-(SS16). We devise an *ad hoc* procedure for estimating the 66 model parameters and discuss aspects of this procedure in Section 7.3, Chapter 4 and in Appendix D. The resulting parameter sets are included in Appendix E. Results of model simulations are presented in Section 7.4 with comparisons to data in the biological literature. Section 7.5 demonstrates how exogenous AMH inputs, AMH agonists and AMH antagonists affect model behavior. Finally, we summarize and discuss the results.

7.2 Biological Background and Model Development

As described in Chapter 2, the menstrual cycle is regulated by a hormonal feedback mechanism between the pituitary/hypothalamus and the ovaries. The gonadotropins FSH and LH are produced in the pituitary and regulate the development of follicles in the ovaries. The ovaries produce E2, P4, InhA and InhB which control the pituitary's synthesis and release of the gonadotropin hormones during the various stages of the cycle (Yen [86]). The ovaries also produce AMH which affects early follicular development (Skinner [72]).

Here we extend previous models for monthly cycling (see Chapters 5 and 6) to the reproductive life span of a woman by beginning at the primordial stage of follicle development and

continuing through primary, preantral, and small antral stages (see Figure 2.3). We also include equations for InhB and AMH since these are important markers of ovarian follicle reserve [9].

The follicular stages in our model in developmental order are primordial ($Primor$), primary ($Primar$), preantral follicles ($PrAnF$), small antral follicles ($SmAnF$), recruited follicles (ReF), growing follicles (GrF), the dominant follicle ($DomF$), ovulatory follicle (Ov), and four luteal stages (Lut_1 through Lut_4). Figure 2.3 depicts the stages of follicular development, the hormones produced by each stage, and which stages are affected by the pituitary hormones LH and FSH.

A primordial follicle consists of an oocyte surrounded by squamous (flat) granulosa cells. If the primordial follicle does not atrophy, it passes to the primary stage where granulosa cells become cuboidal and theca cells are recruited. The primary stage is considered the initial stage of follicular growth ([72, 43, 82]), although Hansen *et al.* [28] referred to primary follicles as non-growing because their growth is gonadotropin independent. The transition from the primordial to the primary is stimulated and inhibited by a variety of ovarian factors (Skinner [72] and Reddy *et al.* [60]). Skinner [72] discussed granulosa and theca cell products that promote the primordial to the primary transition such as KL, KGF and bFGF growth factors. On the other hand, the hormone AMH produced by primary, preantral and small antral follicles is known to inhibit the transition from the primordial to the primary pool (Skinner [72] or Reddy *et al.* [60]). Also Reddy *et al.* [60] described ovarian genetic factors such as oocyte PTEN and Foxo3a which suppress the activation of the primordial follicle pool and hence the transition to the primary pool. The first ovarian stage in our model, $Primor$, represents the primordial pool of follicles. The differential equation for this stage is a single term representing the decay rate of the primordial pool and is directly proportional to $Primor$ and inversely proportional to both $Primor$ and AMH (see equation (SS1)). This term models inhibitory signals between primordial follicles and the inhibitory role of AMH on the primordial to primary transition. The decay term from (SS1) appears as a growth term in (SS2) for the number of primary follicles, $Primar$. The factor of r_{surv} represents the fraction of primordial follicles that are not lost to atresia before becoming primary follicles, i.e., r_{surv} is the survival rate. The amount of AMH in (SS1)-(SS2) is given by (A5) appearing below.

$$\frac{d}{dt}\,Primor = -\frac{r_1\,Primor}{1 + c_{prm}\,Primor + c_{AMH}\,AMH} \tag{SS1}$$

$$\frac{d}{dt}\,Primar = r_{surv}\,\frac{r_1\,Primor}{1 + c_{prm}\,Primor + c_{AMH}\,AMH} - r_2\,Primar \tag{SS2}$$

The $Primar$ stage is followed by $PrAnF$ and $SmAnF$ (equations (SS3)-(SS4)), which represent preantral and small antral follicles, respectively. These stages, and all subsequent follicular stages, represent volumes instead of numbers of follicles. Thus, we multiply the transfer term from $Primar$ to $PrAnF$ in (SS3) by a parameter for the average volume per preantral follicle ($vol2$). A follicle which ultimately releases its ovum spends several months [52] developing from a preantral follicle into an ovulatory follicle, Ov in (SS8). During that time the maturing follicle acquires FSH receptors and its future growth becomes gonadotropin dependent as indicated by the decay term in (SS3), and the growth terms in (SS4). These terms have the form of an increasing Hill function of FSH in agreement with Zeleznik [88] who suggested that FSH levels must rise above a threshold to initiate follicular development. Thus the sustained growth of the small antral stage, $SmAnF$ in (SS4), depends on FSH attaining a threshold serum concentration. The exponents α and β are referred to as Hill coefficients and we determine these parameter values through our estimation procedure.

$$\frac{d}{dt}PrAnF = vol2 \cdot r_2 \cdot Primar - r_3 \frac{FSH^\alpha}{Km_{F1}^\alpha + FSH^\alpha} PrAnF \tag{SS3}$$

$$\frac{d}{dt}SmAnF = r_3 \frac{FSH^\alpha}{Km_{F1}^\alpha + FSH^\alpha} PrAnF + \left[r_4 \frac{FSH^\beta}{Km_{F2}^\beta + FSH^\beta} - r_5 \right] SmAnF \tag{SS4}$$

At the beginning of a woman's monthly cycle, 6 to 12 follicles are recruited from the pool of early antral follicles to grow under the influence of FSH and LH with the opportunity to reach ovulatory size (Figure 2.3). The growth of the recruited follicles, ReF in (SS5), depends on $SmAnF$ and on FSH reaching an early follicular phase threshold, see (SS5). AMH is thought to decrease the FSH-sensitivity of late antral follicles (see (SS6)), playing a role in the selection of the dominant follicle [82]. Typically one follicle is selected to be dominant and then to release its ovum in response to a surge of LH. The state variables in (SS5)-(SS12) represent tissue volumes of 8 distinct stages of the ovary during the follicular and luteal phases of the cycle (see Harris-Clark *et al.*, [30]). ReF, GrF and $DomF$ denote the recruited follicles, the growing follicles and the preovulatory or dominant follicle, respectively. Ov represents a periovulatory stage and Lut_i, $i = 1, ..., 4$, denote four luteal stages. As in previous models, we take the serum concentrations of the ovarian hormones to be proportional to the tissue volumes during the appropriate stages of the cycle giving the 5 auxiliary equations (A1)-(A5).

$$\frac{d}{dt}\,ReF = r_5\,SmAnF + \left[c_1\,\frac{FSH^{\gamma}}{Km_{F3}^{\gamma} + FSH^{\gamma}} - c_2\,LH^{\delta}\right]\,ReF \tag{SS5}$$

$$\frac{d}{dt}\,GrF = c_2\,LH^{\delta}\,ReF + \left[c_3\,\frac{FSH}{1+\frac{AMH}{Ki_{AMH}}} - c_4\,LH\right]\,GrF \tag{SS6}$$

$$\frac{d}{dt}\,DomF = c_4\,LH\cdot GrF - c_5\,LH^{\omega}\,DomF \tag{SS7}$$

$$\frac{d}{dt}\,Ov = c_5\,LH^{\omega}\,DomF + c_6\,LH\cdot Ov - c_7\,Ov \tag{SS8}$$

$$\frac{d}{dt}\,Lut_1 = c_7\,Ov - k_1\,Lut_1 \tag{SS9}$$

$$\frac{d}{dt}\,Lut_2 = k_1\,Lut_1 - k_2\,Lut_2 \tag{SS10}$$

$$\frac{d}{dt}\,Lut_3 = k_2\,Lut_2 - k_3\,Lut_3 \tag{SS11}$$

$$\frac{d}{dt}\,Lut_4 = k_3\,Lut_3 - k_4\,Lut_4\ . \tag{SS12}$$

In terms of these stages, the ovarian hormones are given by:

$$E_2 = e_0 + e_1\,GrF + e_2\,DomF + e_3\,Lut_4 \tag{A1}$$

$$P_4 = p_0 + p_1\,Lut_3 + p_2\,Lut_4 \tag{A2}$$

$$InhA = h_0 + h_1\,DomF + h_2\,Lut_2 + h_3\,Lut_3 \tag{A3}$$

$$InhB = j_0 + j_1\,SmAnF + j_2\,Ov \tag{A4}$$

$$AMH = a_1\,Primar + a_2\,PrAnF + a_3\,SmAnF \tag{A5}$$

The ovarian hormones regulate the synthesis and release of FSH and LH by the hypothalamus and pituitary as described by four differential equations (SS13)-(SS16), which are similar to the equations in Harris-Clark *et al.* [30] and Selgrade 2010 [68] (see equations (S1)-(S4) in Chapter 3). The state variables RP_{LH} and RP_{FSH} represent the amounts of these hormones in the pituitary and LH and FSH represent the blood concentrations of these hormones. The equation (SS15) for RP_{FSH} is similar to that in Selgrade 2010 [68] (see equation (S3) in Chapter 3) except the synthesis term has InhA and InhB inhibition instead of inhibition by a single inhibin (assumed to be Inhibin A). Because hormone synthesis is biochemically more complicated than release, the time-delay parameters d_E, d_P, d_{InhA} and d_{InhB} are assumed only for the synthesis terms and describe the periods between the time when changes in serum levels of E2, P4, InhA and InhB occur and the time when subsequent changes in LH and FSH synthesis rates occur. Based on results of previous work [30, 46, 66], a Hill coefficient of 8 provides

the appropriate steepness for the LH synthesis curve in (SS13) so that simulations will closely approximate LH data in the literature [83, 49].

$$\frac{d}{dt}\,RP_{LH} = \frac{V_{0,LH} + \dfrac{V_{1,LH}\,E_2^8(t-d_E)}{Km_{LH}^8 \;+\; E_2^8(t-d_E)}}{1 + P_4(t-d_P)/Ki_{LH,P}} \;-\; \frac{k_{LH}\;[1 + c_{LH,P}\,P_4]\;RP_{LH}}{1 + c_{LH,E}\,E_2} \tag{SS13}$$

$$\frac{d}{dt}\,LH = \frac{1}{v}\,\frac{k_{LH}\;[1 + c_{LH,P}\,P_4]\;RP_{LH}}{1 + c_{LH,E}\,E_2} \;-\; cl_{LH}\,LH \tag{SS14}$$

$$\frac{d}{dt}\,RP_{FSH} = \frac{V_{FSH}}{1 + \frac{InhA(t-d_{InhA})}{Ki_{FSH,InhA}} + \frac{InhB(t-d_{InhB})}{Ki_{FSH,InhB}}} \;-\; \frac{k_{FSH}\;[1 + c_{FSH,P}\,P_4]\;RP_{FSH}}{1 + c_{FSH,E}\,E_2^2} \tag{SS15}$$

$$\frac{d}{dt}\,FSH = \frac{1}{v}\,\frac{k_{FSH}\;[1 + c_{FSH,P}\,P_4]\;RP_{FSH}}{1 + c_{FSH,E}\,E_2^2} \;-\; cl_{FSH}\,FSH \tag{SS16}$$

7.3 Methods

Estimating the 66 parameter values in system (SS1)-(SS16) and auxiliary equations (A1)-(A5) requires multiple data sets and considerations of parameter sensitivity and correlation. Data are available in the biological literature for blood levels of the pituitary and ovarian hormones but not for the state variables of eqs. (SS3)-(SS12). However, some information is known about realistic values for volumes of ovarian stages (e.g., Nussey and Whitehead [52]). Attempting to be faithful to the biology and to use valid numerical techniques leads us to develop an *ad hoc*, iterative procedure for estimating the parameters. Some details of our process are described in the following subsections and in Appendix D and the resulting parameter sets are included in Appendix E.

7.3.1 Data used during parameter identification (PID) and model comparison

Data used during parameter identification are for primordial and primary follicle counts, and plasma concentrations of AMH, E2, P4, InhA, InhB, LH, and FSH. All data are obtained from the literature [28, 24, 41, 75, 77, 79, 80, 83]. Data for follicle counts and AMH are for ages 20

to 51 years. Data for E2, P4, InhA, InhB, LH, and FSH are for women between ages 20 and 34 years. Additional data for InhB and FSH are for women between ages 35 and 46 years. For more information on the residuals used during parameter identification see Appendix D.

Hansen *et al.* (2008) [28] reported data for gonadotropin independent follicle counts. We take these data to represent the sum of primordial and primary follicle counts. The data were reported in a table along with the age of the subjects. The number of subjects between age 20 and 51 years totaled 103. We refer to this data as $\text{Hansen}_{\text{data}}$ (see Figure 7.1).

Plasma concentration data for AMH from women of age 20 years to 51 years are taken from several sources [24, 41, 75, 77, 79, 80] (see Figure 7.2). No single clinical data set provided ample samples for all ages. Some of the data sets spanned only a portion of the ages of interest, and all but one of the data sets had sparse sample sizes for most of the ages. Van Beek *et al.* [79] had data spanning ages 20 to 38 years, each age having a sample size of less than 10. Data from van Disseldorp *et al.* [80] covered ages 26 to 47, and only 6 of the 22 ages had sample sizes of at least 10. Hagen *et al.* [24] had data spanning the entire range of interest, however all but one age had sample sizes of 6 or less. Data from Tehrani *et al.* [77] spanned ages 20 to 50, but only 6 of these ages had sample sizes of at least 10. Data from Sowers *et al.* [75] was an exception, having a sample size of 50 people for each of the ages reported, however the data set only covered ages 42 to 47. Combining the data from these six sources results in a data set covering ages 20 to 51, where all but 4 of the ages have sample sizes of at least 10 and most ages have sample sizes greater than 20. AMH data sets were in ng/mL except for Hagen which was converted from pmol/L to ng/mL using the conversion 1 pmol/L = 7.14 ng/mL [27]. The resulting data set is a set of average AMH concentrations by age for ages 20 to 51, obtained from a compiled sample of 849 points. We refer to this compiled data as AMH_{data} (see Figure 7.3).

Daily plasma concentrations of E2, P4, InhA, InhB, LH and FSH for women from ages 20-34 (n = 23) are taken from Welt *et al.* (1999) [83] (see Figure 2.2 and Table 2.1), and we use this data to compare the model solved at age 30. We refer to this data as $\text{E2}_{\text{data}}, \text{P4}_{\text{data}}$, etc. InhB and FSH daily plasma concentrations for women from ages 35-46 (n = 21) from Welt et al. (1999) [83] (see Table 2.2) are used to compare the model solved at age 40. We refer to this data as $\text{InhB}_{\text{data,older}}$ and $\text{FSH}_{\text{data,older}}$. We include InhB and FSH data for older women in order to capture the decrease of InhB and increase of FSH with age [83, 25, 61] that make these hormones markers of reduced ovarian function. We do not include hormones from the older age group that showed no significant difference between the two age groups, i.e. LH and P4 (p-value > 0.05, not significant) [83]. InhA showed a significant difference (p-value < 0.04) between the two age groups at only one data point (between ovulation and the luteal phase) [83], but we did not consider this to be an important characteristic to capture with our model, thus InhA data for the older women is not included in our comparison. Welt *et al.*

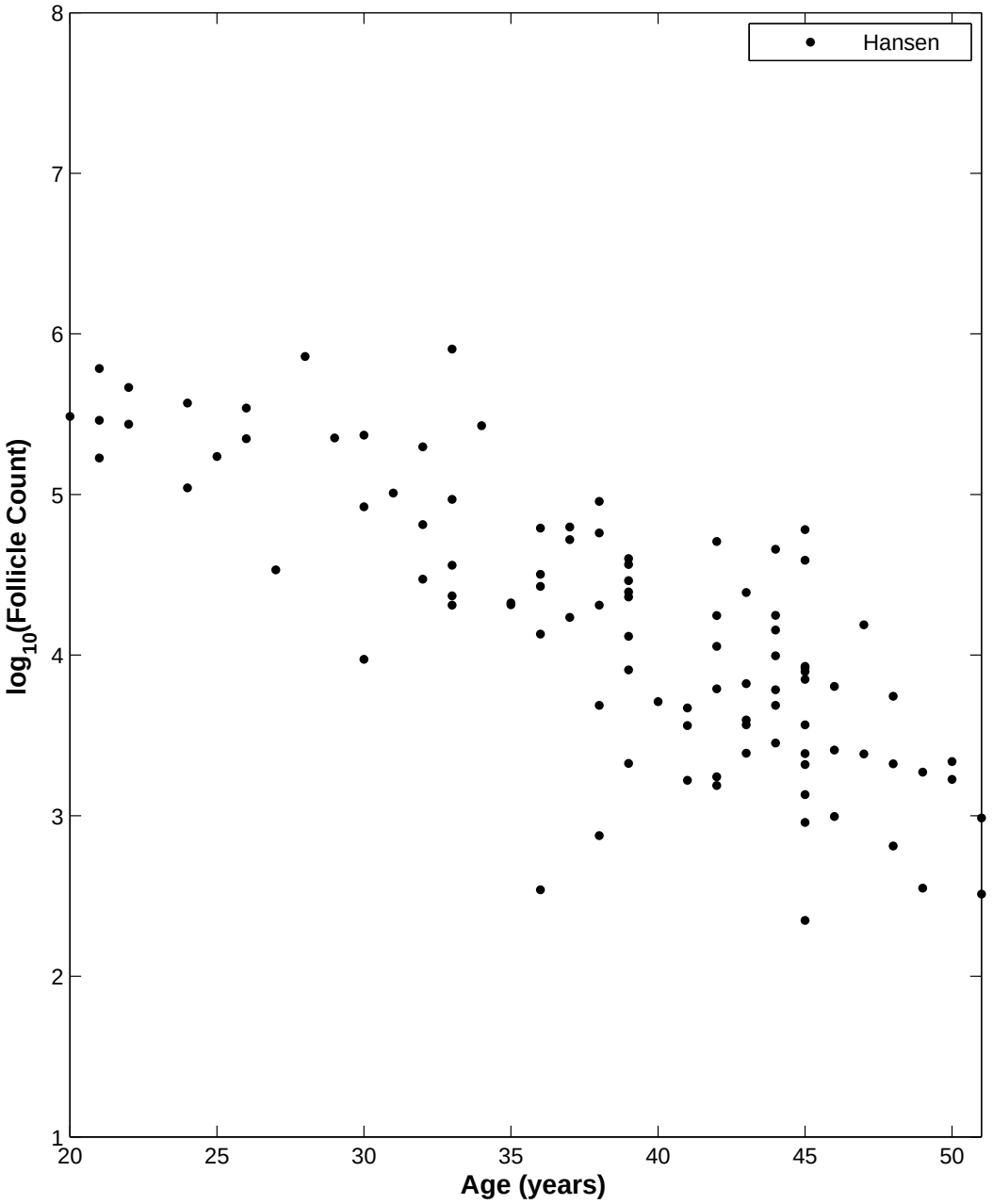

Figure 7.1: Gonadotropin independent follicle count data from Hansen *et al.* 2008 [28] plotted against age. We refer to this dataset as $\text{Hansen}_{\text{data}}$. During parameter identification the sum of primordial and primary follicle counts is optimized against this data (see Appendix D).

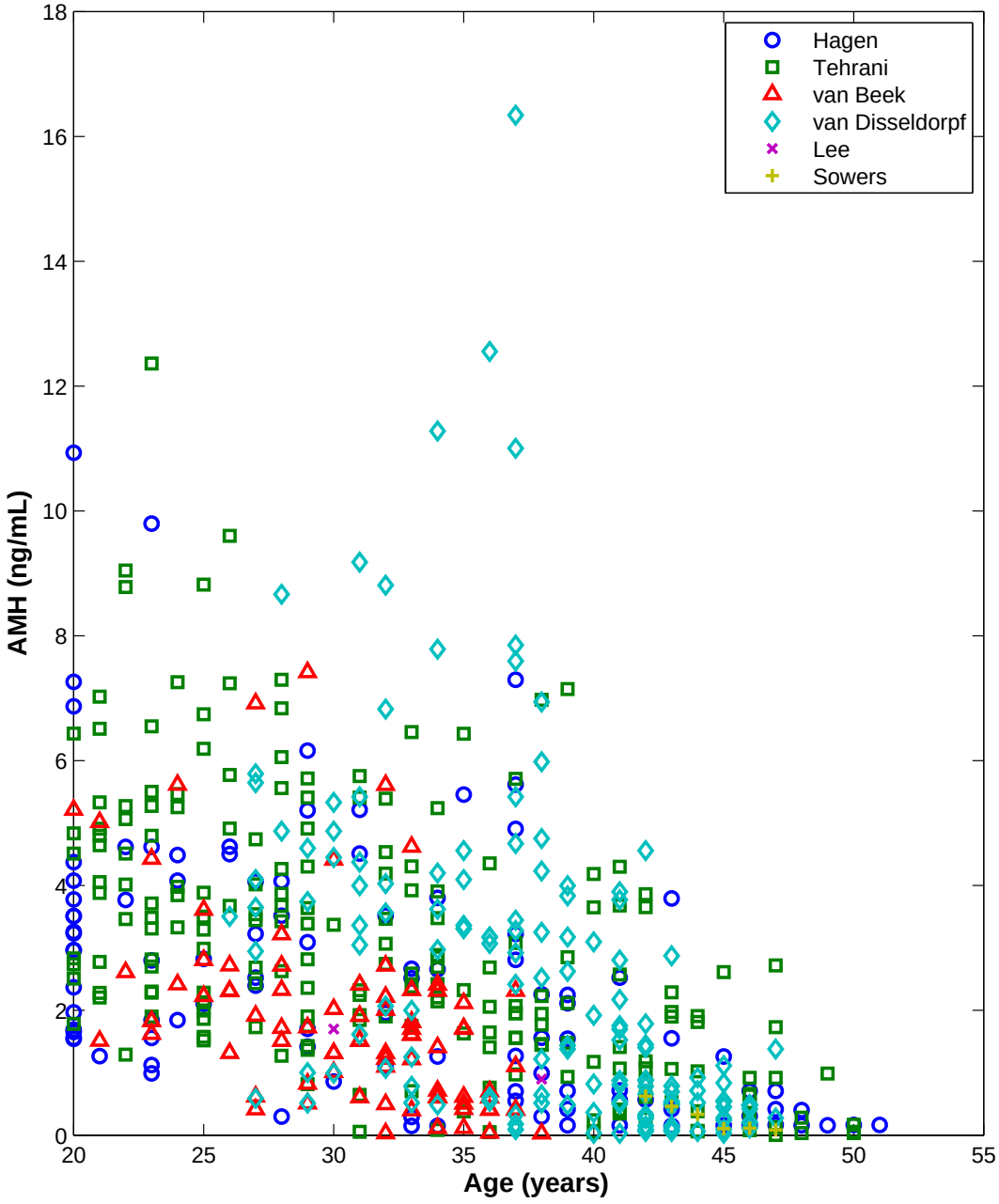

Figure 7.2: AMH plasma concentration data taken from several sources [24, 41, 75, 77, 79, 80] plotted against age. We refer to this dataset as AMH_{data}. During parameter identification simulated AMH (equation A5) is optimized against this data (see Appendix D).

[83] noted a significant increase in follicluar phase E2 in the older group as compared with the younger group (p-value < 0.02), however other sources have cited decreased E2 concentrations in the menopausal transition [9, 10], or no significant difference between women of 22-34 years and those of 41-46 years old (p-value > 0.05, not significant) [81]. Thus we do not include E2 concentrations from the Welt data for the older women in our analysis.

7.3.2 Sensitivity, correlation, and uncertainty quantification

The model presented here has a large number of parameters, and a number of state variables for which there are no direct experimental data. Attempting to identify all of the parameters at once leads to poor convergence of the numerical optimization schemes, and limited parameter identifiability. In the presence of poor convergence, it may be helpful to examine the sensitivity of the model to the parameters and correlations among the parameters. Insensitivity of a model to a parameter means that large changes in the parameter have little effect on the model output. This leads to greater uncertainty of the optimal parameter value and can prevent an optimization algorithm from converging. If a pair of parameters is correlated then changing one parameter is related to changing the other parameter, which may limit parameter identifiability.

The five most sensitive parameters in our model according to the regular sensitivities are c_6, $c_{LH,E}$, c_2, $c_{FSH,E}$ and c_3. In contrast, the most sensitive parameters according to the *relative* sensitivities are δ, Km_{LH}, c_1, r_5, and c_{LHP}. This difference in the sensitivity rankings is due to the magnitudes of the parameters. The parameters $c_{LH,E}$, $c_{FSH,E}$, c_2 and c_3 are smaller in magnitude than many of the other parameters (see Tables E.2 and E.3 in Appendix E), so it is reasonable that a small absolute change in these parameters could result in a larger change in the model output. The relative sensitivities effectively look at how the percent change in the parameters affects the model output.

The parameter r_{surv} shows correlations with a_1 and r_2 (see Eqs. (SS1)-(SS2) and (A5)), with correlation coefficients of 0.938 and 0.997, respectively. Thus we estimate r_{surv}, and fix it during optimization. The parameter r_{surv} is estimated from the decline of $\text{Hansen}_{\text{data}}$ and the estimated monthly pool of primary follicles. The approximate decline of the primordial pool from at age 20 is 22,000 per year (taken as the slope of the power fit to data in Hansen *et al.* [28]), or approximately 1833 per month. According to Nussey and Whitehead (2001) [52], it takes about 120 days (4 months) for a new primary follicle to reach the preantral stage (0.2 mm in diameter). If we assume there are 100 primary follicles at any time in a woman of age 20, developing over a course of 4 months, then there is an average of 25 follicles per month leaving the primary pool. The difference between the average decrease in the primordial stage and the average decrease in the primary stage is modeled as atresia in the primordial to primary transition. The difference of 1833 primordial follicles leaving the primordial pool per month,

and 25 follicles per month maturing in the primary stage, means approximately 1.4% of the primordial follicles leaving the primordial pool survive through the primary stage and 98.6% are lost to atresia. We model this loss as a survival factor in the primordial to primary transition. From this, we have $r_{surv} = 0.014$.

The parameters r_2 and a_1 (Eqs. (SS2) and (A5)) are correlated with a correlation coefficient of 0.937. The correlation between r_2 and a_1 comes from the fact that a_1 determines the magnitude of AMH in terms of the magnitude of $Primar$, which is governed by r_2. Fixing r_2 during optimization results in unwanted transient behavior in the solution profile for $Primar$ when any of the parameters in the growth term for $Primar$ are changed. For example, decreasing r_1 without changing r_2 creates a steep initial drop in the profile for $Primar$, while increasing r_1 without changing r_2 creates a steep initial climb. In order to avoid this transient behavior, we replace r_2 in the equation for $Primar$ with

$$r_2 = \widehat{r}_2 \cdot \frac{r_{surv} \cdot r_1 \cdot 265000}{1 + c_{prm} \cdot 265000 + c_{AMH} \cdot a_1 \cdot 100},$$

and fix $\widehat{r}_2$ during optimization. The value of 0.01 for $\widehat{r}_2$ eliminates the unwanted transient behavior (at this value the right hand side of equation (SS2) is zero at age 20).

Correlation of parameters in the remaining ovarian system equations (Eqs. (SS3)-(SS12)) is due in part to the fact that we do not have data for the ovarian stages themselves, but only for the ovarian hormones modeled by the auxiliary equations (A1)-(A4). Theoretically, the follicular stages could grow to any magnitude during optimization, since the auxiliary coefficients ultimately scale them to fit the data. To avoid this, we determine approximate values for the auxiliary coefficients and fix them during optimization. The auxiliary coefficients represent hormone production per ovarian stage volume, and thus can be approximated with knowledge of the hormone levels during the different stages and approximate volumes of each follicular stage. The volume of the dominant follicle at ovulation, Ov, is taken to be 4000 mm^3 assuming that it is approximately a sphere of diameter 20 mm [52]. Assuming that the ovary is largest around the time of ovulation, we also take Lut_1 to be 4000 mm^3. Then we take the maximum values for the other six follicular stages to differ by increments of 1000 mm^3 as follows: $ReF = Lut_4 = 1000$, $GrF = Lut_3 = 2000$, and $DomF = Lut_2 = 3000$. Finally, we take the maximum for $SmAnF$ to be 10 mm^3. Assuming these maximum values for the follicular stages, and noting the hormone levels of the data from Welt *et al.* [83] during these different phases of the cycle, we are able to determine approximate values for the auxiliary coefficients that will result in the necessary hormone levels. The auxiliary coefficients (see Table E.4, Appendix E) are fixed during optimization so that the follicular stages remain at realistic sizes.

Additional correlations exist among parameters for which we have no empirical data. For these correlations, we fix the least sensitive parameters. The parameters $V_{1,LH}$ and Km_{LH} (see

Eq. SS13) are correlated with correlation coefficient 0.946. $V_{1,LH}$ is the less sensitive parameter, thus we fix it during optimization. The parameter V_{FSH} is correlated with $Ki_{FSH,IhA}$ and $Ki_{FSH,IhB}$ (see Eq. SS15) with correlation coefficients 0.974 and 0.967. $Ki_{FSH,IhA}$ and $Ki_{FSH,IhB}$ are correlated with correlation coefficient 0.916. Of these parameters, V_{FSH} is the most sensitive (according to relative sensitivities), thus $Ki_{FSH,IhA}$ and $Ki_{FSH,IhB}$ are fixed during optimization. The parameters Km_{F2} and r_5 are correlated with correlation coefficient 0.988, and r_5 is more sensitive. The parameters ω and c_5 are correlated with correlation coefficient 0.956, and ω is more sensitive.

7.3.3 Tests for significance

Tests for significant difference between the model simulations at age 30 versus age 40 (see Section 7.4.2) are performed by using two-tailed two sample t-tests on the means from independent samples of 500 Monte Carlo simulations for each of the two ages. The Monte Carlo simulations are performed by sampling parameters from log-normal distributions with means and standard deviations corresponding to the obtained parameter values and standard errors, respectively (see Appendix E). Only the subset of parameters that are varied during optimization are sampled during Monte Carlo simulation. The means and standard deviations of the simulations are computed separately for each model output (i.e. each hormone or follicular stage), and for each day of the cycle. For each model output there is a family of 28 hypotheses, each corresponding to a day of the monthly cycle. Thus we use the Bonferroni correction [56] to control the overall error rate, i.e., for an overall significance level of α, or an overall confidence of $100 \cdot (1-\alpha)\%$, we reject the individual null hypotheses with significance level $\alpha/28$. We use the significance levels of $\alpha = 0.05$ and 0.01 to be significant and very significant, respectively. Hence, in order to achieve overall confidence of 95% and 99%, we restrict the individual p-values to be less than $0.05/28 \approx 0.00179$ and less than $0.01/28 \approx 0.000357$, respectively.

7.3.4 Model-specific treatment of multiple time scales

The primordial pool of follicles declines over the lifetime, a timespan of decades. The decline of AMH from mid-reproductive age to menopause follows a similar trend. Data for the primordial pool and AMH are thus on the order of years. The remaining hormones in our model, E2, P4, InhA, and InhB produced in the ovaries and LH and FSH produced in the pituitary, display daily variations and cycle monthly. The follicular stages that respond to the pituitary hormones ($PrAnF$ and subsequent stages, see equations (SS3) through (SS12)) will also exhibit monthly cycling behavior. Therefore, our model exhibits the time scales of days and of years.

The multiple time scales in this model have the potential of creating numerical and computational difficulties. In order to approximate the daily data of the monthly cycling hormones

(E2, P4, InhA, InhB, LH and FSH), the model equations (SS1)-(SS16) must be solved with a time step less than 1 day. However, to capture the declining trend of the primordial pool and AMH throughout a woman's lifetime, the model equations must be solved over a time span of several decades. Integrating the system from age 20 to age 50 using Matlab's dde23 takes over 8 minutes on a quad-core PC equipped with a generation 7 Intel chip and 8.00 GB RAM. The system of differential equations has 66 parameters, an optimization scheme that integrates the entire system over this time period would take over 8 hours just to change each parameter once, let alone converge to an optimal parameter set. This presents a problem for parameter identification.

In order to use data of the two different time scales in parameter identification for our system, the parameters a_2 and a_3 in equation (A5) are set to zero, allowing for the decoupling of equations (SS1), (SS2), and (A5) from the rest of the system. This system of two ordinary differential equations is solved from age 20 to age 51 using ode23 and optimized against $\text{Hansen}_{\text{data}}$ and AMH_{data} (see Appendix D for residual used during PID).

Once a parameter set is obtained for this small system (see Appendix E for parameter values), the remaining equations (SS3)-(SS16) and (A1)-(A4) can be solved at any age by using initial conditions for $Primor$ and $Primar$ obtained from the simulation to equations (SS1)-(SS2) integrated up to the required age. The initial conditions for the remaining state variables (see equations (SS3) - (SS16)) can obtained at a specific age by fixing $Primor$ and $Primar$ and integrating the remaining equations for two-month time spans until the stable attractor has been reached. Centering the LH peak at day 14, the value of a stage at day 1 is taken to be the initial condition for that stage. When the change in initial condition from one cycle to the next is less than 1%, we assume we have found the stable attractor. The initial conditions for age 20, 30 and 40 are included in Table E.5.

Obtaining parameter values for the remaining parameters involves solving the delay differential equations (SS3)-(SS16) using dde23 and auxiliary equations (A1)-(A4), for two-month time spans starting at age 30, i.e., time $t_{30} = 30 \times 365$ days and at age 40, i.e., time $t_{40} = 40 \times 365$ days. These solutions are then fit to data for women of ages 20 to 34 and ages 35 to 46, respectively, from Welt *et al.* [83]. For more information on the residuals used during optimization see Appendix D.

In situations where there are multiple stable attractors for the same parameter set, there is a real possibility that simulations starting at age 40 might settle on a different stable attractor than simulations starting at age 30. For any parameter set tested for this model, numerical experiments indicate that there appears to be just one stable attractor for the total time span. Updating the initial conditions at each step during optimization insures that the solution profile is close to this stable attractor. Also, simulation of our model from age 30 through age 40 using the reported parameter set (see Appendix E) is in agreement with the model simulated starting

at age 40 with initial condition reported in Appendix E.

Setting a_2 and a_3 equal to zero is a simplification of the model that is made to decrease computational cost during parameter identification. However, there is some biological evidence for emphasizing the primary follicle pool. Maciel *et al.* [43] reported that at any time during the monthly cycle, there are between two and three times as many primary follicles as there are preantral and small antral follicles together. Though individual small antral follicles express more AMH than individual preantral and primary follicles [82], the relative proportions secreted by each cohort is not known.

Since preantral and small antral follicles are cycling monthly, daily levels of AMH throughout the menstrual cycle may be helpful in identifying parameters a_2 and a_3 as compared to a_1. However there is some debate over whether AMH levels exhibit significant daily variability across the menstrual cycle [44, 85]. Younger women appear to show more variability than older women [76]. In this study we are interested in average monthly AMH, as this is the marker for follicle reserve. We believe that modeling AMH as proportional to the primary follicle count is sufficient for this end.

7.4 Simulations and Results

7.4.1 PID of the primordial to primary transition and AMH

Setting a_2 and a_3 equal to zero in equation (A5) allows for equations (SS1)-(SS2) and auxiliary equation (A5) to be decoupled from the larger system, as they no longer depend on the remaining equations. This smaller system is solved from age 20 through age 51 and optimized against the follicle data, $\text{Hansen}_{\text{data}}$, and AMH data, AMH_{data}.

The initial condition for the primordial pool is taken from the Hansen *et al.* [28] (see the equation on page 703) as the power fit to data evaluated at age 20 giving 265,000 follicles. The initial condition for the number of primary follicles at age 20 is taken to be 100. This value is derived from Broekmans et al. (2009) [9] which asserted that there are between 20 and 150 early growing follicles (sized 0.05 mm to 2 mm in diameter) at any time in a woman of age 25 to 40. According to Nussey and Whitehead (2001) [52], preantral and small antral follicles are between between 0.2 mm and 2 mm in diameter, and according to Maciel *et al.* [43] there are between two and three times as many primary follicles as there are preantral and small antral combined. Thus, using the maximum estimate in Broekmans *et al.* [9] for age 20, we assume there are approximately 100 primary follicles and 50 preantral and small antral follicles at age 20.

Correlation of parameters was handled as described in Section 7.3.2. The remaining parameters represent an uncorrelated set, and the numerical optimization algorithm NLSQ_ERR [89]

applied to this smaller system converges. The optimized parameters for this smaller system are included in Table E.1 of Appendix E. Model output for equations (SS1)-(SS2) and (A5) are plotted against data in Figure 7.3.

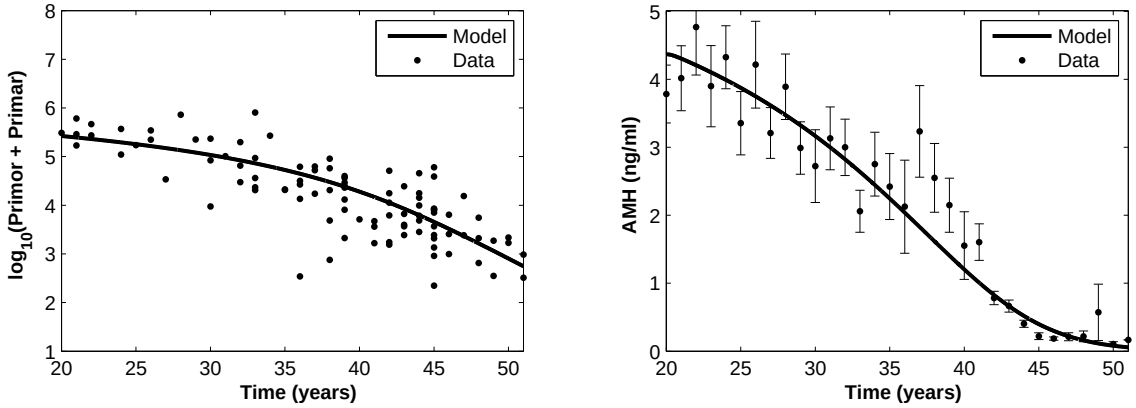

Figure 7.3: Equations (SS1)-(SS2) and (A5) are solved using the optimized parameters (Table E.1, Appendix E), starting at age 20 and using the initial conditions $Primor_0$=265,000, and $Primar_0 = 100$. The sum of the model solutions $Primor$ and $Primar$ is log transformed and plotted against log(Hansen$_{\text{data}}$) [28]. The model for AMH is plotted against composite AMH$_{\text{data}}$ [24, 41, 75, 77, 79, 80] (mean ± SEM).

7.4.2 PID of monthly cycling follicular stages and hormones, and key changes with age

Equations (SS3)-(SS16) can be solved at any age by using initial conditions for $Primor$ and $Primar$ obtained from the solution to equations (SS1)-(SS2) evaluated at the required age. The simulations for equations (SS1)-(SS2) evaluated at age 30 (t_{30}) and age 40 (t_{40}) give the approximate primordial and primary follicle counts as $Primor(t_{30}) = 108,000$ and $Primar(t_{30}) = 72.5$ for age 30, and $Primor(t_{40}) = 19,000$ and $Primar(t_{40}) = 27.6$ for age 40. The initial conditions for the remaining stages for a certain age can be obtained by fixing $Primor$ and $Primar$, which vary little on the time scale of months, and integrating the remaining equations until they have approached the stable attractor. The model simulations are centered with the LH peak at day 14 of the cycle, and day 1 is taken to be the initial condition. This procedure for determining the initial conditions is done whenever the parameter set is varied, and thus must be done at each step in an optimization scheme.

Using the numerical optimization algorithm NLSQ_ERR, we observed that the changes in

the logs of the parameters with each iteration converged to less than 10^{-3}. Since the logs of the parameters were optimized (see Section 4.3), this signifies that the parameters have converged to within 0.1%, and so can be reported to within 3 significant digits. The parameters are reported in Tables E.2, E.3, and E.4. The standard errors (see Section 4.4) associated with this parameter set are also included in Appendix E, and provide an indication of the uncertainty in the presented parameter values. The parameter set reported here provides the smallest observed residual. Running 5000 Monte Carlo simulations, sampling parameters from log-normal distributions with means and standard errors as in Appendix E, revealed no parameter set with smaller residual. The simulations obtained from this parameter set are included in Figures 7.4 to 7.6.

The simulated hormone profiles for LH, E_2, P_4 and $InhA$ are plotted in Figure 7.4 against data for younger women, and the hormone profiles for FSH and $InhB$ are plotted in Figure 7.5 against data from Welt *et al.* [83] for both younger and older women. Figure 7.6 contains the solution profiles for the follicular stages $PrAnF$ through Lut_4 (the states associated with equations (SS3)-(SS12)).

The hormone profiles for LH, E_2, P_4 and $InhA$ (Figure 7.4) are not significantly different for the two age groups, but $InhB$ and FSH (Figure 7.5) are very significantly different (overall confidence 99%). The simulations exhibit lower $InhB$ and higher FSH during the follicular phase for age 40 as compared to age 30, and these differences are similar to those observed in the Welt *et al.* [83] data. The Welt data also exhibits differences in luteal InhB. We may be able to model this difference by including additional stages in the definition of $InhB$. However, since observations reported by others (e.g. van Zonneveld *et al.* [81]) indicate that luteal InhB is not significantly different between the two age groups, we decided not to complicate the model with features that do not necessarily reflect the physiology.

$InhB$ is produced by early growing follicles, which have declined in number between ages 30 and 40 (Figure 7.6), thus the solution profile for $InhB$ is lower at age 40 than it is at age 30 (Figure 7.5). Since $InhB$ inhibits FSH synthesis (see eq. (SS15)), the decreased $InhB$ causes an increase in follicular phase FSH. These differences in $InhB$ and FSH simulations correspond to differences in the data (Figure 7.5). LH, E_2, P_4 and $InhA$ are indicative of the ovulatory follicle and corpus luteum which are similar in ovulatory women of these two age groups [81]. Increased sensitivity to FSH of growing follicles caused by decreased AMH (see eq. (SS6)) allows for full development of the growing follicles, and thus the dominant follicle, ovulatory follicle and corpus luteum in older women. The volumes of stages GrF, $DomF$ through Lut_4 are not significantly different between age 30 and age 40 (overall confidence 95%), and this similarity may be observed in Figure 7.6. Since these stages contribute to the hormones E_2, P_4 and $InhA$ (see eqs. (A1)-(A3)), these hormones are similar between the two age groups and this similarity extends to the LH profiles because LH depends only on E_2 and P_4.

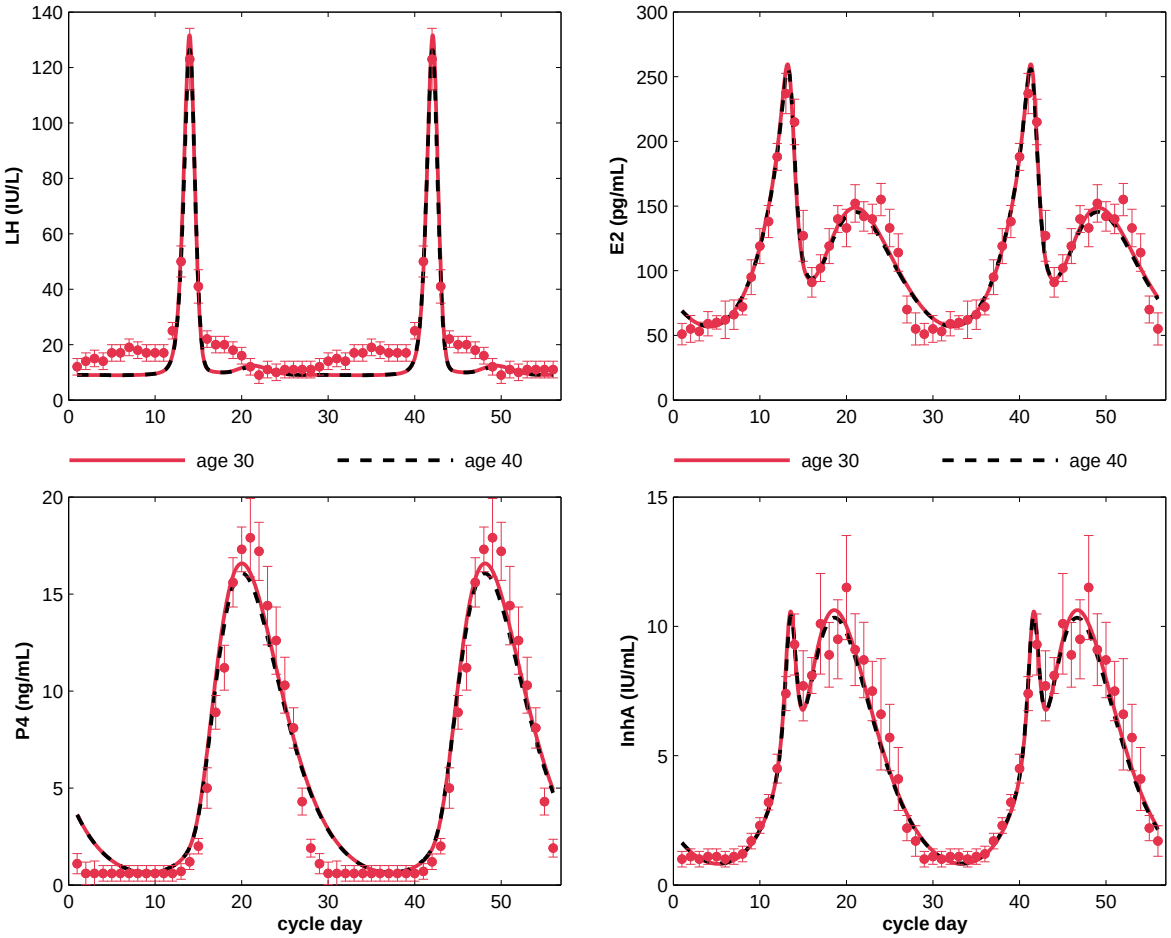

Figure 7.4: Hormone profiles from the model solved at ages 30 (red solid curves) and 40 (black dashed curves) are plotted against data (red dots, mean ± SD) from Welt et al. [83] for women ages 20 to 34 years. Note that the hormone profiles for LH, E_2, P_4 and $InhA$ are very similar between the two ages. LH, E_2, P_4 and $InhA$ are indicative of the ovulatory follicle and corpus luteum, which are similar in ovulatory women of these two age groups [83, 81].

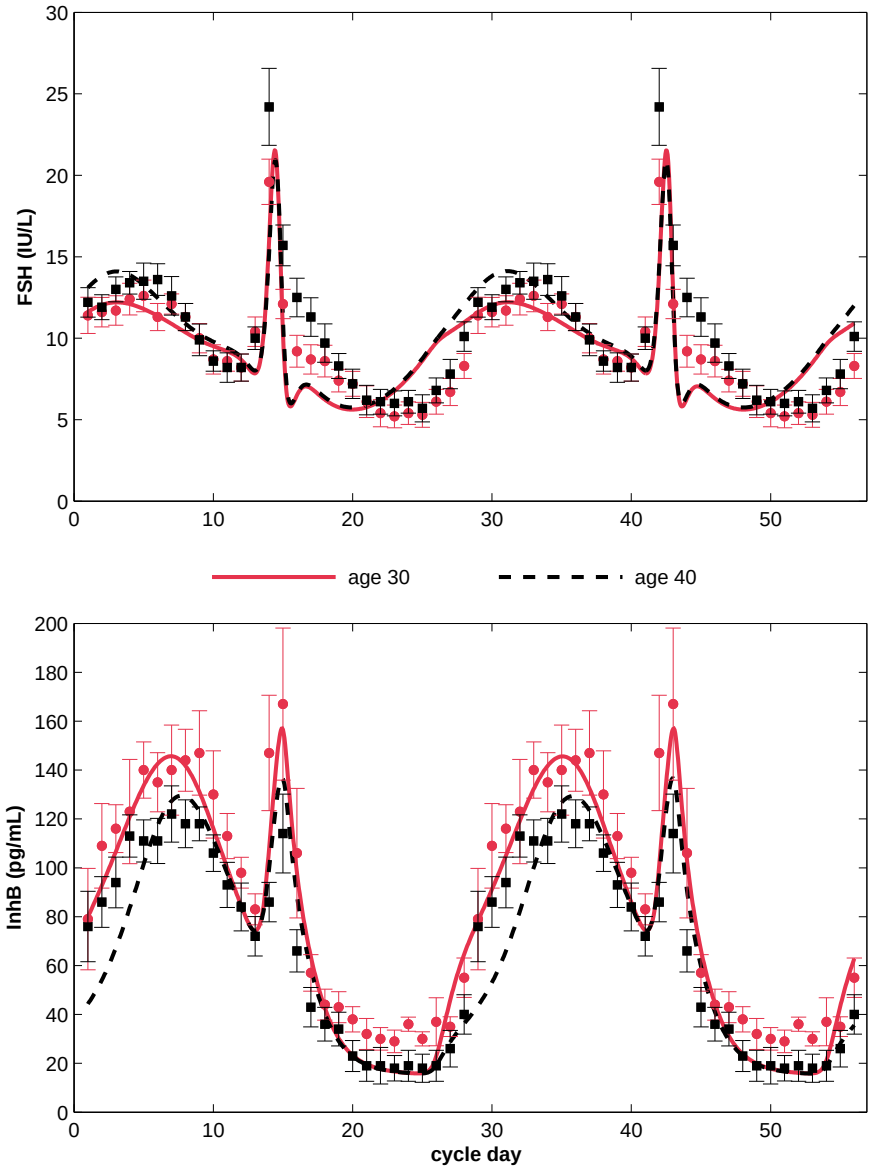

Figure 7.5: Hormone profiles from the model solved at ages 30 (red solid curves) and 40 (black dashed curves) are plotted against data (red dots, mean ± SD) for younger women (ages 20 to 34) and data (black squares, mean ± SD) for older women (ages 35 to 46) from Welt *et al.* [83]. In the older women, early to mid follicular phase (days 1 to 9) $InhB$ is lower and early to mid follicular phase FSH is higher. $InhB$ is produced by early growing follicles which have declined in number between age 30 and 40. The rise in follicular phase FSH is in response to the decreased $InhB$.

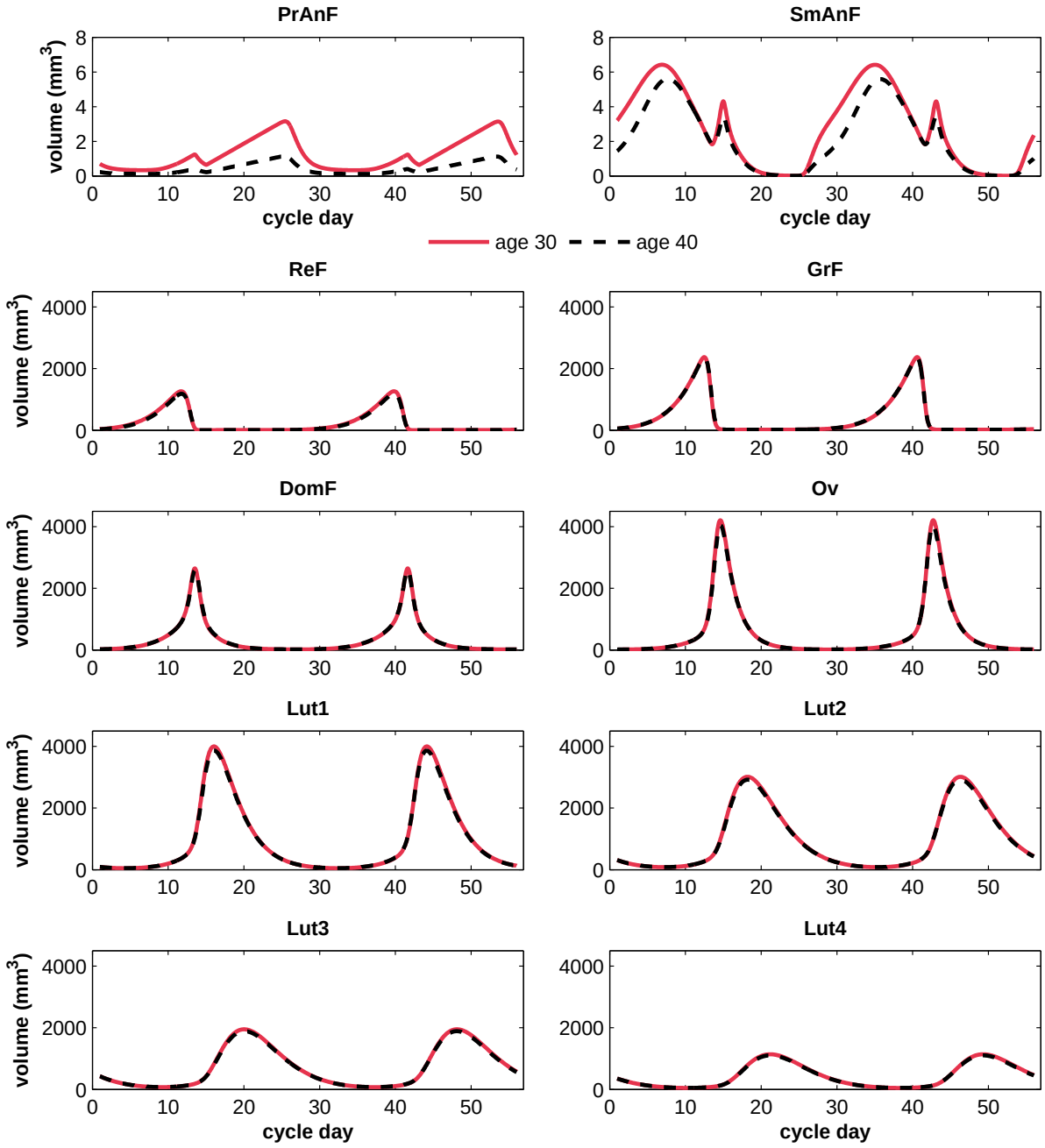

Figure 7.6: Comparison of follicular stages solved at ages 30 (red solid curves) and 40 (black dashed curves). The solution profiles for $PrAnF$, $SmAnF$, and ReF are significantly different between the two ages (overall confidence 99%). This is due to the decreased number of primordial follicles that are available to develop into preantral and small antral follicles at age 40. Note that the increased sensitivity to FSH of the growing follicles (GrF) caused by decreased AMH aids in the full development of the dominant follicle and corpus luteum ($DomF$ through $Lut4$), despite decreased volume of the early antral stages ($PrAnF$, $SmAnF$, and ReF).

7.5 Exogenous AMH, AMH agonists and AMH antagonists

The role that AMH plays in the primordial to primary transition suggests several uses of AMH for fertility treatment, for delaying menopause and for contraception. Since AMH inhibits the transition of follicles from the primordial to the primary stages, AMH or an AMH agonist could be given to premenopausal women to slow this transition and hence may delay the loss of fertility due to low antral follicle count [9]. This treatment would be for women who are waiting to get pregnant until they are older and are worried about the decline of fertility with age due to declining follicle reserve. In the extreme case, if the transition is slowed enough then the number of growing follicles may be decreased enough to prevent ovulation during treatment. Thus AMH or an AMH agonist could be used as a contraceptive. Alternatively, an AMH antagonist could be given to women who are trying to become pregnant but face difficulty due to low antral follicle count. This would be a short term fertility treatment and could possibly be combined with existing fertility treatments such as FSH administration. Our model can be used to simulate outcomes of these treatments. Recall that the numerical optimization algorithms converged to an optimal parameter set for the small system (equations (SS1), (SS2), and (A5)). Hence the following simulated treatments use an optimal fit to $\text{Hansen}_{\text{data}}$ and AMH_{data} as the control.

7.5.1 Exogenous AMH Treatment to Delay Menopause

Predictions for treatment with exogenous AMH from age 25 to 35 with doses that would achieve 5 ng/mL and 20 ng/mL increases in serum AMH are included in Figure 7.7. The treatment is modeled as a constant (5 ng/mL or 20 ng/mL) added to the equation (A5) between the ages 25 and 35. The rate of decline of the primordial pool is decreased during the treatment period, and resumes a normal course after the treatment is ended. The number of primary follicles that are developing during the treatment period is decreased, and this decline is dose-dependent. The 5 ng/mL treatment delays infertility due to low follicle count by 2 years, while the 20 ng/mL treatment delays this by 5 years. After the treatment is ended, normal monthly cycling resumes and behaves as it would for a woman 2 or 5 years younger, respectively. If the woman would have stopped ovulating around age 48 without treatment, she would now stop ovulating around age 50, or age 53, respectively. Note that these treatments are not expected to prevent infertility due to factors other than low follicle count.

7.5.2 Exogenous AMH Treatment as a Contraceptive

In theory, if enough AMH is given during treatment, the number of developing primary follicles would decrease to zero. In order to use AMH as a contraceptive method, the dosage should be large enough to decrease the primary follicle number to a level below what is necessary

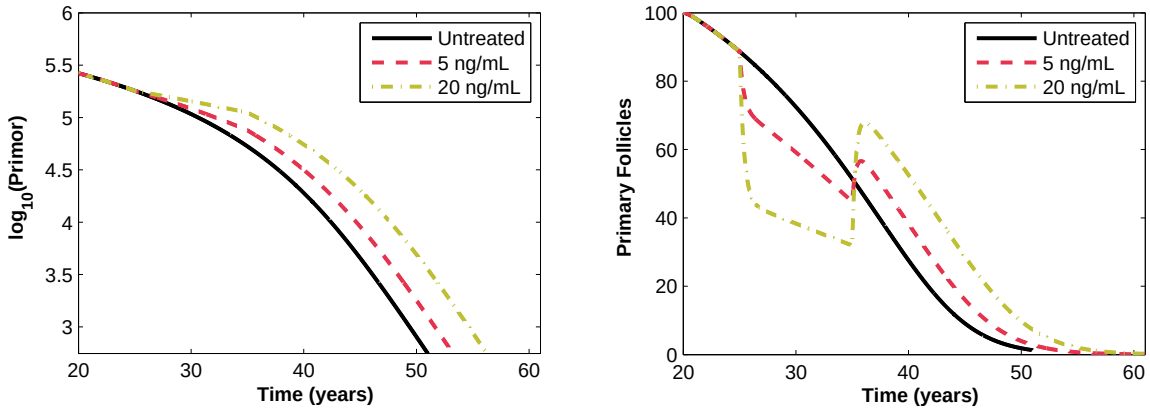

Figure 7.7: Predicted follicle numbers for individuals given exogenous AMH from age 25 to 35. Predictions plotted are for treatments that would achieve 5 ng/mL (red dashed curves) or 20 ng/mL (yellow dot-dashed curves) increase in serum AMH. The 5 ng/mL treatment delays infertility due to low follicle count by 2 years and the 20 ng/mL treatment delays this by 5 years. The number of primary follicles that are developing during the treatment period is decreased, and this decline is dose-dependent.

for ovulation. According to Broekmans *et al.* 2004 [8], the average age at last child birth (in a population not applying contraceptive measures) is around 41 years. This can be used as a proxy for the age at natural loss of fertility. Broekmans *et al.* 2009 [9] cites that the average age at the onset of cycle irregularity is about 46 years, and the average age at menopause (age at final menstrual period) is 51 years. Our simulations at these ages correspond to primary follicle counts of 23, 7, and 1, respectively. An AMH treatment that decreases the simulated primary follicle count to below 23 may be sufficient, but a more conservative treatment that decreases it to below 7 or 1 is more likely to prevent ovulation.

Our simulation predicts that a dose of 55 ng/mL AMH is required to push the primary follicle count of the average 25 year old woman down to that of a woman of age 41. To decrease the primary follicle count to that of a woman of age 46 and 51, doses of 220 ng/mL and 1300 ng/mL AMH, respectively, are required. Figure 7.8 plots these treatments given from age 25 to 35. This is a wide range of possible doses required to prevent ovulation. This range could be used as a starting point for determining the therapeutic threshold.

The doses of AMH for possible contraceptive use mentioned here are much higher than levels found naturally circulating in women, the first being about 10 times, the second about 50 times, and the third about 300 times the natural level of AMH in normal mid-reproductive age women. Thus exogenous AMH for the purpose of contraceptive use may be unrealistic. Studies would need to be performed on the effects, if any, of AMH on other systems in the body to

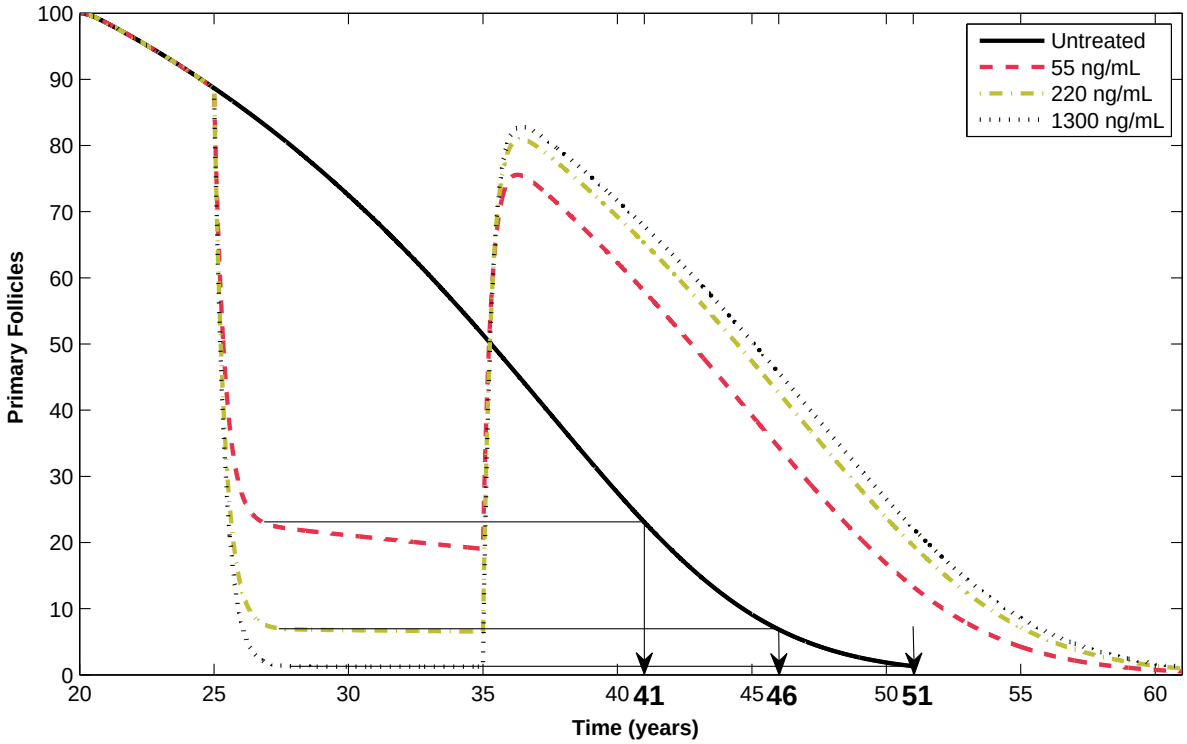

Figure 7.8: The number of primary follicles is plotted for an AMH contraceptive treatment of 55 ng/mL (red dashed line), 220 ng/mL (yellow dot-dashed line), and 1300 ng/mL (black dotted line) from age 25 to 35, plotted against the untreated primary follicle profile (black solid line). These are the doses required to decrease the primary follicle count of the average 25 year old to the level of the average 41, 46 and 51 year old, respectively. Arrows trace the follicle counts resulting from these treatments across to the untreated curve, and down to the corresponding age on the horizontal axis. These ages correspond to the average ages of natural loss of fertility, onset of cycle irregularity, and menopause, respectively [8, 9].

determine plausibility of exogenous AMH treatments of this magnitude.

7.5.3 An AMH Antagonist Fertility Treatment

Figure 7.9 includes predictions for treatments with AMH antagonists for one year starting at age 35 or at age 40 where the antagonists block 75% or 95% of AMH action on the primordial to primary transition. The antagonist action is modeled as a factor of 0.25 or 0.05 multiplying the AMH term in the denominator of equations (SS1) and (SS2). The factor represents the percentage of AMH action not blocked by the antagonist. For the duration of the treatment, the weaker antagonist increases primary follicle numbers by 8 for age 35 (a 16% increase) and by 3 for age 40 (a 12% increase). The stronger antagonist increases primary follicle numbers by 10 for age 35 (a 20% increase) and by 4 for age 40 (a 15% increase). An AMH antagonist could be used to increase small growing follicle numbers. This could be useful by itself, or as part of other fertility treatments such as exogenous FSH. The AMH antagonist would increase the number of small growing follicles available to respond to FSH. Note that these treatments are not expected to improve fertility in women who experience infertility due to factors other than low follicle count.

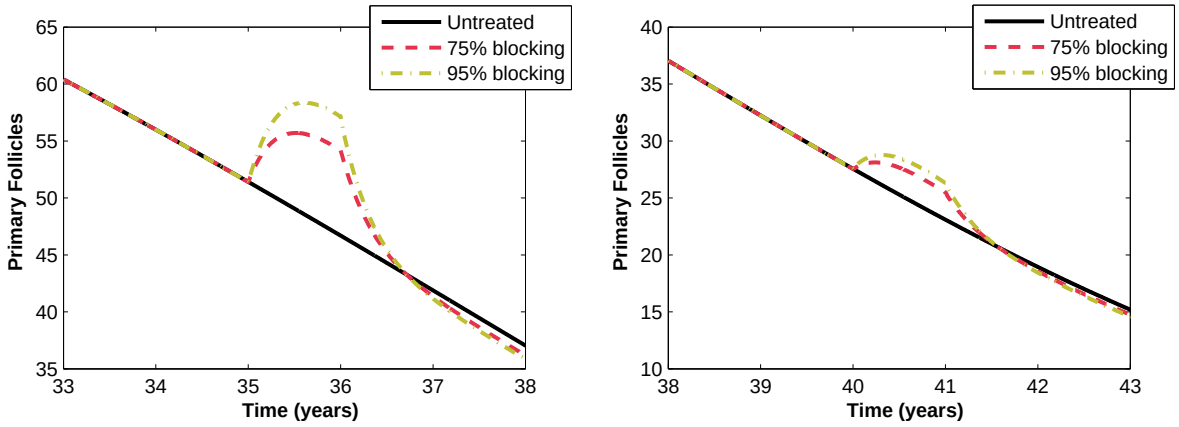

Figure 7.9: Predicted primary follicle numbers for individuals treated for one year at age 35 (left) and at age 40 (right) with an AMH antagonist that blocks 75% (red dashed curves) and 95% (yellow dot-dashed curves) of AMH action on the primordial to primary transition.

7.6 Summary and Discussion

This chapter presents a model for hormonal regulation of the menstrual cycle of an adult woman from age 20 to 51. Our system of 16 nonlinear, delay differential equations with 66 parameters tracks normal cycling from a woman's peak reproductive years to menopause. In order to capture age-related changes in hormone levels and in cycle behavior, we model the gradual loss of inactive primordial follicles throughout a woman's life (Figure 7.3) due to atresia or conversion to the active primary state. The decline in the number of follicles with age results in a noticeable decrease in AMH that begins in a woman's 20's (Figure 7.3) and a decrease in $InhB$ between ages 30 and 40 (Figure 7.5). These hormones are produced by preantral and early antral follicles (Figure 7.6). The drop in $InhB$ causes a rise in follicular phase FSH (Figure 7.5). Levels of $E2$, $P4$, $InhA$ and LH (Figure 7.4) do not exhibit significant changes between age 30 and 40 primarily because they depend on dominant follicle and corpus luteum development (Figure 7.6).

In order to obtain the 66 model parameters we develop an *ad hoc* procedure which results in a model predicting hormonal levels over multiple time scales. This is accomplished by optimizing the parameters of the system (SS1)-(SS2) for the primordial and primary follicles. Then the output of the optimized model (SS1)-(SS2) at any age is used to initiate simulations of the full system (SS1)-(SS16) at that age (see Section 7.4.2).

The age at which simulated cycling ceases because of a constant low LH level seems to be sensitive to parameters and may not represent the actual mechanism of loss of fertility with age. Changes to the model that may account for anovulation and the cessation of cycling would be incorporating thresholds for ovulation and atresia of the dominant follicle if it fails to ovulate. This could be accomplished with a threshold function for LH necessary for ovulation or a threshold for the number of follicles required for dominant follicle selection and ovulation. The latter option would require tracking the numbers of follicles that are developing during the preantral through growing follicle stages. At this point, the model only tracks the numbers of primordial and primary follicles with the remaining follicle stages represented as volumes. Such considerations will be topics of future work.

The fact that AMH inhibits the transition of follicles from the primordial stage to primary stage suggests several treatments using exogenous AMH to slow the activation of primordial follicles, or using an AMH antagonist to increase the number of growing follicles. Figure 7.7 shows that treatments with various doses of AMH may reduce the number of follicles entering the active pool and, hence, delay menopause as measured by the number of primordial follicles remaining in the ovaries. Model simulations show that high amounts of AMH are needed to reduce active follicle numbers to contraceptive levels (see Figure 7.8). Finally, Figure 7.9 shows how an AMH antagonist may temporarily increase the number of small growing follicles which

may improve fertility in a woman who is experiencing infertility due to low follicle count. These hypotheses would need to be investigated clinically.

The material in this chapter was previously published in the paper "A Lifelong Model for the Female Reproductive Cycle with an Antimüllerian Hormone Treatment to Delay Menopause" by Margolskee and Selgrade, 2013 [47]. We would like to thank Charles E. Smith for assistance regarding several statistical issues and two anonymous reviewers whose suggestions improved the paper.

Chapter 8

Summary and Future Work

Chapter 5 explored the affect of changing Km_{LH} in the Hill function in (S1) on the existence of one or more periodic solutions to (S1)-(S13). Km_{LH} is the half-saturation constant in the Hill function for the synthesis of LH (see eq. (S1)). It signifies the level of E2 required for significant LH synthesis. Bifurcation diagrams with respect to this parameter reveal an interval of parameter values for which a unique stable periodic solution exists and this solution represents a menstrual cycle during which ovulation occurs. The existence of multiple stable periodic solutions at a single parameter set indicates the possibility that a woman could be perturbed from an ovulatory cycle to an anovulatory one, or vice versa, due to outside forces.

Chapter 6 presented a variation on previous models to include the phenomenon of waves of follicular development throughout the monthly cycle. The appearance of follicle waves was accomplished by changing a combination of parameters which had the effect of decreasing the impact of the LH surge on the transition from ReF to GrF. This allows for a second wave of follicles to mature to the growing follicle stage in the luteal phase. Atresia of the second wave of follicles in the absence of an LH surge was included as a decay term of the stage $DomF$. It is interesting that changing a few parameter values could produce a second wave of follicular development in the existing model. Further analysis could be done on using this model to simulate follicle waves. Experimental data such as follicle diameter and growing follicle counts reported in Baerwald *et al.* 2003 [3] could be used for model fitting and/or validation.

Chapter 7 presented a variation on previous models to simulate key hormonal changes with age. Previous models could simulate the hormone profiles of women of different ages by supplying separate parameter sets for each age. Incorporating the constantly declining primordial pool of follicles that a woman is born with successfully simulates the decline in AMH from age 20 to 51, the decline in InhB and the subsequent rise in follicular phase FSH between ages 30 and 40. Model simulations using the administration of exogenous AMH show that the transfer of non-growing primordial follicles to the active state can be slowed enough to provide more

follicles for development later in life and to cause a delay in the onset of menopause as measured by the number of primordial follicles remaining in the ovaries.

This model successfully illustrates the decline in the pool of primordial follicles and decrease in AMH from age 20 to menopause, and the age-related changes in InhB and FSH hormone levels between mid-reproductive age and the early menopausal transition. However, the onset of menopause as measured by the cessation of monthly cycling has not been captured adequately by the model in its current form. Refinements could include incorporating an LH threshold for ovulation below which the dominant follicle fails to ovulate (similar to the atresia term in Chapter 6), or tracking follicle numbers beyond the primordial and primary stages through the antral stages insuring that a fraction of a follicle does not grow and ovulate. This latter modification may require a discrete model, or a model where the numbers of equations represent the numbers of growing follicles such as the follicle selection model described by Lacker, 1988 [40].

The mechanism of initiation of monthly cycling at puberty could also be explored in more detail and incorporated into the model. In female pre-adolescents, although primordial follicle count is high, serum AMH concentrations are low and gradually increase to their normal level by about age 8 [24]. The GnRH secretory system is fully developed during the fetal period, and experiences periods of activation during the fetal and very early neontal periods [17]. Puberty is marked by reactivation of the GnRH signaling pathway in the hypothalamus, and subsequent production of pituitary hormones and ovarian response. However, the gradual increase in AMH appears to occur prior to this change in gonadotropin production. Presumably AMH levels are increasing due to the transition of primordial follicles to the primary stage, but the mechanism behind this activation is unclear.

The model simulations in Chapter 7 began with age 20. Modeling the mechanism of puberty could have significant clinical impact for conditions such as precocious puberty and delayed or absent puberty. Though incorporation into the model may be problematic because the timing of puberty is affected by many internal and external factors such as growth, nutrition, body fat/composition, and stress (Ebling, 2005 [17]).

The model of Chapter 7 successfully illustrates the decline in the pool of primordial follicles and decrease in AMH from age 20 to menopause as reported in the biological literature. Model simulations show that administration of exogenous AMH has the potential to slow the transfer of non-growing primordial follicles to the active state. We mention the application of this to delaying menopause and as a contraceptive measure. It is also conceivable that exogenous AMH could be used in treating early onset puberty because it may prevent activation of primordial follicles from resting state, and thus the cascade of follicle development and ovarian hormone production.

REFERENCES

[1] F. Alvarez-Blasco, J. Botella-Carretero, J. S. Millan, and H. Escobar-Morreale, *Prevalence and characteristics of the polycystic ovary syndrome in overweight and obese women*, Archives of Internal Medicine, 166 (2006), pp. 2081–2086.

[2] R. Azziz, K. Woods, R. Reyna, T. Key, E. Knochenhauser, and B. Yildiz, *The prevalence and features of the polycystic ovary syndrome in an unselected population*, J. Clin. Endocrinol. Metab., 89 (2004), pp. 2745–2749.

[3] A. Baerwald, G. Adams, and R. Pierson, *Characterization of ovarian follicular wave dynamics in women*, Biol. Reprod., 69 (2003), pp. 1023–1031.

[4] H. Banks, M. Davidian, and J. Samuels, *An inverse problem statistical methodology summary*, 2007. http://www.ncsu.edu/crsc/reports/ftp/pdf/crsc-tr07-14.pdf.

[5] H. Boer, C. Stötzel, S. Röblitz, P. Deuflhard, R. Veerkamp, and H. Woelders, *A simple mathematical model of the bovine estrous cycle: Follicle development and endocrine interactions*, J. Theor. Biol., 278 (2011), pp. 20–31.

[6] R. Bogumil, M. Ferin, J. Rootenberg, L. Speroff, and R. Vande-Wiele, *Mathematical studies of the human menstrual cycle. I. Formulation of a mathematical model*, J. Clin. Endocrinol. Metab., 35 (1972), pp. 126–143.

[7] R. Bogumil, M. Ferin, and R. Vande-Wiele, *Mathematical studies of the human menstrual cycle II: Simulation of a model of the human menstrual cycle*, J. Clin. Endocrinol. Metab., 35 (1972), pp. 144–156.

[8] F. Broekmans, M. Faddy, G. Scheffer, and E. te Velde, *Antral follicle counts are related to age at natural fertility loss and age at menopause*, J. North Amer. Menopause Soc., 11 no. 6 (2004), pp. 607–614.

[9] F. Broekmans, M. Soules, and B. Fauser, *Ovarian aging: mechanisms and clinical consequences*, Endocr. Rev., 30 (2009), pp. 465–493.

[10] H. Burger, G. Hale, D. Robertson, and L. Dennerstein, *A review of hormonal changes during the menopausal transition: focus on findings from the Melbourne Women's Midlife Health Project*, Hum. Reprod. Update, 13 no. 6 (2007), pp. 559–565.

[11] D. Cacuci, *Sensitivity and Uncertainty Analysis Theory*, Chapman & Hall/CRC, Boca Raton, 2003.

[12] Y. Cobel Jr., P. Kohler, C. Cargille, and G. Ross, *Production rates and metabolic clearance rates of human follicle-stimulating hormone in premenopausal and postmenopausal women*, J. Clin. Investig., 48 (1969), pp. 359–363.

[13] G. Derry and P. Derry, *Characterization of chaotic dynamics in the human menstrual cycle*, Nonlinear Biomedical Physics, 4 no. 5 (2010).

[14] P. Deuflhard, *Newton Methods for Nonlinear Problems–Affine Invariance and Adaptive Algorithms*, Springer-Verlag, Berlin, 2004.

[15] E. Doedel, *AUTO: A program for the automatic bifurcation analysis of autonomous systems*, Congressus Numerantium, 30 (1981), pp. 265–284.

[16] A. Durlinger, J. Visser, and A. Themmen, *Regulation of ovarian function: the role of anti-mullerian hormone*, Reprod., 124 (2002), pp. 601–609.

[17] F. Ebling, *The neuroendocrine timing of puberty*, Reprod., 129 (2005), pp. 675–683.

[18] K. Engelborghs, T. Luzyanina, and D. Roose, *Numerical bifurcation analysis of delay differential equations*, Jour. of Comput. and Appl. Math., 125 (2000), pp. 265–275.

[19] B. Ermentrout, *Simulating, Analyzing, and Animating Dynamical Systems*, SIAM, Philadelphia, PA, 2002.

[20] P. Franchimont, K. Henderson, G. Verhoeven, M. Hazee-Hagelstein, C. Charlet-Renard, A. Demoulin, J. Bourguignon, and M. Lecomte-Yerna, *Inhibin: Mechanisms of action and secretion*, Intragonadal Regulation of Reproduction, (1981), pp. 167–191.

[21] O. Ginther, L. Knopf, and J. Kastelic, *Temporal associations among ovarian events in cattle during oestrous cycles with two and three follicular waves*, J. Reprod. Fertil., 87 (1989), pp. 223–230.

[22] M. Golubitsky and D. G. Schaeffer, *Singularities and Groups in Bifurcation Theory*, vol. 1, Springer-Verlag, New York, 1985.

[23] N. Groome, P. Illingworth, M. O'brien, R. Pai, F. Rodger, J. Mather, and A. McNeilly, *Measurement of dimeric inhibin B throughout the human menstrual cycle*, J. Clin. Endocrinol. Metab., 81 no. 4 (1996), pp. 1401–1405.

[24] C. Hagen, L. Aksglaede, K. Sorensen, K. Main, M. Boas, L. Cleemann, K. Holm, C. Gravholt, A. Andersson, A. Pedersen, J. Petersen, A. Linneberg, S. Kjaergaard, and A. Juul, *Serum levels of anti-mullerian hormone as a marker of ovarian function in 926 healthy females from birth to adulthood and in 172 Turner syndrome patients*, J. Clin. Endocrinol. Metab., 95 (2010), pp. 5002–5010.

[25] G. Hale, X. Zhao, C. Hughes, H. Burger, D. Robertson, and I. Fraser, *Endocrine features of menstrual cycles in middle and late reproductive age and the menopausal transition classified according to the staging of reproductive aging workshop (STRAW) staging system*, J. Clin. Endocrinol. Metab., 92 (2007), pp. 2060–3067.

[26] J. Hale, *Theory of Differential Equations*, Springer-Verlag, 1977.

[27] R. Hampl, M. Snajderova, and T. Mardesic, *Antimullerian hormone (AMH) not only a marker for prediction of ovarian reserve*, Physiol. Res., 60 (2011), pp. 217–223.

[28] K. Hansen, N. Knowlton, A. Thyer, J. Charleston, M. Soules, and N. Klein, *A new model of reproductive aging: the decline in ovarian non-growing follicle number from birth to menopause*, Hum. Reprod., 23 no. 3 (2008), pp. 699–708.

[29] L. Harris, *Differential equation models for the hormonal regulation of the menstrual cycle*, PhD thesis, North Carolina State University, Raleigh, North Carolina, 2001. http://www.lib.ncsu.edu/resolver/1840.16/4693.

[30] L. Harris-Clark, P. Schlosser, and J. Selgrade, *Multiple stable periodic solutions in a model for hormonal control of the menstrual cycle*, Bull. Math. Biol., 65 (2003), pp. 157–173.

[31] P. Hudson, I. Dougas, P. Donahoe, R. Cat, J. Epstein, R. Pepinsky, and D. MacLaughlin, *An immunoassay to detect human mullerian inhibiting substance in males and females during normal development*, J. Clin. Endocrinol. Metab., 70 (1990), pp. 16–22.

[32] P. D. I. Reinecke, *A complex mathematical model of the human menstrual cycle*, J. Theor. Biol., 247 (2007), pp. 303–330.

[33] I. Ipsen, C. Kelley, and S. Pope, *Rank-deficient nonlinear least squares problems and subset selection*, Siam J. Numer. Anal., 49 (2011), pp. 1244–1266.

[34] L. P. Jr. and S. Luxenberg, *Biological modeling on a microcomputer using standard spreadsheet and equation solver programs: The hypothalamic-pituitary-ovarian axis as an example*, Comput. Biomed. Res., 25 (1992), pp. 117–130.

[35] F. Karsch, D. Dierschke, R. Weick, J. H. T. Yamaji, and E. Knobil, *Positive and negative feedback control by estrogen of luteinizing hormone secretion in the rhesus monkey*, Endocrinol., 92 (1973), pp. 799–804.

[36] J. Keener and J. Sneyd, *Mathematical Physiology I: Cellular Physiology*, Springer-Verlag, New York, 2nd ed., 2009.

[37] C. Kelley, *Iterative Methods for Optimization*, vol. 18 of Frontiers in Applied Mathematics, SIAM, Philadelphia, 1999.

[38] N. A. Klein, A. J. Harper, B. S. Houmard, P. M. Sluss, and M. R. Soules, *Is the short follicular phase in older women secondary to advanced or accelerated dominant follicle development?*, J. Clin. Endocrinol. Metab., 87 (2002), pp. 5746–5750.

[39] P. Kohler, G. Ross, and W. Odell, *Metabolic clearance and production rates of human luteinizing hormone in pre- and postmenopausal women*, J. Clin. Investig., 47 no. 1 (1968), pp. 38–47.

[40] H. Lacker, *How do the ovaries count?*, Math. Biosci., 90 (1988), pp. 305–332.

[41] M. Lee, P. Donahoe, T. Hasegawa, B. Silverman, G. Crist, S. Best, Y. Hasegawa, R. Noto, D. Schoenfeld, and D. MacLaughlin, *Mullerian inhibiting*

substance in humans: normal levels from infancy to adulthood, J. Clin. Endocrinol. Metab., 81 (1996), pp. 571–576.

[42] J. Liu and S. Yen, *Induction of midcycle gonadotropin surge by ovarian steroids in women: A critical evaluation*, J. Clin. Endocrinol. Metab., 57 (1983), pp. 797–802.

[43] G. Maciel, E. Baracat, J. Benda, S. Markham, K.Hensinger, R. Chang, and G. Erickson, *Stockpiling of transitional and classic primary follicles in ovaries of women with polycystic ovary syndrome*, J. Clin. Endocrinol. Metab., 89 (2004), pp. 5321–5327.

[44] A. L. Marca, G. Stabile, A. C. Artenisio, and A. Volpe, *Serum anti-mullerian hormone throughout the human menstrual cycle*, Hum. Reprod., 21 no. 12 (2006), pp. 3103–3107.

[45] A. Margolskee, *ddeRK4*, 2012. http://www4.ncsu.edu/∼amargol/research/ddeRK4.html.

[46] A. Margolskee and J. Selgrade, *Bifurcation analysis of a model for hormonal regulation of the menstrual cycle with inhibin delay*, Math. Biosci., 234 (2011), pp. 95–107.

[47] ——, *A lifelong model for the female reproductive cycle with an antimllerian hormone treatment to delay menopause*, J. Theor. Biol., 326 no. 7 (2013), p. 2135.

[48] J. McIntosh and R. McIntosh, *Mathematical Modeling and Computers in Endocrinology*, Springer-Verlag, Berlin, 1980.

[49] R. McLachlan, N. Cohen, K. Dahl, W. Bremner, and M. Soules, *Serum inhibin levels during the periovulatory interval in normal women: Relationships with sex steroid and gonadotrophin levels*, Clin. Endocrinol., 32 (1990), pp. 39–48.

[50] R. McLachlan, N. Cohen, K. Dahl, and M. S. W.J. Bremner, *Serum inhibin levels during the periovulatory interval in normal women: Relationships with sex steroid and gonadotrophin levels*, Clin. Endocrinol., 32 (1990), pp. 39–48.

[51] J. Meiss, *Differential Dynamical Systems*, SIAM, Philadelphia, 2007.

[52] S. Nussey and S. Whitehead, *Endocrinology: An Integrated Approach*, Taylor & Francis, London, 2001.

[53] W. Odell, *The reproductive system in women*, in: *Endocrinology*, Grune & Stratton, New York, 1979, pp. 1383–1400.

[54] S. Ojeda, *Female reproductive function*, in: *Textbook of Endocrine Physiology*, Oxford University Press, Oxford, 2nd ed., 1992, pp. 134–188.

[55] M. Olufsen and J. Ottesen, *A practical approach to parameter estimation applied to model predicting heart rate regulation*, J. Math. Biol., (2012), pp. 1–30.

[56] R. Ott and M. Longnecker, *An Introduction to Statistical Methods and Data Analysis*, Brooks/Cole Cengage Learning, 6th ed., 2010.

[57] R. Pasteur, *A multiple-inhibin model for the human menstrual cycle*, PhD thesis, North Carolina State University, Raleigh, North Carolina, 2008. http://www.lib.ncsu.edu/resolver/1840.16/5587.

[58] A. Ralston and P. Rabinowitz, *A First Course in Numerical Analysis*, Mcgraw-Hill, New York, 2nd ed., 1978.

[59] S. Ramaswamy, C. Pohl, A. McNeilly, S. Winters, and T. Plant, *The time course of follicle-stimulating hormone suppression by recombinant human inhibin A in the adult rhesus monkey*, Endocrinology, 139 (1998), pp. 3409–3415.

[60] P. Reddy, W. Zheng, and K. Liu, *Mechanisms maintaining the dormancy and survival of mammalian primordial follicles*, Trends Endocrinol. Metab., 21 (2009), pp. 96–103.

[61] D. Robertson, G. Hale, I. Fraser, C. Hughes, and H. Burger, *A proposed classification system for menstrual cycles in the menopause transition based on changes in serum hormone profiles*, Menopause: J. North Amer. Menopause Soc., 15 no. 6 (2008), pp. 1139–1144.

[62] D. Robertson, G. Hale, D. Jolley, I. Fraser, C. Hughes, and H. Burger, *Interrelationships between ovarian and pituitary hormones in ovulatory menstrual cycles across reproductive age*, J. Clin. Endocrinol. Metab., 94 (2009), pp. 138–144.

[63] D. Robertson, M. Prisk, J. McMaster, D. Irby, J. Findlay, and D. deKretser, *Serum FSH-suppressing activity of human recombinant inhibin A in male and female rats*, J. of Reproduction & Fertility, 91 (1991), pp. 321–328.

[64] D. Robertson and P. F. R. Hertan, *Is the action of inhibin mediated via a unique receptor?*, Reviews of Reproduction, 5 (2000), pp. 131–135.

[65] R. Robinson, *An Introduction to Dynamical Systems: Continuous and Discrete*, Pearson Prentice Hall, New Jersey, 2004.

[66] P. Schlosser and J. Selgrade, *A model of gonadotropin regulation during the menstrual cycle in women: Qualitative features*, Environ. Health Perspect., 108 suppl. 5 (2000), pp. 873–881.

[67] R. Scott and H. Burger, *Mechanism of action of inhibin*, Biol. of Reproduction, 24 (1981), pp. 541–550.

[68] J. Selgrade, *Bifurcation analysis of a model for hormonal regulation of the menstrual cycle*, Math. Biosci., 225 (2010), pp. 108–114.

[69] J. Selgrade, L. Harris, and R. Pasteur, *A model for hormonal control of the menstrual cycle: structural consistency but sensitivity with regard to data*, J. Theor. Biol., 260 (2009), pp. 572–580.

[70] J. Selgrade and P. Schlosser, *A model for the production of ovarian hormones during the menstrual cycle*, Fields Inst. Comm., 21 (1999), pp. 429–446.

[71] L. Shampine and S. Thompson, *Solving DDEs in MATLAB*, Appl. Numer. Math., 37 (2001), pp. 441–458.

[72] M. Skinner, *Regulation of primordial follicle assembly and development*, Hum. Reprod. Update, 11 no. 5 (2005), pp. 461–471.

[73] A. Sonin, *The physical basis of dimensional analysis*, Dept. of Mech. Eng. MIT, 2nd ed., 2001.

[74] M. Soules, S. Sherman, E. Parrott, R. Rebar, N. Santoro, W. Utian, and N. Woods, *Stages of reproductive aging workshop (STRAW)*, J. Womens Health & Gender-Based Med., 10 (2001), pp. 843–848.

[75] M. Sowers, A. Eyvazzadeh, D. McConnell, M. Yosef, M. Jannausch, D. Zhang, S. Harlow, and J. Randolph Jr., *Anti-mullerian hormone and inhibin B in the definition of ovarian aging and the menopause transition*, J. Clin. Endocrinol. Metab., 93 (2008), pp. 3478–3483.

[76] M. Sowers, D. McConnel, K. Gast, H. Zheng, B. Nan, J. McCarthy, and J. Randolph, *Anti-Mullerian hormone and inhibin B variability during normal menstrual cycles*, Fertil. Steril., 94 no. 4 (2010).

[77] F. Tehrani, M. Solaymani-Dodaran, M. Hedayati, and F. Azizi, *Is polycystic ovary syndrome an exception for reproductive aging?*, Hum. Reprod., 25 (2010), pp. 1775–1781.

[78] A. Treloar, R. Boynton, B. Behn, and B. Brown, *Variation of the human menstrual cycle through reproductive life*, International Jour. of Fertility, 12 (1967), pp. 77–126.

[79] R. van Beek, M. van den Heuvel-Eibrink, J. Laven, F. de Jong, A. Themmen, F. Hakvoort-Cammel, C. van den Bos, H. van den Berg, R. Pieters, and S. de Muinck Keizer-Schrama, *Anti-mullerian hormone is a sensitive serum marker for gonadal function in women treated for Hodgkin's lymphoma during childhood*, J. Clin. Endocrinol. Metab., 92 (2007), pp. 3189–3874.

[80] J. van Disseldorp, M. Faddy, A. Themmen, F. de Jong, P. Peeters, Y. van der Schouw, and F. Broekmans, *Relationship of serum antimullerian hormone concentration to age at menopause*, J. Clin. Endocrinol. Metab., 93 (2008), pp. 2129–2134.

[81] P. van Zonneveld, G. Scheffer, F. Broekmans, M. Blankenstein, F. Jong, C. Looman, J. Habbema, and E. te Velde, *Do cycle disturbances explain the age-related decline of female fertility? Cycle characteristics of women aged over 40 years compared with a reference population of young women*, Hum. Reprod., 18 (2003), pp. 495–501.

[82] J. Visser, F. de Jong, J. Laven, and A. Themmen, *Anti-mullerian hormone: a new marker for ovarian function*, Soc. for Reprod. and Fertil., 131 (2006), pp. 1–9.

[83] C. Welt, D. McNicholl, A. Taylor, and J. Hall, *Female reproductive aging is marked by decreased secretion of dimeric inhibin*, J. Clin. Endocrinol. Metab., 84 (1999), pp. 105–111.

[84] Y. White, D. Woods, Y. Takai, O. Ishihara, H. Seki, and J. Tilly, *Oocyte formation by mitotically active germ cells purified from ovaries of reproductive-age women*, Nature Medicine, 18 no. 3 (2012), pp. 413–421.

[85] D. Wunder, N. Bersinger, M. Yared, R. Kretschmer, and M. Birkhauser, *Statistically significant changes of antimullerian hormone and inhibin levels during the physiologic menstrual cycle in reproductive age women*, Fertil. Steril., 89 (2008), pp. 927–933.

[86] S. Yen, *The human menstrual cycle: Neuroendocrine regulation*, in: *Reproductive Endocrinology: Physiology, Pathophysiology and Clinical Management*, W.B. Saunders Co., Philadelphia, 4th ed., 1999, pp. 191–217.

[87] ——, *Polycystic ovarian syndrome (hyperandrogenic chronic anovulation)*, in: *Reproductive Endocrinology: Physiology, Pathophysiology and Clinical Management*, W.B. Saunders Co., Philadelphia, 4th ed., 1999, pp. 436–478.

[88] A. Zeleznik, *The physiology of follicle selection*, Reprod. Biol. Endocrinol., 2 (2004), p. 31.

[89] ZIB, *Zuse Institut Berlin: Newton Lib.* http://www.zib.de/en/numerik/software/newton lib.html.

APPENDICES

Appendix A

ddeRK4

```
% ddeRK4
% Last updated 10/12/2012
% Alison Margolskee
%
% delay differential equation solver using explicit 4th order
% fixed-step Runge Kutta integrator and Quartic Hermite
% interpolating polynomial to determine lagged values from stored history
% For implementation in Matlab Version 7.12

function sol = ddeRK4(ddefun,lags, history, t0, tf, h, options,varargin)

% Output:
% sol
%   .x = time steps
%   .y = solution at time steps .x
%   .yp = derivative at time steps .x
%       allows user to perform hermite interpolation to
%       obtain solution at time points not in .x, if desired
%
% Input:
% ddefun = delay differential equation
%       has the form dydt = ddefun(t, y, z, varargin)
%       where t = time, y = state variable (can be a col. vector or a scalar)
%       and z = [ y(tau1), y(tau2), ... ]
%               row vector of delayed state variables
```

```
%               (or matrix if y is a column vector)
% lags = (tau1, tau2, ....) = delays (must be positive)
% history = constant initial history or function of time defined on
%       the interval [t0 - max(lags), t0]
% t0 = initial time
% tf = final time
% h = time step
% options
%   .Nsteps = #steps to skip between writing to output
%       this option allows you to integrate with a
%       small step and save storage by skipping
%       steps in storage (default = 0)
%   .transient = time to run integrator before storing
%       allows integrator to approach a stable attractor before
%       storing the solution (default = t0)
% varargin = extra arguments to feed to ddefun

if min(lags)<=0
    error('Error: delays must be positive');
end
if max(lags) + 2*h > (tf - t0)
    error('Error: maximum delay must be less than tf - t0 by at least
              two time steps')
end

%%%%%%%%%% Set up options %%%%%%%%%%%%

defaultopt.Nsteps = 0;
defaultopt.transient = t0;

if nargin < 7
    options = defaultopt;
elseif isempty(options)
    options = defaultopt;
else
    allfields = {'Nsteps';'transient'};
    for i = 1:length(allfields)
```

```
        try
            options.(cell2mat(allfields(i,:)));
        catch ME
            options.(cell2mat(allfields(i,:))) ...
                = defaultopt.(cell2mat(allfields(i,:)));
        end
    end

end

Nsteps = options.Nsteps;
transient = options.transient;

%%%%%%%%%%%%%%%%%%%%%%%%%%%%%%%%%%%%%%%%%%%%


%%%%% Determine initial y, yp and z
if isnumeric(history)
  y0 = history;
  sol.history = history;
else
  y0 = feval(history,t0,varargin{:});
  sol.history = history;
end
neq = length(y0);

Z0 = zeros(neq, length(lags));
for j = 1:length(lags)
    if isnumeric(history)
        Z0(:,j) = history;
    else
        Z0(:,j) = feval(history,t0 - lags(j),varargin{:});
    end
end

yp0 = feval(ddefun,t0,y0,Z0,varargin{:});
```

```
% total time interval for integrator
tspan=t0:h:tf;

%%%%%%%%%% Initialize output %%%%%%%%%%
% tout, yout, and ypout
temp = find(transient <= tspan,1,'first');
tout = tspan(temp:(Nsteps+1):end);

yout = zeros(neq,length(tout));
ypout = zeros(neq,length(tout));
nout = 0;
nsteps = 0;

if t0 >= transient
    nout = nout + 1;
    nsteps = nsteps + 1;
    yout(:,1) = y0;
    ypout(:,1) = yp0;
end


%%%%%% Initialize History Storage %%%%%
% Thist, Yhist and YPhist
% determine size of storage for history
Nhist = find( max(lags) >= tspan - t0, 1, 'last') + 2;
Thist = tspan(1:Nhist) - max(lags) - 2*h;

Yhist = zeros(neq, Nhist);
Yhist(:,:) = y0*ones(1, Nhist);

YPhist = zeros(neq, Nhist);
YPhist(:,:) = yp0*ones(1, Nhist);


%%%%%%  Set up RK4 algorithm %%%%%%%%%%
C=[0, 1/2, 1/2, 1, 1];
A=[
```

```
    0   1/2 0   0
    0   0   1/2 0
    0   0   0   1
    0   0   0   0];
B=[1/6  1/3 1/3 1/6]';

hA = h*A;
hB = h*B;
hC = h*C;
%%%%%%%%%%%%%%%%%%%%%%%%%%%%%%%%%%%%%%%%

y = y0;

f=zeros(neq,4);
f(:,1) = yp0;

%%%% Perform RK4 step for each time point t in tspan %%%
for nspan = 2:length(tspan)

    t=tspan(nspan-1);

    %%%%%%%%%%%% Set up RK4 time points %%%%%%%%%%%%%%%%
    t2 = t + hC(2);
    t3 = t + hC(3);
    t4 = t + hC(4);
    tnew = t + hC(5);

    %%%%%%%%%% Determine lagged values Z2, Z3, Z4, Znew

    Z2 = zeros(neq, length(lags));
    Z3 = zeros(neq, length(lags));
    Z4 = zeros(neq, length(lags));
    Znew = zeros(neq, length(lags));

    for j = 1:length(lags)
        % If lagged times are <= t0, use user-defined history
        if t4 - lags(j) <= t0
```

```
    if isnumeric(history)
        Z2(:,j) = history;
        Z3(:,j) = history;
        Z4(:,j) = history;
        Znew(:,j) = history;
    else
        Z2(:,j) = feval(history,t2 - lags(j),varargin{:});
        Z3(:,j) = feval(history,t3 - lags(j),varargin{:});
        Z4(:,j) = feval(history,t4 - lags(j),varargin{:});
        Znew(:,j) = feval(history,tnew - lags(j),varargin{:});
    end
elseif t2 - lags(j) <= t0
    if isnumeric(history)
        Z2(:,j) = history;
        Z3(:,j) = history;
    else
        Z2(:,j) = feval(history,t2 - lags(j),varargin{:});
        Z3(:,j) = feval(history,t3 - lags(j),varargin{:});
    end
else
    indices = find(t2 - lags(j) >= Thist(1:end-1));

    D = indices(end);

    %%%%%%%%%%%%%%%%%%% Quartic Hermite Interpolation %%%%%%%%%%
    % interpolating polynomial of the form
    %
    %     p= @(t,a,x) a(:,1) + a(:,2)*(t-x(1)) ...
    %       + a(:,3)*(t-x(1)).^2 ...
    %       + a(:,4)*(t-x(1)).^2.*(t-x(2)) ...
    %       + a(:,5)*(t-x(1)).^2.*(t-x(2)).^2 ;
    %
    %     dp= @(t,a,x) a(:,2) + 2*a(:,3)*(t-x(1)) ...
    %       + a(:,4)*(2*(t-x(1))*(t-x(2))+(t-x(1))^2) ...
    %       + a(:,5)*(2*(t-x(1))*(t-x(2))^2 ...
    %       + 2*(t-x(1))^2*(t-x(2))) ;
    %
```

```
alpha = zeros(length(y0),5);

% a(:,1) = p(x(1),a,x)
alpha(:,1)=Yhist(:,D-1);

% a(:,2) = dp(x(1),a,x)
alpha(:,2)=YPhist(:,D-1);

% a(:,3) = (y(:,2) - p(x(2),a,x) )/(x(2)-x(1))^2;
alpha(:,3) = ...
    ( (Yhist(:,D) - alpha(:,1) )/(Thist(D)-Thist(D-1))...
    - alpha(:,2) )/(Thist(D)-Thist(D-1))- alpha(:,3) ;

% a(:,4) = (dy(:,2) - dp(x(2),a,x) )/(x(2)-x(1))^2;
alpha(:,4) = ...
    ( (YPhist(:,D) - alpha(:,2) )/(Thist(D)-Thist(D-1)) ...
    - 2*alpha(:,3) )/(Thist(D)-Thist(D+1)) - alpha(:,4) ;

% a(:,5) = (y(:,3) - p(x(3),a,x))/((x(3)-x(1))^2*(x(3)-x(2))^2);
alpha(:,5)=( ( ( ( Yhist(:,D+1) ...
    - alpha(:,1))/(Thist(D+1)-Thist(D-1)) ...
    - alpha(:,2) )/(Thist(D+1)-Thist(D-1)) ...
    - alpha(:,3) )/(Thist(D+1)-Thist(D)) ...
    - alpha(:,4) )/(Thist(D+1)-Thist(D)) - alpha(:,5);

%%%%%% Evaulate lagged values with interpolating polynomial
Z2(:,j) = alpha(:,1) + (t2 - lags(j) - Thist(D-1))*(alpha(:,2)...
    + (t2 - lags(j) - Thist(D-1)) *( alpha(:,3) ...
    + (t2 - lags(j) - Thist(D))*( alpha(:,4) ...
    + alpha(:,5)*(t2 - lags(j) - Thist(D))  ) ) );

Z3(:,j) = alpha(:,1) + (t3 - lags(j) - Thist(D-1))*(alpha(:,2)...
    + (t3 - lags(j) - Thist(D-1)) *( alpha(:,3) ...
    + (t3 - lags(j) - Thist(D))*( alpha(:,4) ...
    + alpha(:,5)*(t3 - lags(j) - Thist(D))  ) ) );

Z4(:,j) = alpha(:,1) + (t4 - lags(j) - Thist(D-1))*(alpha(:,2)...
```

```
            + (t4 - lags(j) - Thist(D-1)) *( alpha(:,3) ...
            + (t4 - lags(j) - Thist(D))*( alpha(:,4) ...
            + alpha(:,5)*(t4 - lags(j) - Thist(D))  ) ) );

        Znew(:,j) = alpha(:,1) ...
            + (tnew - lags(j) - Thist(D-1))*(alpha(:,2)...
            + (tnew - lags(j) - Thist(D-1)) *( alpha(:,3) ...
            + (tnew - lags(j) - Thist(D))*( alpha(:,4) ...
            + alpha(:,5)*(tnew - lags(j) - Thist(D))  ) ) );
        %%%%%%%%%%%%%%%%%%%%%%%%%%%%%%%%%%%%%%%%%%%%%%%%%%%%%%%%%%%%%%%%%%%%%%%

    end
end

%%%%%%%%%%%%%% Determine ynew %%%%%%%%%%%%%%%%%%%%%

f(:,2) = feval(ddefun,t2,y+f*hA(:,2),Z2,varargin{:});
f(:,3) = feval(ddefun,t3,y+f*hA(:,3),Z3,varargin{:});
f(:,4) = feval(ddefun,t4,y+f*hA(:,4),Z4,varargin{:});

ynew = y + f*hB;

%%%%%%%%%%%%%%%% Update history %%%%%%%%%%%%%%%%%%%%
Yhist(:,1:Nhist-1) = Yhist(:,2:Nhist);
Yhist(:,Nhist) = ynew;

YPhist(:,1:Nhist-1) = YPhist(:,2:end);
YPhist(:,Nhist) = feval(ddefun,tnew,ynew,Znew,varargin{:});

Thist(1:Nhist-1) = Thist(2:Nhist);
Thist(Nhist) = tnew;
%%%%%%%%%%%%%%%%%%%%%%%%%%%%%%%%%%%%%%%%%%%%%%%%%%%%

if tnew >= transient
    if ~mod(nsteps, Nsteps+1)
        % if after transient period, and
        % if Nsteps have been reached, write to yout
```

```
            nout = nout + 1;
            yout(:,nout) = Yhist(:,Nhist);
            ypout(:,nout) = YPhist(:,Nhist);
        end
        nsteps = nsteps + 1;
    end

    y = ynew;
    f(:,1) = YPhist(:,Nhist);
end

sol.x = tout;
sol.y = yout;
sol.yp = ypout;
```

Appendix B

Bifurcation theory

Meiss 2007 [51] described a bifurcation as a "qualitative change in dynamics occurring upon a small change in a parameter." Bifurcations can occur when equilibria are created or destroyed or when a change in the stability of an equilibrium is observed in response to a change in parameter value. For example, in a saddle-node bifurcation varying a parameter results in the merging and disappearance of a saddle equilibrium and a node (see Figure B.1). A pitchfork bifurcation and a transcritical bifurcation are two more examples of bifurcations involving the destruction/creation and changes in stability of equilibria (see Figure B.2).

$$\dot{x} = -x \tag{B.1}$$

$$\dot{y} = -(y^2 + \mu) \tag{B.2}$$

The equations above represent a two-dimensional system that exhibits a saddle-node bifurcation in the parameter μ. Setting the right-hand sides equal to zero, we find the equilibrium solutions to be $(0,-\sqrt{-\mu})$ and $(0,\sqrt{-\mu})$. We can already see that there are two equilibria for $\mu < 0$, one equilbrium when $\mu = 0$, and no equilibria when $\mu > 0$. Linearizing about the equilibria, we can determine their stability.

$$\text{Linearization about } (0, -\sqrt{-\mu}): \qquad \begin{bmatrix} -1 & 0 \\ 0 & 2\sqrt{-\mu} \end{bmatrix}$$

$$\text{Linearization about } (0, \sqrt{-\mu}): \qquad \begin{bmatrix} -1 & 0 \\ 0 & -2\sqrt{-\mu} \end{bmatrix}$$

The eigenvalues for $(0,-\sqrt{-\mu})$ are -1 and $2\sqrt{-\mu}$, thus this equilibrium is a saddle (when $\mu < 0$). For $(0,\sqrt{-\mu})$ the eigenvalues are -1 and $-2\sqrt{-\mu}$, thus this equilibrium is a stable node

(when $\mu < 0$). These equilibria only exist for $\mu \leq 0$. When μ crosses 0, we have a degenerate equilbrium at $(0, 0)$. When μ is positive, there are no equilibrium solutions. Figure B.1 depicts the dynamics of this bifurcation.

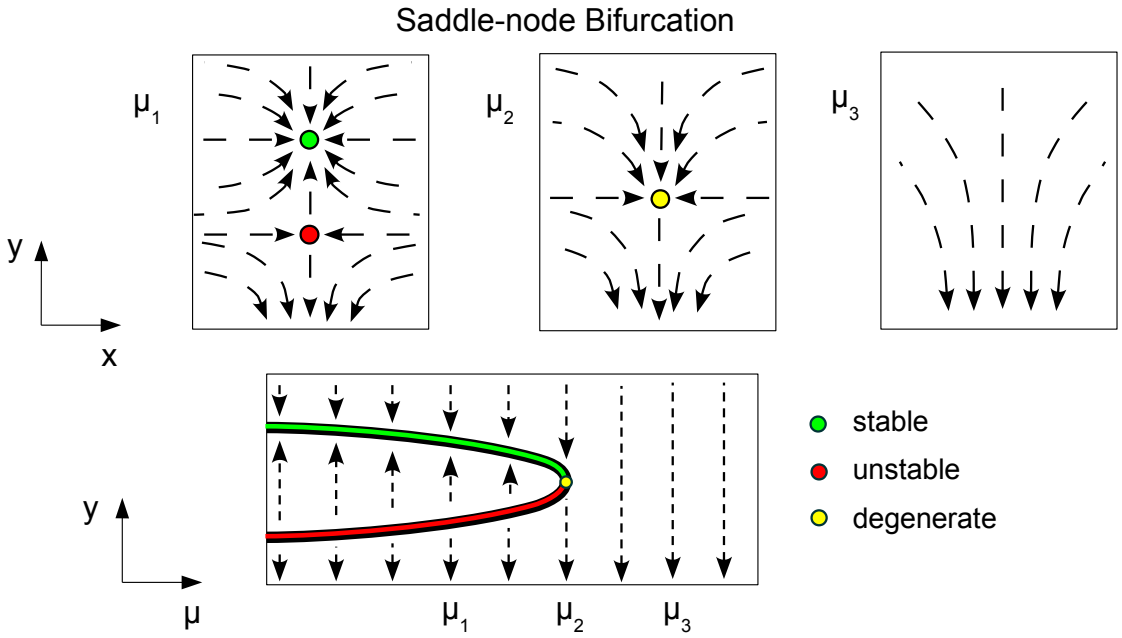

Figure B.1: Saddle-node bifurcation depicted in the phase space (top) and the corresponding bifurcation diagram plotted against the varied parameter "μ". In this bifurcation an unstable saddle equilibrium and a stable node combine and disappear.

$$\dot{x} = -x \tag{B.3}$$

$$\dot{y} = -(y^2 + \mu) \cdot y \tag{B.4}$$

The equations above represent a two-dimensional system that exhibits a pitchfork bifurcation in the parameter μ. The equilibria for this system are (0,0), and $(0,\pm\sqrt{-\mu})$, the latter of which only exist for $\mu \leq 0$. When μ crosses 0, we have a degenerate equilbrium at $(0, 0)$. When μ is positive, there is only one equilibrium solution (0,0). The stability of the equilibria can be determined by looking at the linearization. The eigenvalues for $(0,\pm\sqrt{\mu})$ are -1 and 2μ, thus these equilibria are stable nodes (when $\mu < 0$). For $(0, 0)$ the eigenvalues are -1 and $-\mu$, thus this equilibrium is an unstable node for $\mu < 0$, and a stable node for $\mu > 0$. Figure B.2 depicts

the dynamics of this bifurcation.

$$\dot{x} = -x \tag{B.5}$$

$$\dot{y} = -(y + \mu) \cdot y \tag{B.6}$$

The equations above represent a two-dimensional system that exhibits a transcritical bifurcation in the parameter μ. The equilibria for this system are $(0, 0)$ and (0,-μ). When μ crosses 0, these two equilibria come together creating a degenerate equilbrium at $(0, 0)$. When μ is positive, the equilibria have crossed to opposite sides of each other. The stability of the equilibria can be determined by looking at the linearization. The eigenvalues for $(0, 0)$ are -1 and -μ, thus this equilibrium is unstable when $\mu < 0$ and stable when $\mu > 0$. For $(0,-\mu)$ the eigenvalues are -1 and μ, thus this equilibrium is stable when $\mu < 0$, and unstable when $\mu > 0$. Figure B.2 depicts the dynamics of this bifurcation.

Each of the bifurcations mentioned thus far can also occur between combinations of stable and unstable periodic solutions, by just applying the stability analysis to the return map of the periodic orbits. There are also bifurcations that can involve both equilibria and periodic solutions. For example, a Hopf bifurcation occurs when a stable equilibrium with a pair of complex eigenvalues becomes unstable and gives rise to a stable periodic orbit (see Figure B.3).

$$\dot{x} = \left(\mu - \left(x^2 + y^2\right)\right) \cdot x + y \tag{B.7}$$

$$\dot{y} = \left(\mu - \left(x^2 + y^2\right)\right) \cdot y - x \tag{B.8}$$

The equations above represent a two-dimensional system that exhibits a hopf bifurcation in the parameter μ. There is a single equilibrium for this system at $(0, 0)$. The linearization about $(0, 0)$ reveals a pair of complex eigenvalues $\mu \pm i$. For $\mu < 0$, this equilibrium is a stable spiral, for $\mu > 0$, this equilibrium is an unstable spiral. For $\mu > 0$ there is also a periodic orbit encircling $(0, 0)$. The orbit has the form of a circle of radius $\sqrt{\mu}$ centered at $(0, 0)$. This can be more easily observed if the system is expressed in polar coordinates:

$$\dot{r} = (\mu - r^2) \cdot r \tag{B.9}$$

$$\dot{\theta} = -1 \tag{B.10}$$

Here we can see that when $r = \sqrt{\mu}$, we have $\dot{r} = 0$, implying that the circle of radius $\sqrt{\mu}$ is invariant under this system of differential equations. This along with the constant rotation in

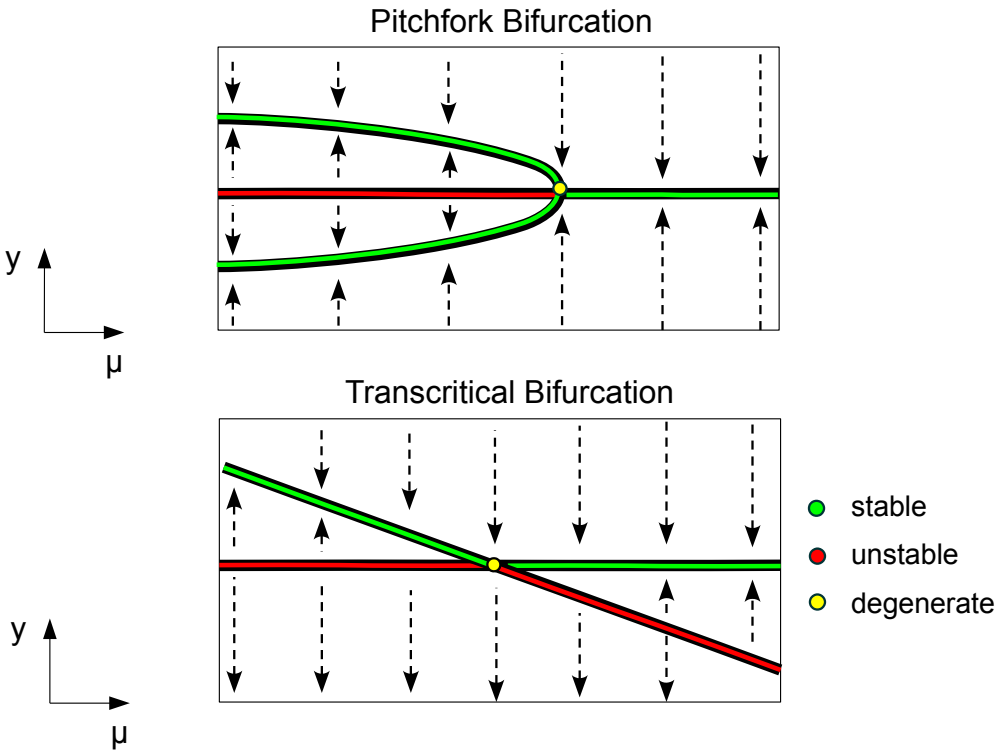

Figure B.2: Bifurcation diagrams are plotted against the varied parameter "μ". In the pitchfork bifurcation (top) two stable equilibria combine and disappear while crossing an unstable equilibrium which then becomes stable. In the transcritical bifurcation (bottom) one unstable and one stable equilibrium cross and switch stability.

the direction of $-\theta$ reveals that this invariant set is the circle of radius $\sqrt{\mu}$ centered at $(0, 0)$.

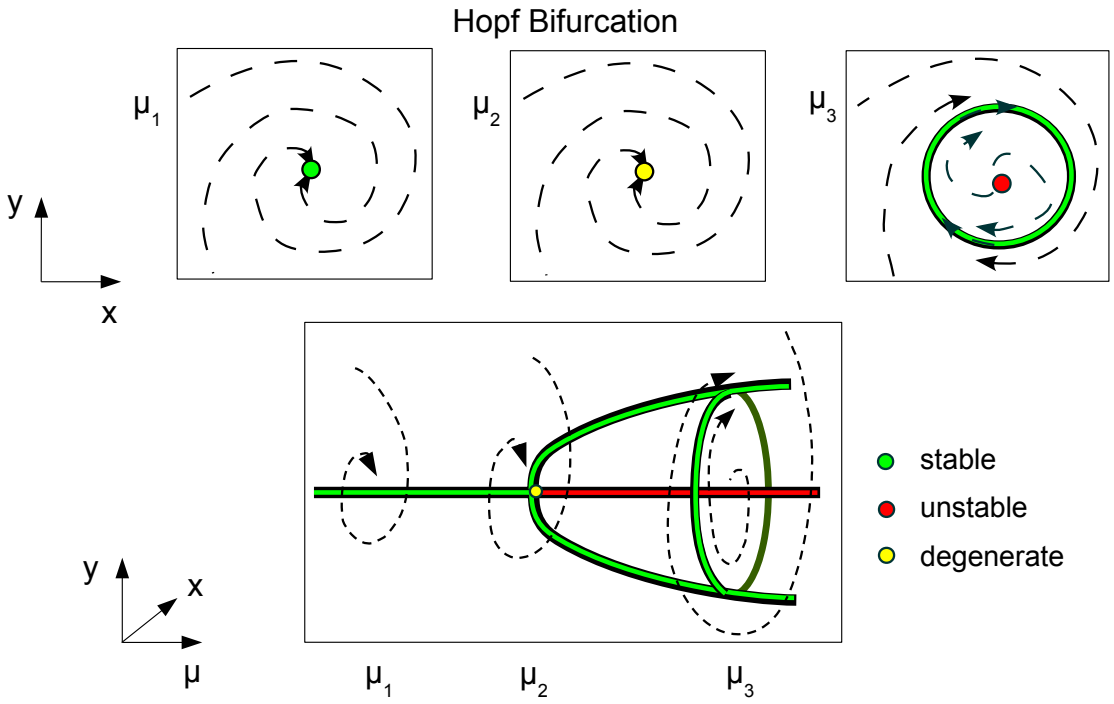

Figure B.3: A hopf bifurcation is depicted in the phase space (top) and the corresponding bifurcation diagram is plotted against the varied parameter "μ". In this bifurcation a stable equilibrium with a pair of complex eigenvalues becomes unstable and gives rise to a stable periodic orbit.

Appendix C

Using DDE-BIFTOOL

In this section we discuss how to produce a bifurcation diagram using the Matlab package DDE-BIFTOOL [18]. We start with several files that need to be created. These include a file to set the path to the toolbox, a file defining the right hand side of the system of delay differential equations, a file specifying the location of the delays in the parameter list, and a file containing the derivative of the delay system with respect to the state variables and parameters. Then we describe the steps to creating a branch of steady state solutions, including setting up the steady state solution structure, finding/verifying that a point is a steady state, computing the stability of steady state, and continuing a branch starting from a few steady state solution points. Finally we discuss finding a hopf bifurcation and creating a branch of periodic orbits emanating from a hopf bifurcation.

C.1 Files we need to create:

The following subsections describe files that must be created and saved in the current folder or added to the path in Matlab. The files are sys_init.m, sys_rhs.m, sys_tau.m, sys_deriv.m, and must have these specific names. The file 'sys_init.m' is the system initialization function. It lets Matlab know where to find the DDE-BIFTOOL functions, and is called at the beginning of bifurcation analysis. The file 'sys_rhs.m' contains the right hand side of the system of differential equations. The file 'sys_tau.m' tells Matlab which parameters are the delays. The file 'sys_deriv.m' contains the Jacobian matrices. It can be replaced by 'df_deriv.m' from the DDE-BIFTOOL package, which is a default file that computes the Jacobians using finite differences. Engelborghs recommends that the first derivatives with respect to the state variables be computed since they are important in the bifurcation analysis.

C.1.1 sys_init.m

```
function [name,dim]=sys_init()

name='mentsrualcycle';
dim=13;
path(path,'./DDEBIFTOOL_203/ddebiftool/');

return;
```

C.1.2 sys_rhs.m

```
function dydt=sys_rhs(y,Q)

r_LH=14; vol=2.5; a_FSH=8.21; a=8;

v_0LH=Q(1); v_1LH=Q(2); Km_LH=Q(3); Ki_LHP=Q(4); k_LH=Q(5); c_LHP=Q(6);
c_LHE=Q(7); d_E=Q(8); d_P=Q(9); v_FSH=Q(10); Ki_FSHIh=Q(11); k_FSH=Q(12);
c_FSHP=Q(13); c_FSHE=Q(14); d_Ih=Q(15); alpha=Q(16); beta=Q(17); gamma=Q(18);
b=Q(19); c_1=Q(20); c_2=Q(21); c_4=Q(22); c_5=Q(23); c_8=Q(24); d_1=Q(25);
d_2=Q(26); k_1=Q(27); k_2=Q(28); k_3=Q(29); k_4=Q(30); e_0=Q(31); e_1=Q(32);
e_2=Q(33); e_3=Q(34); p_0=Q(35); p_1=Q(36); p_2=Q(37); h_0=Q(38); h_1=Q(39);
h_2=Q(40); h_3=Q(41);

% Auxiliary equations
E_2=e_0+e_1*y(6,1)+e_2*y(7,1)+e_3*y(13,1);
P_4=p_0+p_1*y(12,1)+p_2*y(13,1);
Ih=h_0+h_1*y(7,1)+h_2*y(11,1)+h_3*y(12,1);

E2_lag=e_0+e_1*y(6,2)+e_2*y(7,2)+e_3*y(13,2);
P4_lag=p_0+p_1*y(12,3)+p_2*y(13,3);
Ih_lag=h_0+h_1*y(7,4)+h_2*y(11,4)+h_3*y(12,4);

% System of Differential Equations:
dydt(1,1)=(v_0LH+v_1LH*(E2_lag/Km_LH)^a/(1+(E2_lag/Km_LH)^a))...
```

```
        /(1+P4_lag/Ki_LHP) - k_LH*((1+c_LHP*P_4)/(1+c_LHE*E_2))*y(1,1);
dydt(2,1)=(1/vol)*k_LH*((1+c_LHP*P_4)/(1+c_LHE*E_2))*y(1,1)-r_LH*y(2,1);
dydt(3,1)=v_FSH/(1+Ih_lag/Ki_FSHIh)...
        - k_FSH*((1+c_FSHP*P_4)/(1+c_FSHE*E_2^2))*y(3,1);
dydt(4,1)=(1/vol)*k_FSH*((1+c_FSHP*P_4)/(1+c_FSHE*E_2^2))*y(3,1)...
        - a_FSH*y(4,1);
dydt(5,1)=b*y(4,1)+(c_1*y(4,1)-c_2*y(2,1)^alpha)*y(5,1);
dydt(6,1)=c_2*(y(2,1)^alpha)*y(5,1)+(c_4*(y(2,1)^beta)-c_5*y(2,1))*y(6,1);
dydt(7,1)=c_5*y(2,1)*y(6,1)-c_8*y(2,1)^gamma*y(7,1);
dydt(8,1)=c_8*y(2,1)^gamma*y(7,1)-d_1*y(8,1);
dydt(9,1)=d_1*y(8,1)-d_2*y(9,1);
dydt(10,1)=d_2*y(9,1)-k_1*y(10,1);
dydt(11,1)=k_1*y(10,1)-k_2*y(11,1);
dydt(12,1)=k_2*y(11,1)-k_3*y(12,1);
dydt(13,1)=k_3*y(12,1)-k_4*y(13,1);
```

C.1.3 sys_tau.m

```
function tau=sys_tau()

tau=[8, 9, 15];

return;
```

C.1.4 sys_deriv

```
function J=sys_deri(y,Q,nx,np,v)

r_LH=14; vol=2.5; a_FSH=8.21; a=8;

v_0LH=Q(1); v_1LH=Q(2); Km_LH=Q(3); Ki_LHP=Q(4); k_LH=Q(5); c_LHP=Q(6);
c_LHE=Q(7); d_E=Q(8); d_P=Q(9); v_FSH=Q(10); Ki_FSHIh=Q(11); k_FSH=Q(12);
c_FSHP=Q(13); c_FSHE=Q(14); d_Ih=Q(15); alpha=Q(16); beta=Q(17); gamma=Q(18);
b=Q(19); c_1=Q(20); c_2=Q(21); c_4=Q(22); c_5=Q(23); c_8=Q(24); d_1=Q(25);
```

```
d_2=Q(26); k_1=Q(27); k_2=Q(28); k_3=Q(29); k_4=Q(30); e_0=Q(31); e_1=Q(32);
e_2=Q(33); e_3=Q(34); p_0=Q(35); p_1=Q(36); p_2=Q(37); h_0=Q(38); h_1=Q(39);
h_2=Q(40); h_3=Q(41);

% Auxiliary equations
E_2=e_0+e_1*y(6,1)+e_2*y(7,1)+e_3*y(13,1);
P_4=p_0+p_1*y(12,1)+p_2*y(13,1);
Ih=h_0+h_1*y(7,1)+h_2*y(11,1)+h_3*y(12,1);

E2_lag=e_0+e_1*y(6,2)+e_2*y(7,2)+e_3*y(13,2);
P4_lag=p_0+p_1*y(12,3)+p_2*y(13,3);
Ih_lag=h_0+h_1*y(7,4)+h_2*y(11,4)+h_3*y(12,4);

J=[];

if length(nx)==1 && length(np)==0 && isempty(v)
    % first derivatives wrt state variables
    if nx==0 % derivative wrt y(t), i.e. y(:,1)
        J(1,1)=-k_LH*((1+c_LHP*P_4)/(1+c_LHE*E_2));
        J(1,12)=-k_LH*((c_LHP*p_1)/(1+c_LHE*E_2))*y(1,1);
        J(1,13)=-k_LH*y(1,1)*(((c_LHP*p_2)/(1+c_LHE*E_2)) ...
                  + (1+c_LHP*P_4)*(-c_LHE*e_3/(1+c_LHE*E_2)^2));
        J(1,6)=-k_LH*(1+c_LHP*P_4)*y(1,1)*(-c_LHE*e_1/(1+c_LHE*E_2)^2);
        J(1,7)=-k_LH*(1+c_LHP*P_4)*y(1,1)*(-c_LHE*e_2/(1+c_LHE*E_2)^2);
        J(2,1)=-J(1,1)/vol;
        J(2,2)=-r_LH;
        J(2,12)=-J(1,12)/vol;
        J(2,13)=-J(1,13)/vol;
        J(2,6)=-J(1,6)/vol;
        J(2,7)=-J(1,7)/vol;
        J(3,3)=-k_FSH*(1+c_FSHP*P_4)/(1+c_FSHE*E_2^2);
        J(3,12)=-k_FSH*p_1*y(3,1)/(1+c_FSHE*E_2^2);
        J(3,13)=-k_FSH*y(3,1)*((p_2/(1+c_FSHE*E_2^2)) ...
                +(1+c_FSHP*P_4)*(-c_FSHE*2*E_2*e_3)/(1+c_FSHE*E_2^2)^2);
        J(3,6)=-k_FSH*(1+c_FSHP*P_4)*y(3,1)*...
                (-c_FSHE*2*E_2*e_1)/(1+c_FSHE*E_2^2)^2;
        J(3,7)=-k_FSH*(1+c_FSHP*P_4)*y(3,1)*...
```

```
            (-c_FSHE*2*E_2*e_2)/(1+c_FSHE*E_2^2)^2;
    J(4,3)=-J(3,3)/vol;
    J(4,12)=-J(3,12)/vol;
    J(4,13)=-J(3,13)/vol;
    J(4,6)=-J(3,6)/vol;
    J(4,7)=-J(3,7)/vol;
    J(4,4)=-a_FSH;
    J(5,2)=-c_2*alpha*(y(2,1)^(alpha-1))*y(5,1);
    J(5,4)=b+c_1*y(5,1);
    J(5,5)=c_1*y(4,1)-c_2*y(2,1)^alpha;
    J(6,2)=-J(5,2)+(c_4*beta*y(2,1)^(beta-1)-c_5)*y(6,1);
    J(6,5)=c_2*y(2,1)^alpha;
    J(6,6)=c_4*y(2,1)^beta-c_5*y(2,1);
    J(7,2)=c_5*y(6,1)-c_8*gamma*y(7,1)*y(2,1)^(gamma-1);
    J(7,6)=c_5*y(2,1);
    J(7,7)=-c_8*y(2,1)^gamma;
    J(8,2)=c_8*gamma*y(7,1)*y(2,1)^(gamma-1);
    J(8,7)=-J(7,7);
    J(8,8)=-d_1;
    J(9,8)=d_1;
    J(9,9)=-d_2;
    J(10,9)=d_2;
    J(10,10)=-k_1;
    J(11,10)=k_1;
    J(11,11)=-k_2;
    J(12,11)=k_2;
    J(12,12)=-k_3;
    J(13,12)=k_3;
    J(13,13)=-k_4;
elseif nx==1 %derivatives wrt y(t-d_E), i.e. y(:,2)
    J(1,6)=v_1LH*(1/(1+P4_lag/Ki_LHP))*a*e_1*E2_lag^(a-1)*...
            (Km_LH^a)/(Km_LH^a+E2_lag^a)^2;
    J(1,7)=v_1LH*(1/(1+P4_lag/Ki_LHP))*a*e_2*E2_lag^(a-1)*...
            (Km_LH^a)/(Km_LH^a+E2_lag^a)^2;
    J(1,13)=v_1LH*(1/(1+P4_lag/Ki_LHP))*a*e_3*E2_lag^(a-1)*...
            (Km_LH^a)/(Km_LH^a+E2_lag^a)^2;
    J(13,13)=0;
```

```
    elseif nx==2 %derivatives wrt y(t-d_P), i.e. y(:,3)
        J(1,12)=(v_0LH+v_1LH*(E2_lag/Km_LH)^a/(1+(E2_lag/Km_LH)^a))*...
                (-p_1/Ki_LHP)/(1+P4_lag/Ki_LHP)^2;
        J(1,13)=(v_0LH+v_1LH*(E2_lag/Km_LH)^a/(1+(E2_lag/Km_LH)^a))*...
                (-p_2/Ki_LHP)/(1+P4_lag/Ki_LHP)^2;
        J(13,13)=0;
    elseif nx==3 %derivatives wrt y(t-d_Ih), i.e. y(:,4)
        J(3,7)=v_FSH*(-1/Ki_FSHIh)*h_1/(1+Ih_lag/Ki_FSHIh)^2;
        J(3,11)=v_FSH*(-1/Ki_FSHIh)*h_2/(1+Ih_lag/Ki_FSHIh)^2;
        J(3,12)=v_FSH*(-1/Ki_FSHIh)*h_3/(1+Ih_lag/Ki_FSHIh)^2;
        J(13,13)=0;
    end;
elseif length(nx)==0 && length(np)==1 && isempty(v)
    % derivatives wrt the parameters
    if np==1 % derivative wrt v0_LH
        J(1,1)=1/(1+P4_lag/Ki_LHP);
        J(13,1)=0;
    elseif np==2 % derivative wrt v1_LH
        J(1,1)=(E2_lag^a/(Km_LH^a+E2_lag^a))/(1+P4_lag/Ki_LHP);
        J(13,1)=0;
    elseif np==3 % derivative wrt Km_LH
        J(1,1)=v_1LH*(a*Km_LH^(a-1))*...
                (E2_lag^a*(-1)/(Km_LH^a+E2_lag^a)^2)/(1+P4_lag/Ki_LHP);
        J(13,1)=0;
    elseif np==4 % derivative wrt Ki_LHP
        J(1,1)=(v_0LH+v1_LH*(E2_lag^a/(Km_LH^a+E2_lag^a)))*...
                (P4_lag/(Ki_LHP+P4_lag)^2);
        J(13,1)=0;
    elseif np==5 % derivative wrt k_LH
        J(1,1)=-(1+c_LHP*P_4)*y(1,1)/(1+c_LHE*E_2);
        J(2,1)=-J(1,1)/vol;
        J(13,1)=0;
    elseif np==6 % derivative wrt c_LHP
        J(1,1)=-k_LH*P_4*y(1,1)/(1+c_LHE*E_2);
        J(2,1)=-J(1,1)/vol;
        J(13,1)=0;
    elseif np==7 % derivative wrt c_LHE
```

```
    J(1,1)=-k_LH*y(1,1)*(1+c_LHP*P_4)*(-E2)/(1+c_LHE*E_2)^2;
    J(2,1)=-J(1,1)/vol;
    J(13,1)=0;
elseif np==8 || 9 || 15 % derivatives wrt delays
    J(13,1)=0;
elseif np==10 % derivative wrt v_FSH
    J(3,1)=1/(1+Ih_lag/Ki_FSHIh);
    J(13,1)=0;
elseif np==11 % derivative wrt Ki_FSHIh
    J(3,1)=v_FSH*Ih_lag/(Ki_FSHIh+Ih_lag)^2;
    J(13,1)=0;
elseif np==12 % derivative wrt k_FSH
    J(3,1)=-(1+c_FSHP*P_4)*y(3,1)/(1+c_FSHE*E_2^2);
    J(4,1)=-J(3,1)/vol;
    J(13,1)=0;
elseif np==13 % derivative wrt c_FSHP
    J(3,1)=-k_FSH*P_4*y(3,1)/(1+c_FSHE*E_2^2);
    J(4,1)=-J(3,1)/vol;
    J(13,1)=0;
elseif np==14 % derivative wrt c_FSHE
    J(3,1)=-k_FSH*(1+c_FSHP*P_4)*y(3,1)*(-E_2^2)/(1+c_FSHE*E_2^2)^2;
    J(4,1)=-J(3,1)/vol;
    J(13,1)=0;
elseif np==16 % derivative wrt alpha
    J(5,1)=-c_2*y(5,1)*log(y(2,1))*y(2,1)^alpha;
    J(6,1)=-J(5,1);
    J(13,1)=0;
elseif np==17 % derivative wrt beta
    J(6,1)=c_4*y(6,1)*log(y(2,1))*y(2,1)^beta;
    J(13,1)=0;
elseif np==18 % derivative wrt gamma
    J(7,1)=-c_8*y(7,1)*log(y(2,1))*y(2,1)^gamma;
    J(8,1)=-J(7,1);
    J(13,1)=0;
elseif np==19 % derivative wrt b
    J(5,1)=y(4,1);
    J(13,1)=0;
```

```
elseif np==20 % derivative wrt c_1
    J(5,1)=y(4,1)*y(5,1);
    J(13,1)=0;
elseif np==21 % derivative wrt c_2
    J(5,1)=-y(2,1)^alpha*y(5,1);
    J(6,1)=-J(5,1);
    J(13,1)=0;
elseif np==22 % derivative wrt c_4
    J(6,1)=y(2,1)^beta*y(6,1);
    J(13,1)=0;
elseif np==23 % derivative wrt c_5
    J(6,1)=-y(2,1)*y(6,1);
    J(7,1)=-J(6,1);
    J(13,1)=0;
elseif np==24 % derivative wrt c_8
    J(7,1)=-y(2,1)^gamma*y(7,1);
    J(8,1)=-J(7,1);
    J(13,1)=0;
elseif np==25 % derivative wrt d_1
    J(8,1)=-d_1*y(8,1);
    J(9,1)=-J(8,1);
    J(13,1)=0;
elseif np==26 % derivative wrt d_2
    J(9,1)=-y(9,1);
    J(10,1)=-J(9,1);
    J(13,1)=0;
elseif np==27 % derivative wrt k_1
    J(10,1)=-y(10,1);
    J(11,1)=-J(10,1);
    J(13,1)=0;
elseif np==28 % derivative wrt k_2
    J(11,1)=-y(11,1);
    J(12,1)=-J(11,1);
    J(13,1)=0;
elseif np==29 % derivative wrt k_3
    J(12,1)=-y(12,1);
    J(13,1)=-J(12,1);
```

```
elseif np==30 % derivative wrt k_4
    J(13,1)=-y(13,1);
elseif np==31 % derivative wrt e_0
    J(1,1)=v_1LH*(a*E2_lag^(a-1)*Km_LH^a/(Km_LH^a+E2_lag^a)^2)...
            /(1+P4_lag/Ki_LHP)-k_LH*(1+c_LHP*P_4)*y(1,1)*(-c_LHE)...
            /(1+c_LHE*E_2)^2;
    J(2,1)=(k_LH/vol)*(1+c_LHP*P_4)*y(1,1)*(-c_LHE)/(1+c_LHE*E_2)^2;
    J(3,1)=-k_FSH*(1+c_FSHP*P_4)*y(3,1)*(-c_FSHE*2*E_2)...
            /(1+c_FSHE*E_2^2)^2;
    J(4,1)=-J(3,1)/vol;
    J(13,1)=0;
elseif np==32 % derivative wrt e_1
    J(1,1)=v_1LH*(a*y(6,2)*E2_lag^(a-1)*...
            Km_LH^a/(Km_LH^a+E2_lag^a)^2)/(1+P4_lag/Ki_LHP)...
            -k_LH*(1+c_LHP*P_4)*y(1,1)*(-c_LHE*y(6,1))/(1+c_LHE*E_2)^2;
    J(2,1)=(k_LH/vol)*(1+c_LHP*P_4)*y(1,1)*(-c_LHE*y(6,1))...
           /(1+c_LHE*E_2)^2;
    J(3,1)=-k_FSH*(1+c_FSHP*P_4)*y(3,1)*(-c_FSHE*2*y(6,1)*E_2)...
            /(1+c_FSHE*E_2^2)^2;
    J(4,1)=-J(3,1)/vol;
    J(13,1)=0;
elseif np==33 % derivative wrt e_2
    J(1,1)=v_1LH*(a*y(7,2)*E2_lag^(a-1)*...
            Km_LH^a/(Km_LH^a+E2_lag^a)^2)/(1+P4_lag/Ki_LHP)...
            -k_LH*(1+c_LHP*P_4)*y(1,1)*(-c_LHE*y(7,1))/(1+c_LHE*E_2)^2;
    J(2,1)=(k_LH/vol)*(1+c_LHP*P_4)*y(1,1)*(-c_LHE*y(7,1))...
            /(1+c_LHE*E_2)^2;
    J(3,1)=-k_FSH*(1+c_FSHP*P_4)*y(3,1)*(-c_FSHE*2*y(7,1)*E_2)...
             /(1+c_FSHE*E_2^2)^2;
    J(4,1)=-J(3,1)/vol;
    J(13,1)=0;
elseif np==34 % derivative wrt e_3
    J(1,1)=v_1LH*(a*y(13,2)*E2_lag^(a-1)*...
            Km_LH^a/(Km_LH^a+E2_lag^a)^2)/(1+P4_lag/Ki_LHP)...
            -k_LH*(1+c_LHP*P_4)*y(1,1)*(-c_LHE*y(13,1))/(1+c_LHE*E_2)^2;
    J(2,1)=(k_LH/vol)*(1+c_LHP*P_4)*y(1,1)*(-c_LHE*y(13,1))...
            /(1+c_LHE*E_2)^2;
```

```
    J(3,1)=-k_FSH*(1+c_FSHP*P_4)*y(3,1)*(-c_FSHE*2*y(13,1)*E_2)...
             /(1+c_FSHE*E_2^2)^2;
    J(4,1)=-J(3,1)/vol;
    J(13,1)=0;
elseif np==35 % derivative wrt p_0
    J(1,1)=(v_0LH+v_1LH*E2_lag^a/(Km_LH^a+E2_lag^a))*...
            (-1/Ki_LHP)/(1+P4_lag/Ki_LHP)^2...
            - k_LH*y(1,1)*c_LHP/(1+c_LHE*E_2);
    J(2,1)=(k_LH/vol)*y(1,1)*c_LHP/(1+c_LHE*E_2);
    J(3,1)=-k_FSH*y(3,1)*c_FSHP/(1+c_FSHE*E_2^2);
    J(4,1)=-J(3,1)/vol;
    J(13,1)=0;
elseif np==36 % derivative wrt p_1
    J(1,1)=(v_0LH+v_1LH*E2_lag^a/(Km_LH^a+E2_lag^a))*...
            (-y(12,3)/Ki_LHP)/(1+P4_lag/Ki_LHP)^2-k_LH*y(1,1)*...
            c_LHP*y(12,1)/(1+c_LHE*E_2);
    J(2,1)=(k_LH/vol)*y(1,1)*c_LHP*y(12,1)/(1+c_LHE*E_2);
    J(3,1)=-k_FSH*y(3,1)*c_FSHP*y(12,1)/(1+c_FSHE*E_2^2);
    J(4,1)=-J(3,1)/vol;
    J(13,1)=0;
elseif np==37 % derivative wrt p_2
    J(1,1)=(v_0LH+v_1LH*E2_lag^a/(Km_LH^a+E2_lag^a))*...
            (-y(13,3)/Ki_LHP)/(1+P4_lag/Ki_LHP)^2-k_LH*y(1,1)*...
            c_LHP*y(13,1)/(1+c_LHE*E_2);
    J(2,1)=(k_LH/vol)*y(1,1)*c_LHP*y(13,1)/(1+c_LHE*E_2);
    J(3,1)=-k_FSH*y(3,1)*c_FSHP*y(13,1)/(1+c_FSHE*E_2^2);
    J(4,1)=-J(3,1)/vol;
    J(13,1)=0;
elseif np==38 % derivative wrt h_0
    J(3,1)=v_FSH*(-1/Ki_FSHIh)/(1+Ih_lag/Ki_FSHIh)^2;
    J(13,1)=0;
elseif np==39 % derivative wrt h_1
    J(3,1)=v_FSH*(-y(7,4)/Ki_FSHIh)/(1+Ih_lag/Ki_FSHIh)^2;
    J(13,1)=0;
elseif np==40 % derivative wrt h_2
    J(3,1)=v_FSH*(-y(11,4)/Ki_FSHIh)/(1+Ih_lag/Ki_FSHIh)^2;
    J(13,1)=0;
```

```
    elseif np==41 % derivative wrt h_3
        J(3,1)=v_FSH*(-y(12,4)/Ki_FSHIh)/(1+Ih_lag/Ki_FSHIh)^2;
        J(13,1)=0;
    end
else
    J=df_deriv(y,Q,nx,np,v);
end;

if isempty(J)
    err=[nx np size(v)]
    error('SYS_DERI: requested derivative could not be computed!');
end;

return;
```

C.2 Steady State Solutions

We start our analysis by calling 'sys_init'. To find a steady state solution, we start with a guess, and then correct it using the command `p_correc`. A point may need to be corrected a few times until success=1. The values for the parameter vector, Q, and the initial guess for the steady state, IC, should be defined prior to running the following code.

```
[name,n]=sys_init

stst.kind = 'stst';
stst.parameter = [Q];
stst.x = [IC]';

method = df_mthod('stst');
[stst,success] = p_correc(stst,[],[],method.point)
```

For the parameter values of Chapters 3 and 5, and Km_LH=50, the steady state that is stst.x = [440.8492; 34.7994; 36.3527; 13.3224; 7.3883; 12.0259; 20.6372; 22.5986; 20.1773; 20.5442; 16.3758; 13.2933; 13.2933].

We can compute the stability of the steady state solution using the command `p_stabil`. The command `df_mthod('stst')` provides the default options for computing the stability. If we find that only a few characteristic roots were computed, we can change `method.stability.minimal_real_part` to a more negative value.

```
method=df_mthod('stst');
stst.stability=p_stabil(stst,method.stability);
figure(1); clf;
p_splot(stst);
```

See Figure C.1 for the stability plot of the steady state solution that we found above. From the stability plot, we can see that the steady state solution at Km_LH=50 is a stable solution (all of the characteristic roots have negative real part). Eigenvalues with real part less than 0 are colored in green by default, while eigenvalues with real part greater than 0 are colored in red.

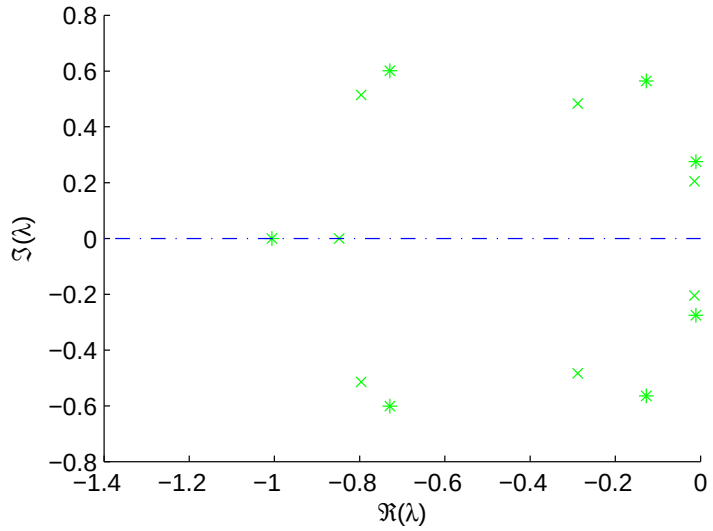

Figure C.1: Eigenvalues of the steady state solution at Km_LH=50

C.3 Creating a Branch of Steady State Solutions

We can use the steady state point we just found as a first point in a branch of steady state solutions. First we obtain an empty branch with free parameter Km_LH limited by Km_LH in [50, 300] and delta Km_LH < 10 between points.

```
stst_branch=df_brnch(3,'stst') % df_brnch(free_par,kind)
stst_branch.parameter
stst_branch.parameter.min_bound
stst_branch.parameter.min_bound(4,:)=[3 50]; % [par minbound]
stst_branch.parameter.max_bound(1,:)=[3 300]; % [par maxbound]
stst_branch.parameter.max_step(1,:)=[3 10]; % [par maxstep]
```

To start a branch, we need two points. We set the first point equal to the steady state point that we just found. To obtain a second point we change the parameter Km_LH slightly and correct.

```
stst_branch.point=stst;
method=df_mthod('stst');
stst.parameter(3)=stst.parameter(3)+2;
success=0;
i=0;
while success==0 && i<5
        i=i+1;
        [stst,success]=p_correc(stst,[],[],method.point)
end
stst_branch.point(2)=stst;
```

Once we have two starting points and suitable method parameters, we can start varying Use the command `br_contn` to continue the branch with a certain number of points. When continuing a branch, it may be necessary to adjust some of the default continuation options. In to continue the branch of steady state solutions for the system discussed here, it was necessary to set `stst_branch.method.continuation.steplength_condition` equal to 0. If you want to continue the branch in the other direction you can reverse order of branch points using the command `br_rvers`, and `br_contn` then continues the branch to the left.

```
stst_branch.method.continuation.steplength_condition=0;
[stst_branch,s,f,r]=br_contn(stst_branch,50)
```

Use the command `br_plot` to plot the branch. Obtain the input variables `xm` and `ym` from `df_measr`. The first argument of `df_measr` indicates that we do not want to plot the stability information along the branch. The plotting functions of DDE-BIFTOOL by default display the first state variable of the system. In order to plot a different state variable, set `ym.row` equal to the order in which that variable appears. For example, to plot LH, we set `ym.row` equal to 2 since it is the second equation in our system. Figure C.2 displays the branch of steady state solutions.

```
figure;
[xm,ym]=df_measr(0,stst_branch);
ym.row=2;
br_plot(stst_branch,xm,ym,'b');
br_plot(stst_branch,xm,ym,'b.');
xlabel('KmLH');
ylabel('LH');
title('Branch of Steady State Solutions');
```

C.4 Finding Hopf Bifurcations

We can find Hopf bifurcations by computing the stability along the branch of steady state solutions. Where a pair of complex eigenvalues crosses the imaginary axis we have a potential Hopf bifurcation. Use the command `stst_branch` to compute the stability along the steady state branch.

```
stst_branch=br_stabl(stst_branch,0,1)
```

Plot the real part of the approximated roots of the characteristic equation along the branch using the `br_plot` command. The '1' in the first argument of `df_measr` indicates that we wish to plot the stability information associated with our branch.

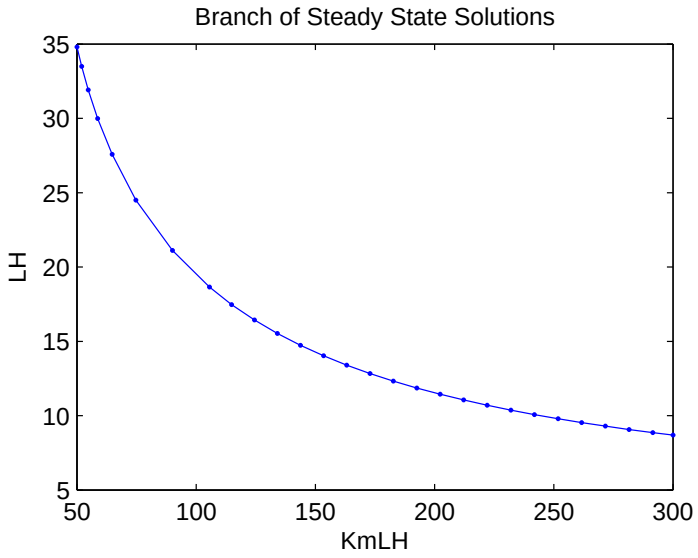

Figure C.2: Branch of steady state solutions.

```
[xm,ym]=df_measr(1,stst_branch);
figure;
br_plot(stst_branch,xm,ym,'b');
xlim([50 300]);
xlabel('KmLH');
ylabel('R(\lambda)');
plot([50 300], [0 0],'-.');
```

In order to discern which real parts correspond to real e-values vs. complex pairs, you can compare Figures C.1 and C.3. The plot for this range of Km_LH values shows us that there are candidates for Hopf bifurcations at about Km_LH=65.5 and KmLH=248.2 (see Figure C.3). In order to check that these are indeed Hopf bifurcations, we need to know their position in the branch, or their point number. Plot the branch against the point number by removing the argument `xm` in the command `br_plot`. The two candidate Hopf points that we observed occur at point number 5 and 23 (see Figure C.3).

```
figure;
br_plot(stst_branch,[],ym,'b');
br_plot(stst_branch,[],ym,'b.');
plot([0 30],[0 0],'-.');
```

```
xlim([0 30]);
ylim([-0.03 0.03]);
ylabel('R(\lambda)');
xlabel('point number');
```

Now we can check these points to see if they are Hopf points. First we convert the points to a structure that DDE-BIFTOOL associates with hopf points using the command `p_tohopf`. Then we use the `p_correc` command to correct the points.

```
hopf1=p_tohopf(stst_branch.point(5));
hopf2=p_tohopf(stst_branch.point(23));

method=df_mthod('hopf');
success=0;
i=0;
while success==0 && i<5
    i=i+1;
    [hopf1,success]=p_correc(hopf1,3,[],method.point)
end

success=0;
i=0;
while success==0 && i<5
    i=i+1;
    [hopf2,success]=p_correc(hopf2,3,[],method.point)
end
```

Now that we have a Hopf point, we can start a branch of periodic solutions from this point.

C.5 Branch of Periodic Solutions emanating from a Hopf point

Starting from the first hopf point, we initialize branch of periodic solutions. We found it necessary to change some of the methods to get the branch to continue.

```
psol2_branch = df_brnch(3,'psol');
```

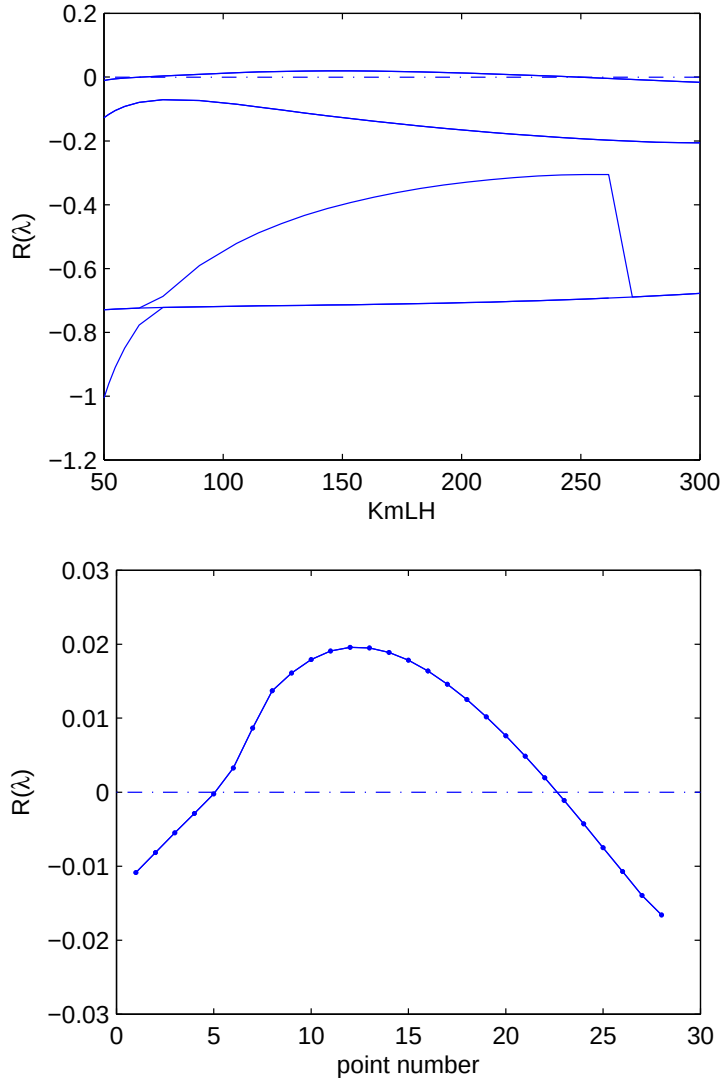

Figure C.3: Stability information along the branch of steady state solutions. Potential Hopf points occur at about Km_LH=65.5 (about point 5) and Km_LH=248.2 (about point 23)

```
psol2_branch.parameter.min_bound(4,:) = [3 55];
psol2_branch.parameter.max_bound(1,:) = [3 350];
psol2_branch.parameter.max_step(1,:) = [3 10];
psol2_branch.method.point.minimal_accuracy = 1;
psol2_branch.method.point.newton_max_iterations = 10;
```

In order to continue a branch, we need at least two starting points. For this system with this set of parameters, it was necessary to provide several points, otherwise the branch would jump back down to the steady state branch. The first point to construct is a degenerate periodic solution (amplitude = 0) from the hopf point.

```
amplitude = 0;
intervals = 20;
degree = 3;
[deg_psol,stepcond] = p_topsol(hopf1,amplitude,degree,intervals);

% we obtain default point method parameters and correct the point
method = df_mthod('psol');
method.point.minimal_accuracy = 1;
[deg_psol,success] = p_correc(deg_psol,[],stepcond,method.point)

deg_psol.mesh = []; % to speed up branch continuation remove the mesh
psol_branch.point = deg_psol;
```

We need several points to start the branch. Using only two points may result in the branch going back to steady state. We use the hopf point to construct several small amplitude periodic solutions.

```
for j=2:5
    amplitude = (j-1)^2;
    intervals = 20;
    degree = 3;
    [psol,stepcond]=p_topsol(hopf1,amplitude,degree,intervals);
    % p_topsol(hopf,amplitude,degree,intervals)
```

```
    % we get default point method parameters and correct the point
    method=df_mthod('psol');
    method.point.newton_max_iterations=10; % changes max iters from 5 to 10
    method.point.minimal_accuracy=1; % changes accuracy from 1e-06 to 1

    [psol,success]=p_correc(psol,3,stepcond,method.point)
    % p_correc(psol,free_param,stepcond,method.point)

    temp=psol;
    temp.mesh=[]; % remove mesh to speed up branch continuation
    psol_branch.point(j)=temp;
end
```

Now that we have several points to start with, we can continue the branch.

```
figure;
[xm,ym]=df_measr(0,psol_branch); % 0 means no stability information
br_plot(psol_branch,xm,ym,'b.-'); % plots initial branch points

[psol_branch,s,f,r]=br_contn(psol_branch,45) % br_contn(branch, max # of pts)
```

By default, DDE-BIFTOOL plots the amplitude of the first state variable against the varied parameter. After the branch is complete, it is possible to plot other state variables, and plot the maximum value along a periodic solution instead of the amplitude. The following code plots the LH value for the branch of steady state solutions and the maximum LH value associated with each solution along the branch of periodic solutions.

```
% Plotting maximum LH value of periodic branch and stst branch together:
figure;
[xm,ym]=df_measr(0,stst_branch);
ym.row=2;
br_plot(stst_branch,xm,ym,'b');
xlim([50 300]);
xlabel('KmLH')
ylim([0 160]);
```

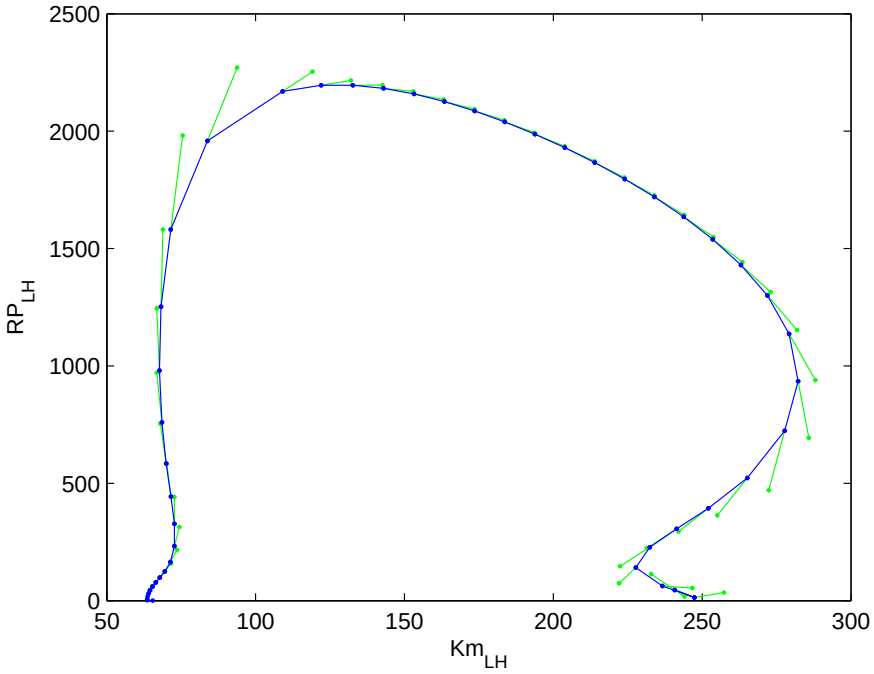

Figure C.4: Branch of periodic solutions

```
ylabel('LH')
[xm,ym]=df_measr(0,psol_branch);
ym.row=2;
ym.col='max';
br_plot(psol_branch,xm,ym,'b.-');
```

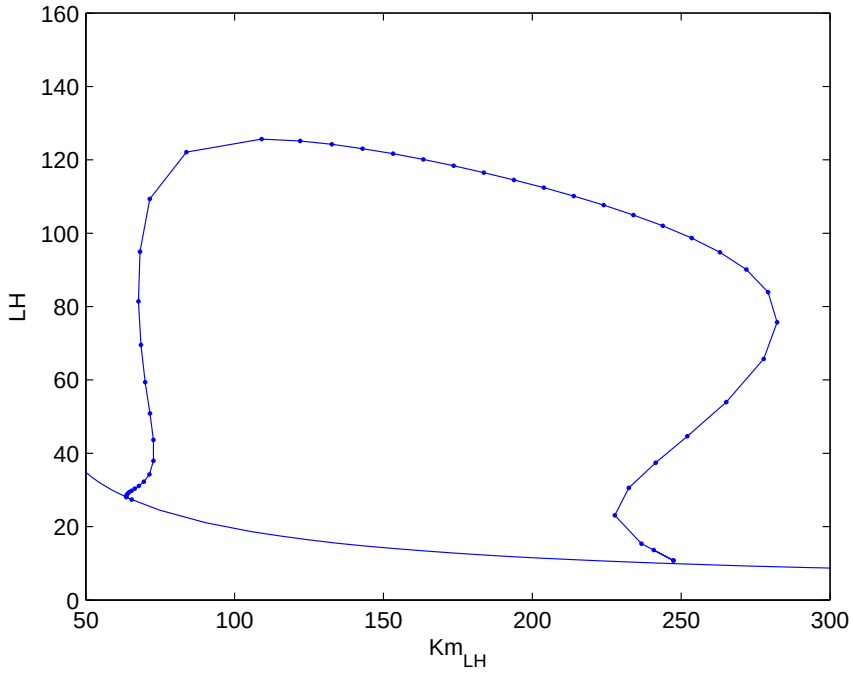

Figure C.5: Final bifurcation diagram combining the branch of steady state solutions and the branch of periodic orbits. The maximum value of LH associated with each solution is plotted against the varied parameter Km_LH.

Appendix D

Residuals used during optimization

The residual vector used in optimization of equations (S1)-(S2) and (A5) is

$$R = \begin{bmatrix} \frac{R_{P_o+P_a}}{\sqrt{n_1}\ \max(\log(\text{Hansen}_{\text{data}}))} \\ \\ \frac{R_{AMH}}{\sqrt{n_2}\ \max(\text{AMH}_{\text{data}})} \end{bmatrix}$$

where

$$R_{P_o+P_a} = [\log(Primor + Primar) - \log(\text{Hansen}_{\text{data}})] \quad \text{and} \quad R_{AMH} = [AMH - \text{AMH}_{\text{data}}],$$

and n_1, n_2 are the sample sizes of $\text{Hansen}_{\text{data}}$ and AMH_{data}, respectively. The error for $Primor+Primar$ is computed using *log* transformed data because the error in the data is consistent with a log-normal distribution. The two residuals $R_{P_o+P_a}$ and R_{AMH} are divided by the maximum value of the respective data so that these terms are on the same scale. The errors are also each divided by the square root of the number of data points so that the sum of squared residuals of a large and a small data set are weighed equally during optimization.

The residual vector used in optimization of equations (S3)-(S12) and (A1)-(A4) is

$$R = \begin{bmatrix} \frac{R_{LH}}{\max(\mathrm{LH_{data}})} \\ \frac{R_{FSH}}{\max(\mathrm{FSH_{data}})} \\ \frac{R_{E2}}{\max(\mathrm{E2_{data}})} \\ \frac{R_{P4}}{\max(\mathrm{P4_{data}})} \\ \frac{R_{InhA}}{\max(\mathrm{InhA_{data}})} \\ \frac{R_{InhB}}{\max(\mathrm{InhB_{data}})} \\ \frac{R_{InhB,40}}{\max(\mathrm{InhB_{data,older}})} \\ \frac{R_{FSH,40}}{\max(\mathrm{FSH_{data,older}})} \end{bmatrix}$$

where

$$R_{LH} = [LH(t_{30}) - \mathrm{LH_{data}}]$$

$$\vdots$$

$$R_{InhB} = [InhB(t_{30}) - \mathrm{InhB_{data}}]$$

$$R_{FSH,40} = [FSH(t_{40}) - \mathrm{FSH_{data,older}}]$$

and

$$R_{InhB,40} = [InhB(t_{40}) - \mathrm{InhB_{data,older}}].$$

Here $\mathrm{LH_{data}}, \mathrm{FSH_{data}}$, etc. are the data for younger women, and $\mathrm{FSH_{data,older}}$ and $\mathrm{InhB_{data,older}}$ are the data for older women from Welt et al. (1999) [83]. The residuals include model output of all 6 hormones at age 30 ($LH(t_{30}), FSH(t_{30})$, etc.) compared to data for younger women, and model output for FSH and $InhB$ at age 40 ($FSH(t_{40})$ and $InhB(t_{40})$) compared to data for older women. FSH and InhB for older women are included because of the decline of follicular phase $InhB$ and subsequent rise in FSH that is seen between age 30 and 40 [83].

Appendix E

Parameters and initial conditions

Table E.1: Optimized parameters for eq. (SS1)-(SS2) and (A5). This parameter set was obtained by minimizing the sum of square residuals of $\log(Primor + Primar)$ against $\log(\text{Hansen}_{\text{data}})$ [28], and $AMH = a_1\, Primar$ against AMH_{data} [24, 31, 41, 75, 77, 79, 80] (see Appendix D). The *'s indicate parameter values that were fixed to avoid correlations among parameters during optimization. For r_2, a scaled version, $\widehat{r}_2$, was fixed (see Section 4.1). See Figure 7.3 for the simulation profiles plotted against data. If no units are given, it is a dimensionless quantity.

Eq. (SS1)-(SS2)			Eq. (A5)		
c_{AMH}	$= 0.226 \pm 0.187$	mL/ng	a_1	$= 0.0437 \pm 0.00463$	ng/(mL follicle)
c_{prm}	$= 1.31\text{E-}05 \pm 2.49\text{E-}06$	follicle^{-1}	a_2	$= 0^*$	
r_{surv}	$= 0.014^*$		a_3	$= 0^*$	
r_1	$= 0.00102 \pm 0.000178$	day^{-1}			
r_2	$= 0.00694^*$	day^{-1}			

Table E.2: Optimized parameters for equations (SS3)-(SS12). This list along with the parameters in Tables E.3 and Table E.4 were obtained by minimizing the sum of square residuals of LH, FSH, E2, P4, InhA, and InhB against data from Welt *et al.* [83] (see Appendix D). The *'s indicate parameter values that were fixed to avoid correlations among parameters during optimization.

Eq. (SS3)-(SS12)					
$vol2$	$= 0.500^*$	mm^3	c_1	$= 0.918 \pm 0.0188$	day^{-1}
Km_{F1}	$= 9.82 \pm 0.306$	IU/L	c_2	$= 0.0575 \pm 0.000499$	$(L/IU)^{\delta}/day$
Km_{F2}	$= 10.4^*$	IU/L	c_3	$= 0.0241 \pm 0.00172$	L/(day IU)
Km_{F3}	$= 5.08 \pm 0.355$	IU/L	c_4	$= 0.0307 \pm 0.00299$	L/(day IU)
Ki_{AMH}	$= 20.7 \pm 1.37$	ng/mL	c_5	$= 0.198^*$	$(L/IU)^{\omega}/day$
α	$= 29.1 \pm 2$		c_6	$= 0.00519 \pm 5.28E\text{-}05$	L/(day IU)
β	$= 2.06 \pm 0.125$		c_7	$= 0.686 \pm 0.0489$	day^{-1}
γ	$= 2.95 \pm 0.137$		k_1	$= 0.416 \pm 0.0258$	day^{-1}
δ	$= 0.999 \pm 0.0245$		k_2	$= 0.405 \pm 0.0181$	day^{-1}
ω	$= 0.363 \pm 0.0142$		k_3	$= 0.551 \pm 0.0218$	day^{-1}
r_3	$= 0.759 \pm 0.0657$	day^{-1}	k_4	$= 0.903 \pm 0.0351$	day^{-1}
r_4	$= 2.23 \pm 0.0967$	L/(day IU)			
r_5	$= 1.21 \pm 0.0487$	day^{-1}			

Table E.3: Parameters for equations (SS13)-(SS16). The *'s indicate parameter values that were fixed during optimization. Some of these were taken from biological sources, others were fixed at nominal values to avoid correlations among parameters during optimization (see Section 3.6). The parameters cl_{LH} and cl_{FSH} were taken from biological sources [39] and [12]. The parameter d_{InhB} was taken to be zero as a result of separate analysis of the FSH equations using time-dependent input functions for the ovarian hormones.

Eq. (S13)-(S16)					
$V_{0,LH}$	$= 343 \pm 16.4$	IU/day	V_{FSH}	$= 616 \pm 11.9$	IU/day
$V_{1,LH}$	$= 8110^*$	IU/day	$Ki_{FSH,InhA}$	$= 2.58^*$	IU/mL
Km_{LH}	$= 247 \pm 4.75$	pg/mL	$Ki_{FSH,InhB}$	$= 120^*$	pg/mL
Ki_{LHP}	$= 155 \pm 17.1$	ng/mL	k_{FSH}	$= 1.04 \pm 0.103$	day^{-1}
k_{LH}	$= 1.01 \pm 0.0709$	day^{-1}	cl_{FSH}	$= 8.21^*$	day^{-1}
cl_{LH}	$= 14.0^*$	day^{-1}	$c_{FSH,P}$	$= 130 \pm 8.61$	mL/ng
c_{LHP}	$= 1.10 \pm 0.101$	mL/ng	$c_{FSH,E}$	$= 0.00525 \pm 0.00058$	mL^2/pg^2
c_{LHE}	$= 0.00398 \pm 7.59E\text{-}05$	mL/pg	d_{InhA}	$= 1.38 \pm 0.0852$	days
d_E	$= 0.187 \pm 0.0457$	days	d_{InhB}	$= 0^*$	days
d_P	$= 2.00 \pm 0.249$	days	v	$= 2.5^*$	L

Table E.4: Parameters for equations (A1)-(A4). These parameters were obtained by using biologically appropriate magnitudes for the follicular state variables, and estimating the values for the coefficients that would achieve good fits to the data from Welt *et al* [83] for younger women. These parameter values were fixed during optimization to avoid correlations among parameters.

Eq. (A1)-(A4)					
e_0	$= 30$	pg/mL	h_0	$= 0$	
e_1	$= 0.04$	pg/(mL mm^3)	h_1	$= 0.0035$	IU/(mL mm^3)
e_2	$= 0.065$	pg/(mL mm^3)	h_2	$= 0.0021$	IU/(mL mm^3)
e_3	$= 0.1$	pg/(mL mm^3)	h_3	$= 0.0021$	IU/(mL mm^3)
p_0	$= 0$	ng/(mL mm^3)	j_0	$= 15$	pg/mL
p_1	$= 0.0085$	ng/(mL mm^3)	j_1	$= 20.2$	pg/(mL mm^3)
p_2	$= 0$	ng/(mL mm^3)	j_2	$= 0.0138$	pg/(mL mm^3)

Table E.5: Initial conditions used when solving the model at ages 30 and 40. Initial conditions for *Primor* and *Primar* were obtained by solving equations (SS1)-(SS2) and (A5) from age 20 up to the required age. Initial conditions for the remaining stages were obtained for a specific age by fixing *Primor* and *Primar*, and allowing the solution to approach the stable attractor. We consider a less than 1% change in initial condition from one cycle to the next as a sign that the stable attractor has been reached. Centering the *LH* peak at day 14, the value of a stage at day 1 is taken to be the initial condition for that stage.

	Age 20	Age 30	Age 40
$Primor$	265000	108000	19000
$Primar$	100	72.5	27.6
$PrAnF$	1.15	0.712	0.237
$SmAnF$	3.98	3.21	1.46
ReF	40.4	37.9	33.2
GrF	53.1	52.9	55.9
$DomF$	23.3	23.0	24.3
Ov	16.0	15.6	16.3
Lut_1	91.3	88.9	89.9
Lut_2	320	313	312
Lut_3	438	429	426
Lut_4	362	355	352
RP_{LH}	78.5	79.5	80.0
LH	9.05	9.05	9.05
RP_{FSH}	12.0	12.7	14.4
FSH	11.0	11.6	13.1